THESIS ON NATURAL AND EXACT SCIENCES B123

Metabolic Flux Analysis of Compartmentalized Systems using Dynamic Isotopologue Modeling

DAVID W. SCHRYER

TUT PRESS

TALLINN UNIVERSITY OF TECHNOLOGY
Institute of Cybernetics
Laboratory of Systems Biology

This dissertation was accepted for the defense of the degree of Doctor of Philosophy (Engineering Physics) on Friday, January 13th, 2012.

Supervisor: Marko Vendelin, PhD,
Laboratory of Systems Biology, Institute of Cybernetics at TUT

Co-supervisors: Pearu Peterson, PhD,
Laboratory of Systems Biology, Institute of Cybernetics at TUT

Professor Toomas Paalme, Chair of Food Processing,
Faculty of Chemical and Materials Technology, TUT

Opponents: Katharina Nöh, PhD,
Institute of Bio- and Geosciences IBG-1, Forschungszentrum Jülich GmbH

Professor Tanel Tenson,
Head of the Antibiotics Group in the Molecular Microbiology Laboratory,
Institute of Technology at the University of Tartu

Defense of the thesis: April 12th, 2012 at 14:00 EET

Declaration: I hereby declare that this doctoral thesis, submitted for the doctoral degree at Tallinn University of Technology, is my original investigation and achievement and has not been submitted for the defense of any academic degree elsewhere.

David W. Schryer

Colophon: This thesis was typeset with LaTeX 2ε using André Miede's *classicthesis* style with modifications by Ardo Illaste and David W. Schryer to conform with TUT style guidelines. The main font is Libertine. ZapfChancery is used for Latin text. Biolinum is used for *sans* serif text.

ISSN 1406-4723
ISBN 978-9949-23-238-3 (publication)
ISBN 978-9949-23-239-0 (PDF)

LOODUS- JA TÄPPISTEADUSED B123

Isotopoloogilise modelleerimise rakendamine heterogeensete bioloogiliste süsteemide ainevahetusvoo analüüsis

DAVID W. SCHRYER

TTÜ
KIRJASTUS

CONTENTS

SUMMARY

This dissertation applies dynamic tracer-based MFA to study the recycling fluxes of energy metabolites in the mammalian heart and the TCA cycle flux of *Saccharomyces uvarum*. Compartmentation of metabolites in these systems complicates their analysis, so methods are discussed to reveal compartmentation using dynamic isotopologue simulation coupled with isotopic transient data measured in biological systems operating at *pseudo* metabolic steady state. A routine was developed to compose dynamic isotopologue models from systems of chemical transformations and, in the case of *Saccharomyces uvarum*, optimization techniques were applied to find flux distributions that best fit with measurements of the isotopic labeling state. To make the optimization process more efficient for application in large metabolic networks, a sparse symbolic Gauss-Jordan elimination routine was developed to express all steady state metabolic solutions in terms of a flux coordinate system suggested by the analyst. Properties of flux coordinate systems were found to be useful in studying systems of chemical transformations in general and genome-scale metabolic networks in particular. Dynamic isotopologue modeling was applied to study the recycling fluxes of energy metabolites in the mammalian heart. A sensitivity analysis of the dynamic isotopologue model revealed that the fluxes found using ^{18}O–assisted ^{31}P–NMR, ^{31}P–NMR saturation transfer, and ^{31}P–NMR inversion and saturation transfer all predict a very similar ^{18}O labeling state of key metabolites, in contrast to statements in the literature. This modeling work shows that the ^{18}O–assisted ^{31}P–NMR method provides a measure of the combined net and exchange fluxes in the creatine kinase and adenylate kinase shuttles, and not net flux as previously stated, thus resolving a long-standing debate in the heart energetics community. Overall, this doctoral work highlights the importance of considering compartmentation while analyzing the metabolic fluxes within eukaryotic systems, and provides techniques to reveal previously unknown manifestations of compartmental biology using dynamic isotopologue modeling.

KOKKUVÕTE

Käesolevas väitekirjas analüüsitakse rakusiseste energiakandjate ringlust imetaja südames ja pärmseene Krebsi tsüklit. Mõlemal juhul rakendatakse dünaamilist isotoopmärgisel põhinevat ainevahetusvoo analüüsi meetodit. Nimetatud süsteemide uurimise muudab keerukaks keskkonna heterogeensusest tulenev ebaühtlane jaotumine rakusiseses ruumis (eng *metabolite compartmentation*), mille täpne struktuur ei ole teada. Väitekirjas koostatakse meetod nimetatud kompartmentatsioon uurimiseks. *Saccharomyces uvarum*'i korral rakendatakse optimeerimismeetodit, et leida parim reaktsioonikiiruste jaotus, metaboliitides mis vastab mõõdetavale isotoopide jaotusele. Optimeerimisprotsessi tõhususe tõstmiseks suurte ainevahetusvõrgustike korral arendatakse välja analüütiline Gauss-Jordani ellimineerimismeetod, mis võimaldab kõiki metaboolseid statsionaarseid olekuid esitada kompaktsel kujul uurija poolt määratud üldises nn reaktsioonikiiruste koordinaatsüsteemis. Selline koordinaatsüsteem on kasulik keemiliste reaktsioonide uurimisel ja eelkõige suurte ainevahetusvõrgustike kirjeldamisel ja analüüsimisel. Dünaamilist isotopoloogide modelleerimist (DIM) rakendatakse energiakandjate ringluse modelleerimiseks imetaja südames. DIM analüüs näitab, et reaktsioonikiirused, mis saadakse kahel erineval viisil - ^{18}O isotoobi ja tuumamagnetresonantsi meetoditega - ennustavad uuritavates metaboliitides väga sarnast isotoobi ^{18}O märgistuse jaotust. See näitab, et nimetatud kahe meetodi tulemused on kooskõlas, vastupidiselt teadusajakirjades varem esinenud arvamustele. Kokkuvõtlikult öeldes juhib käesolev väitekiri tähelepanu metaboliitide kompartmentatsioonile olulisusele reaktsioonikiiruste analüüsimisel eukarüootsetes süsteemides ja annab DIM-l põhineva meetodi metaboliitide heterogeensuse struktuursete ja funktsionaalsete aspektide uurimiseks.

LIST OF PUBLICATIONS

I Schryer DW, Peterson P, Paalme T, Vendelin M. **Bidirectionality and compartmentation of metabolic fluxes are revealed in the dynamics of isotopomer networks**. *International Journal of Molecular Sciences*, 10(4):1697-718, (2009)

II Illaste A, Kalda M, Schryer DW, Sepp M. **Life of mice - development of cardiac energetics**. *Journal of Physiology*, 588(Pt 23):4617-9, (2010)

III Schryer DW, Vendelin M, Peterson P. **Symbolic flux analysis for genome-scale metabolic networks**. *BMC Systems Biology*, 5(1):81, (2011)

IV Schryer DW, Peterson P, Illaste A, Vendelin M. **Sensitivity analysis of flux determination in heart by ^{18}O labeled water ($H_2^{18}O$)–provided labeling using a dynamic isotopologue model of energy transfer pathways** *Submitted*, (2012)

SUMMARY OF AUTHOR'S CONTRIBUTION

I In Publication I, DWS composed the metabolic model, simulated the isotopologue dynamics, performed the optimization, wrote the text, prepared the figures and manuscript.

II In Publication II, all authors contributed to the text and literature review with the first author credited with having contributed more of his time during manuscript preparation.

III DWS and PP developed the GJE technique with DWS providing chemical insight and PP providing mathematical insight. DWS composed the example yeast network and analyzed constraints. All authors contributed to the text and approved the content of the final manuscript.

IV In Publication IV, DWS composed the metabolic model, simulated the isotopologue dynamics, performed the sensitivity analysis, prepared the figures, wrote the bulk of the text, and prepared the manuscript.

LIST OF PRESENTATIONS

I Schryer DW, Peterson P, Paalme T, Vendelin M. **Isotopomeric ^{13}C labeling of amino acids reveal compartmentation in** *Saccharomyces uvarum*. *Biophysical Journal*, 96(3):308a, (2009)

II Illaste A, Schryer DW, Birkedal R, Peterson P, Vendelin M. **Determination of regional diffusion coefficients of fluorescent ATP in rat cardiomyocytes**. *Biophysical Journal*, 98(3):749a, (2010)

III Schryer DW, Peterson P, Illaste A, Vendelin M. **Mathematical model of oxygen labeling to study heart energy transfer**. *Biophysical Journal*, 102(3):141a, (2012)

PREFACE

The work presented in this dissertation was carried out in the Laboratory of Systems Biology in the Institute of Cybernetics at Tallinn University of Technology. The Laboratory of Systems Biology works within the Centre for Nonlinear Studies (CENS). Financial support from the Wellcome Trust and the Archimedes Foundation is appreciated.

The original goal of this work was to extract information about the central metabolic fluxes of a laboratory yeast strain from dynamic isotope labeling data using dynamic tracer-based metabolic flux analysis (MFA). This work was to be performed in collaboration with another research institution. A metabolite quenching apparatus was constructed and isotope labeling experiments were to be performed, however, this collaboration was halted due to funding limitations. Without the option to perform the planned isotope labeling experiments this work was split into a number of related studies and took on a more theoretical bent with the goal of applying dynamic tracer-based MFA techniques in metabolic systems that contain both well characterized and unknown manifestations of metabolic compartmentation. Four publications resulted from this doctoral work, all with the common theme of flux analysis in compartmentalized systems. Two of these papers use dynamic isotopologue modeling.

The work started under the original experimental plan was wrapped up in Publication I. However, this work exposed a significant drawback of numerically stable methods of finding and expressing all steady state flux solutions of a large system of chemical transformations. Publication III provides a very general method to express all steady state solutions using a flux coordinate system whose desired components are specified by the user. The potential use of flux coordinate systems to reveal canonical patterns in genome scale metabolic systems has yet to be explored.

Because the Laboratory of Systems Biology is focused on heart metabolism, the remainder of my studies concerned the recycling fluxes of energy metabolites in heart. This work is summarized in Publication II and Publication IV, with the latter demonstrating the relevance of dynamic isotopologue modeling in the interpretation of isotopic labeling data.

ACKNOWLEDGMENTS

I approached Marko Vendelin to co-supervise my doctoral work with the idea of applying dynamic isotopologue modeling to a laboratory strain of yeast. Marko has an uncanny ability to immediately understand how to solve most numerical problems, and the problem of simulating isotopologue dynamics was particularly easy because he had applied the technique as an undergraduate student and did not consider it difficult then. He accepted the role of being my main supervisor and never wavered in his support of my work at any of the numerous bumpy points along this research path. No student interested in learning the art of numerical simulation or cardiac mechanoenergetics could ask for a more talented and supportive supervisor.

I met Pearu Peterson after he joined the Laboratory of Systems Biology two years into my doctoral studies. Pearu is a truly gifted analytical scientist who is simultaneously modest, patient, and generous with his time; an exception among the exceptional. His patient guidance has forever changed the way I think. No student interested in learning the art of applied mathematics or writing efficient numerical routines could ask for a more talented and supportive supervisor.

Unfortunately, I did not get a chance to work as closely with my other co-supervisor Toomas Paalme. It would have been a pleasure to carry out isotope labeling experiments with Toomas, and I hope future funding opportunities will rectify this loss; There is no other experimental scientist in Estonia better poised and passionate about performing dynamic isotope labeling experiments. Toomas has an extensive knowledge of yeast physiology and metabolism, and has developed specialized fermentation and analytical methods that are ideal for dynamic isotope labeling experiments.

It was a pleasure being part of the first wave of doctoral students in the Laboratory of Systems Biology. We learned much together in the first year and without the support of Mervi, Mari, and Ardo the difficult moments might have been less successful. The next few waves of doctoral students have, without exception, been equally helpful and friendly. Many thanks to Martin, Niina, Natalja, Jelena, Merle, and Päivo.

The most important acknowledgment is saved for my wonderful wife Maris. I would never have started, finished, or enjoyed this work without her support. Even though they cannot read these words yet, our wonderful children, with their endless joy and enthusiasm, have made the dark days in Estonia bright.

I was fortunate to have worked in a laboratory that strives for academic excellence, and unfortunate to have worked in an academic system that has the double edged sword of being grossly underfunded, and grossly inefficient due to structural fragmentation. The resources required to carry out dynamic isotope labeling experiments are not currently available to Estonian researchers despite its unique ability to determine intracellular fluxes. From a strategic point of view this is injudicious because knowledge of these fluxes may be prerequisite to realizing the promises of genetic improvement; A field the Estonian government has made considerable investment in.

On rare occasions I sacrificed time I normally spend with my wife and children to pursue this research. Perhaps a more ambitious schedule would have resulted in more publications, however, it is my belief that the pursuit of truth is best not rushed. The words of Charles Mims come to mind: "The world has waited 4.54 billion years for this particular piece of knowledge. It can wait another week." This *wu wei* (无为) approach diametrically opposes the pressure to publish-or-perish, and often results in more purposeful scientific communication. Having adopted this philosophy, partially completed research was saved for future publication and the content of this dissertation is succinct.

David W. Schryer

ACRONYMS

ADP	adenosine-5'-diphosphate, KEGG: C00008
AdK	adenylate kinase, EC: 2.7.4.3
ATP	adenosine-5'-triphosphate, KEGG: C00002
β-ATP	β phosphoryl group in ATP
γ-ATP	γ phosphoryl group in ATP
ATPase	adenosine triphosphatase, EC: 3.6.1.3
CENS	Centre for Nonlinear Studies
Ca^{2+}	calcium, KEGG: C00076
^{13}C	Stable isotope of carbon with seven neutrons.
CO_2	carbon dioxide, KEGG: C00011
CK	creatine kinase, EC: 2.7.3.2
DNFB	2,4–dinitrofluorobenzene, PubChem: 149192
EET	Eastern European Time (Greenwich Mean Time + 2 hours)
EMU	elementary metabolite unit
FBA	flux balance analysis
GC	gas chromatography
GJE	Gauss–Jordan elimination
IMS	mitochondrial intermembrane space
LC	liquid chromatography
MFA	metabolic flux analysis
MS	mass spectrometer
NMR	nuclear magnetic resonance
ODE	ordinary differential equation
^{18}O	Stable isotope of oxygen with ten neutrons.
^{31}P	Stable isotope of phosphorus with 16 neutrons.
PCA	principal component analysis
PCr	phosphocreatine, KEGG: C02305
P_i	inorganic phosphate, KEGG: C00009
SVD	singular value decomposition
TCA	tricarboxylic acid cycle
TUT	Tallinn University of Technology
$H_2^{18}O$	^{18}O labeled water

THESIS

1

INTRODUCTION

The systems addressed by the science of biology are among the most complex known to humankind. The majority of biological studies make use of deductive reasoning, and typically only a very small subset of the complex biological system is scrutinized. In contrast, systems biology, is holistic and makes use of inductive reasoning, typically by constraining mathematical models with all available data. Because it is well established that system behaviour is often more than the sum of its parts [1], systems biology models aspire to include all relevant complexities to reproduce emergent properties and explore their causes and mechanisms.

A holistic approach to studying biological systems comes with a number of drawbacks, not least of which is avoiding overparameterization. One can only gain insight from models that can be sufficiently constrained with measured data. Another drawback is the inherent difficulty in dealing with complexity; Building models of large systems and gathering the data required to constrain them is a tedious process. Original biological data is disparate and contains a relatively large amount of uncertainty, and often stochastic models and statistical tests are required to evaluate the overall uncertainty of model predictions. Furthermore, we are often ignorant of some fundamental connections between model components which requires an iterative model building/testing/measurement cycle to resolve. This development cycle exacerbates all of the previous drawbacks and makes it easier to apply systems biology techniques on well characterized systems.

Fortunately, a large number of biological studies are devoted to elucidating the function of a small set of organisms. These model organisms are ideal for the development of systems biology tools and techniques, and this doctoral work is no exception. This doctoral work has focused on: (I) the central metabolism of a laboratory strain of yeast, and (II) the energetic metabolism of the mammalian rat heart.

Specifically, this dissertation is concerned with quantifying the metabolic fluxes in these systems. Metabolic fluxes are rarely directly quantifiable, yet are of fundamental importance in defining phenotypes on the cellular level [2], and are ubiquitous in multicellular organisms (*e.g.*, regulation by cytokines and hormones, and the control of growth factor receptor glycosylation by glycolytic fluxes [3]).

A number of techniques have been developed to aid metabolic flux analysis (MFA) with the most prominent being flux balance analysis (FBA) [4], and isotopic tracer-based MFA. Tracer-based MFA works by finding steady state flux distributions that best describe measured labeling states of metabolic isotopologues. Typically, this technique is applied after an isotopic steady labeling state is reached. For recent reviews on isotopically stationary tracer-based MFA please refer to [5–8].

Dynamic tracer-based MFA is the younger brother of the previous approach and bases its flux predictions on information contained in measurements at multiple time points while the isotopic labeling state is changing with time. These measurements are sometimes supplemented with additional measurements at isotopic steady state. A recent review summarizes all studies that have used the dynamic approach in a single table [9].

At least one study has explored the use of tracer-based stimulus-response experiments to identify *in vivo* enzyme kinetics by perturbing the metabolism and tracking the transient response of the labeling state of intermediate metabolites [10]. The move towards the combined use of kinetic modeling and tracer-based MFA is occurring, however, it is currently difficult to apply in practice for a number of reasons:

A. Kinetic models of instationary metabolism require careful consideration to avoid overparameterization.

B. Many kinetic mechanisms have not been completely characterized, and composing a system with a large number of estimated components may result in highly unrealistic model behaviour.

C. After the tedious procedure of creating a large kinetic scheme, simulation of such a system requires specialized techniques to be computationally efficient and avoid numerical instabilities.

D. It is currently difficult to measure pool sizes, let alone changes in pool sizes with current sampling and measurement techniques [11]. Unknown pool parameters complicate the analysis of stimulus-response experiments.

The use of kinetic mechanisms within MFA is discussed in Publication I and Publication III, however, all techniques applied in this dissertation assume strict steady metabolism with stationary metabolic pools.

The implications of assuming stationary metabolism should always be kept in mind while interpreting original data. A widening body of evidence suggests that phenotypic heterogeneity [12–18] and temporal compartmentation [18–25] are fundamental properties of eukaryotic cell metabolism. These phenomena could be the root cause of observed oscillations in eukaryotic gene expression [26–28]. It is not yet clear that the flux distributions found using dynamic tracer-based MFA are sensitive to these phenomena. A judicious analysis from the perspective of dynamic isotopologue simulation is saved for future publication.

The goal of dynamic tracer-based MFA is to find steady state flux distributions that best describe how isotopologue distributions dynamically change after switching the labeling state of a substrate being metabolized by the system under study.

1.1 ANALYTICAL DETERMINATION OF ISOTOPOLOGUE DISTRIBUTIONS

A number of analytical approaches are used to quantify isotopologue distributions: (I) liquid chromatography (LC) coupled to a mass spectrometer (MS), or tandom MS, (II) gas chromatography (GC) coupled to a MS, or tandom MS, and (III) nuclear magnetic resonance (NMR). Due to its non-destructive nature NMR is useful for *in vivo* dynamic measurements, however, it has low sensitivity, cannot resolve the labeling state of intermediate metabolites

with small metabolic pools, and has the potential to introduce error in the measurement of the unlabeled isotopologue as they are found by subtraction from the others [29]. Until recently, NMR was the only method able to measure positional isotopic labeling, however, a new approach developed by Rühl *et al.* uses LC coupled to a tandem MS with an electron collider that allows for the quantification of metabolic fragments [30]. Rühl's method enables the sensitive determination of positional isotope enrichment of intermediate metabolites. The greater sensitivity of MS based techniques allows for the direct quantification of the labeling distribution of intermediate metabolites, such as free amino acids [31].

1.2 FLUX DETERMINATION USING DYNAMIC TRACER-BASED MFA

To find steady state flux distributions using measurements of the isotopic labeling state during the isotopic transient phase, a kinetic model of the labeling dynamics is required. Publication IV provides a general method for deriving ordinary differential equation (ODE) mass balances around the isotopologues of all chemicals in a set of chemical transformations. The result is a set of weakly non-linear ODEs that can be solved using various solvers. This system of equations can be cast into a cascading series of linear differential equations that are solved sequentially with less computational resources in a shorter period of time [32]. To reduce the computational effort even further, the elementary metabolite unit (EMU) method was developed [33] which reduces the number of balances required by balancing the isotopologues of metabolite fragments that remain intact across sets of reactions. The metabolic systems considered in this dissertation are small and do not warrant use of either technique to simulate the isotopologue dynamics more efficiently.

The kinetic model that provides simulated solutions of isotopologue dynamics is solved within an optimization routine to find a set of thermodynamically feasible [34] kinetic parameters that provide the closest prediction to the measured isotopologue data.

1.3 MAIN THEME: FLUX DETERMINATION IN COMPARTMENTALIZED SYSTEMS

One of the most challenging aspects of finding feasible steady state metabolic flux distributions using dynamic tracer-based MFA is the complication introduced by metabolic compartmentation. The added compartmental complexity of eukaryotic cells may be one reason why *Escherichia coli*, *Corynebacterium glutamicum*, and *Synechocystis sp.* have been used as test organisms to develop dynamic tracer-based MFA techniques [9, 11, 35].

> This doctoral work focuses on the use of dynamic tracer-based MFA techniques in metabolic systems that contain both well characterized and unknown manifestations of metabolic compartmentation.

The remainder of this dissertation discusses the original research presented in the four publications that resulted from this doctoral work. Chapter 2 discusses Publication I. This contribution provides methods of revealing compartmentation using information contained in isotopologue dynamics. Chapter 3 discusses Publication III. The symbolic Gauss–Jordan elimination (GJE) algorithm developed in this publication is more general than the main theme of this doctoral work, however, the flux coordinate representation of metabolic

systems has direct implications for the study of complex systems and the optimization of isotopologue dynamics. Chapter 4 discusses Publication II and Publication IV. Publication II is a critique of a study on the postnatal development of compartmentalized energy metabolism in the mouse heart. Although this publication does not use dynamic tracer-based MFA we recommended that the original data be interpreted using modeling techniques. Publication IV uses dynamic tracer-based MFA techniques to study the phosphotransfer fluxes through the creatine kinase (CK) and adenylate kinase (AdK) shuttles in healthy normoxic heart.

The underlying theme linking the contributions within these four papers is perhaps not obvious upon first reading. The most obvious explanation is that each contributes to and overlaps with different branches of biology that use different diction, grapple with different problems, and typically have few common followers. This dissertation presents the commonalities, such as the difficulties in dealing with compartmentalized biology, and strives to present this set as a unified contribution.

2

COMPARTMENTATION IS REVEALED IN ISOTOPOLOGUE DYNAMICS

It is well known that compartmentation complicates the application of tracer-based MFA [7]. Publication I demonstrates that compartmental effects are revealed in isotopologue dynamics, and goes on to discuss other motivations for adopting dynamic tracer-based MFA in place of the stationary tracer-based approach.

In brief Publication I: (I) discusses the additional information contained in the isotopic transient, (II) provides dynamic isotopologue simulations to illustrate how to extract this additional information from transient isotopic data, and (III) attempts to point the way towards the future of dynamic metabolic modeling by integrating dynamic tracer-based MFA with predictive kinetic models.

Wahrheit et al. recently stated that Publication I may be the only publication to date that discusses the potential of using isotopologue transients to describe compartmentation [36]. Other publications in this dissertation contain short discussions of the manifestations of compartmentation. Publication III provides a discussion on the manifestations of compartmentation and strategies to reveal compartmentation, albeit short; this discussion is continued within Publication IV.

2.1 ADDITIONAL INFORMATION CONTAINED IN THE ISOTOPIC TRANSIENT

The transient labeling state is a function of: (I) the net and exchange fluxes, and (II) the pool size of all metabolites. A corollary to this is that all additional information contained in the isotopic transient is convoluted with the dynamic influence of metabolic pool sizes; inaccurate pool measurements complicate the interpretation of isotopic transients.

The following summarizes the additional information that can be obtained using dynamic tracer-based MFA:

A. Determining of the size of unknown metabolic pools.

B. The bidirectionality of reactions in a linear pathway can be determined from measurements of the labeling state of the intermediates.

C. Metabolic compartmentation is revealed if the labeling state of a metabolite becomes enriched more rapidly than a metabolite upstream to the net flux.

D. Metabolic compartmentation or the presence of a previously unknown reaction is revealed if the optimal pool size parameters do not match well with measured metabolic pool sizes.

E. In plant systems and autotrophic microorganisms that utilize CO_2 as the sole carbon source, or other mono atomic labeling systems (*e.g.* $H_2^{18}O$ in Publication IV), the isotopic steady state contains no information. In contrast, kinetic information can be extracted from measured isotopologue dynamics.

2.2 DYNAMIC ISOTOPOLOGUE SIMULATIONS WITHIN PUBLICATION I

Publication I provides two sets of simulations to illustrate the information that can be obtained using dynamic tracer-based MFA. The first set of simulations illustrate how metabolic pool size parameters shift the time scale of the metabolic transient. The second set of simulations illustrate how the shape of the isotopic transient changes with different isotopic substrates. The second set of simulations show that more information can be obtained from isotopic transient data if identical experiments are performed using different isotopic substrates and analyzed together; each substrate reveals information about different parts of the metabolism.

If the timing and shape of isotopic transients does not match with measured data, the discrepancy provides clues about metabolic compartmentation. One such case was considered in Publication I. Looking at Equation 2.1, if the labeling enrichment in metabolite C becomes enriched faster than metabolite B, this indicates that the experimental data should be analyzed with a compartmentalized model of B, shown on the right.

$$\mathrm{A} \rightleftharpoons \mathrm{B} \rightleftharpoons \mathrm{C} \qquad \begin{array}{c} \mathrm{A} \rightleftharpoons \mathrm{B_i} \rightleftharpoons \mathrm{C} \\ \downdownarrows \\ \mathrm{B_j} \end{array} \tag{2.1}$$

However, if B lies on the intersection of two different metabolic pathways and C becomes enriched faster, it may indicate that these pathways use different pools of B that mix, or two fully separated pools of B, shown in the middle and right of Equation 2.2 *in illo ordine*.

$$\begin{array}{ccccc} & & \mathrm{D} & & \\ & & \downdownarrows & & \\ \mathrm{A} & \rightleftharpoons & \mathrm{B} & \rightleftharpoons & \mathrm{C} \\ & & \downdownarrows & & \\ & & \mathrm{E} & & \end{array} \qquad \begin{array}{ccccc} \mathrm{A} & \rightleftharpoons & \mathrm{B_i} & \rightleftharpoons & \mathrm{C} \\ & & \downdownarrows & & \\ \mathrm{D} & \rightleftharpoons & \mathrm{B_j} & \rightleftharpoons & \mathrm{E} \end{array} \qquad \begin{array}{ccccc} \mathrm{A} & \rightleftharpoons & \mathrm{B_i} & \rightleftharpoons & \mathrm{C} \\ & & & & \\ \mathrm{D} & \rightleftharpoons & \mathrm{B_j} & \rightleftharpoons & \mathrm{E} \end{array} \tag{2.2}$$

Of course, all three of the cases in Equation 2.2 may contain a non-reacting side pool of B as in Equation 2.1, and the compartmentalized cases may even contain two such pools.

2.3 DYNAMIC TRACER-BASED MFA USING STEADY STATE DATA

The tricarboxylic acid cycle (TCA) cycle fluxes of *Saccharomyces uvarum* were obtained in Publication I by optimizing parameters of a dynamic isotopologue model using absolute and conditional enrichment measurements of proteinogenic amino acids. This optimization procedure demonstrated that lack of knowledge regarding metabolic pool sizes does not make dynamic tracer-based MFA any less reliable than a steady state model. Both simulation approaches were seen to provide an equally good fit to the same steady state data regardless of the pool parameters.

2.4 SUMMARY OF PUBLICATION I

Publication I reviews research from a diverse set of research areas within the biological and biotechnoligcal sciences. The main purpose of this contribution was to show that adopting dynamic tracer-based MFA in place of isotopically stationary approaches provides additional insight into the compartmentation of metabolic fluxes; a topic of fundamental interest in the biological sciences and the main subject of this work.

Dynamic isotopologue simulation is not commonly used to interpret isotopic tracer movement in large biological systems. For this reason another purpose of this contribution is to illustrate to non practitioners that the most difficult task in applying dynamic tracer-based MFA is our ignorance of the many manifestations of compartmental biology; technical issues are no longer prohibitive.

Publication I also points towards the potential future marriage of phenomenological MFA with predictive kinetic modeling. The attempts to combine these approaches have shown promise, and is predicted to become increasingly important as the gaps in our fundamental knowledge of *in vivo* kinetic mechanisms narrow.

3

USE OF FLUX COORDINATE SYSTEMS

An algorithm was developed in Publication III to express all possible steady state solutions of a large set of chemical transformations in terms of a flux coordinate system. The first description of a flux coordinate system is provided by Quek *et al.* [37]. Publication III generalizes their definition, although, the existence of the contribution by Quek *et al.* was unknown until quite recently.

3.1 DEFINITION OF FLUX COORDINATE SYSTEM

The example network provided in Figure 1 is used to introduce flux coordinate systems. The dynamic mass balance of this system is provided in Equation 3.1:

$$\begin{pmatrix} \frac{dA}{dt} \\ \frac{dB}{dt} \\ \frac{dC}{dt} \\ \frac{dD}{dt} \\ \frac{dE}{dt} \end{pmatrix} = \begin{pmatrix} -1 & 0 & -1 & 0 & 1 & -1 & 0 & 0 \\ 1 & -1 & -1 & -1 & 0 & 0 & 0 & 0 \\ 0 & 1 & 0 & -1 & 0 & 1 & 0 & 0 \\ 0 & 0 & 0 & 1 & 0 & 0 & -1 & 0 \\ 0 & 0 & 1 & 0 & 0 & 0 & 1 & -1 \end{pmatrix} \times \begin{pmatrix} \nu_{A\rightarrow B} \\ \nu_{B\rightarrow C} \\ \nu_{A+B\rightarrow E} \\ \nu_{B+C\rightarrow D} \\ \nu_{A_{in}} \\ \nu_{A\rightarrow C} \\ \nu_{D\rightarrow E} \\ \nu_{E_{out}} \end{pmatrix}. \tag{3.1}$$

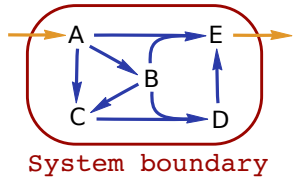

Figure 1 – Small example network to aid in the definition and discussion of flux coordinate systems. Reactions internal to the system are blue, reactions that transport flux into and out of the system are yellow. This open system has eight reactions and five metabolites, thus all steady state flux solutions are found using three parameters.

Setting the left hand side of Equation 3.1 to zero is equivalent to assuming that the mass of all metabolites in the system are steady over time. The result is a homogeneous system of linear equations that when solved, provides all possible steady state flux solutions. The

solution is the kernel of the stoichiometric matrix. In this example, the kernel is a three dimensional linear subspace of an eight dimensional Euclidean space. This linear subspace is spanned by a set of linearly independent basis vectors (columns of a matrix representation of the kernel); many possible sets of basis vectors are possible, each a different representation of the same linear subspace. Steady state flux solutions are expressed through a linear combination of the basis vectors.

As described in Publication III, the kernel can be found using various techniques, including GJE, and singular value decomposition (SVD). The matrix representation of the kernel in Equation 3.2 was found using GJE. The columns of the kernel matrix are the basis vectors. In Equation 3.2, the last three rows of the kernel matrix form an identity matrix where the rows are the independent flux variables in the system. Another kernel matrix is obtained using SVD, and shown in Equation 3.3.

$$\begin{pmatrix} \nu_{A\to B} \\ \nu_{B\to C} \\ \nu_{A+B\to E} \\ \nu_{B+C\to D} \\ \nu_{A_{in}} \\ \nu_{A\to C} \\ \nu_{D\to E} \\ \nu_{E_{out}} \end{pmatrix} = \begin{pmatrix} -1 & 1 & 1 \\ -1 & 1 & 0 \\ 0 & -1 & 1 \\ 0 & 1 & 0 \\ 0 & 0 & 2 \\ 1 & 0 & 0 \\ 0 & 1 & 0 \\ 0 & 0 & 1 \end{pmatrix} \times \begin{pmatrix} \nu_{A\to C} \\ \nu_{D\to E} \\ \nu_{E_{out}} \end{pmatrix}, \tag{3.2}$$

$$\begin{pmatrix} \nu_{A\to B} \\ \nu_{B\to C} \\ \nu_{A+B\to E} \\ \nu_{B+C\to D} \\ \nu_{A_{in}} \\ \nu_{A\to C} \\ \nu_{D\to E} \\ \nu_{E_{out}} \end{pmatrix} = \begin{pmatrix} -0.00459 & 0.47191 & -0.47087 \\ 0.20089 & 0.15114 & -0.55839 \\ -0.61236 & -0.00330 & 0.00266 \\ 0.40688 & 0.32407 & 0.08486 \\ -0.41095 & 0.64155 & 0.17504 \\ 0.20600 & 0.17294 & 0.64325 \\ 0.40688 & 0.32407 & 0.08486 \\ -0.20548 & 0.32078 & 0.08752 \end{pmatrix} \times \begin{pmatrix} \alpha \\ \beta \\ \gamma \end{pmatrix}. \tag{3.3}$$

Note that in Equation 3.3 the rows are ordered as in Equation 3.2, however the 3×3 submatrix formed by the last three rows are dense.

A flux coordinate system is thus defined as a set of basis vectors of a kernel representation that form an identity submatrix. Publication III discusses that the process of GJE naturally creates a flux coordinate system, and that many possible flux coordinate systems are possible.

3.2 SELECTION OF A FLUX COORDINATE SYSTEM

The algorithm developed in Publication III allows the researcher to specify a desired set of fluxes that form the flux coordinate system. However, not all sets of fluxes are able to form a coordinate system (*i. e.*, selecting two fluxes in a linear pathway). If the selected flux

variables cannot form a basis, the routine will discard such flux variables and find a viable flux coordinate system.

As discussed below, the freedom to choose a flux coordinate system is prerequisite to reaping the benefits of using flux coordinate systems.

3.3 BENEFITS OF THE ALGORITHM DEVELOPED IN PUBLICATION III

There are a number of reasons why the symbolic GJE routine developed in Publication III is recommended to be used in place of optimized numerical SVD algorithms:

A. There is no computational penalty to using the symbolic GJE algorithm developed in Publication III compared with optimized numerical SVD algorithms.

B. SVD algorithms create a dense solution that uses more memory than sparse matrix GJE algorithms. With the examples we considered, doubling the network size quadruples the memory requirement of SVD and roughly doubles the memory requirement of GJE when applied to the same system.

C. The coordinate system of the steady state subspace found using SVD has no obvious physical meaning and the components of the basis vectors affect almost all metabolic fluxes making constraints on individual fluxes difficult (see subsection 3.4.1).

D. Inspection of the GJE kernel matrix allows for identification of sub-networks within the larger metabolic network.

E. The flux coordinate system found using GJE can be selected by the user, thus enabling one to reap the benefits of using flux coordinate systems.

F. The ability to select the flux coordinate system means that the basis of the steady state flux subspace is no longer dependent on the original ordering of the rows and columns of the stoichiometric matrix.

The limited scope of Publication III did not allow for discussion regarding some of the potential benefits of using flux coordinate systems.

To the author's best knowledge, Barret *et al.* is the first study to have discussed the benefits of using sparse basis vectors to study the properties of metabolic networks [38]. They developed an algorithm that combined principal component analysis (PCA) and eigenvector rotation and shearing for the purpose of finding a top-down method of determining the molecular mechanisms that control cellular metabolic states. Applied to a subset of the metabolism, their algorithm results in sparse basis vectors that "[provide] a low-dimensional and biochemically interpretable decomposition of the steady flux states of the system" [38]. The sparse basis vectors they found resemble those of a flux coordinate system, however, to find a full flux coordinate system as defined herein, the use of GJE is recommended. The use of GJE also allows for the possibility of finding many flux coordinate systems, or a desired flux coordinate system for the same steady state flux subspace. A set of flux coordinate systems could be analyzed together to gain even deeper insight into the operation of complex metabolic networks.

3.4 FLUX COORDINATES LESSEN THE CURSE OF DIMENSIONALITY

Flux coordinate systems are also useful in the optimization process of tracer-based MFA [39]. It must be admitted that this was the motivation of developing the GJE algorithm in Publication III. Often, the analyst has prior knowledge of a subset of the fluxes being analyzed by tracer-based MFA. These fluxes can be chosen to form the coordinate system that spans the steady state metabolic subspace and constrained to reduce the dimension of the parameter subspace to be traversed by an optimization routine. The example yeast network presented within Publication III was composed to analyze dynamic isotopologue data. A flux coordinate system was chosen to correspond with 26 available biomass production rates. By constraining these fluxes directly, the entire steady state subspace is defined by 13 independent variables. Using the steady state representation found using SVD the optimization routine will need to traverse 39 independent variables to span all possible steady state flux distributions. The high dimensional and convolved steady state representation provided by SVD makes it difficult to traverse all relevant steady state solutions. To avoid this problem, random sampling of the steady state subspace has been applied [38, 40].

The above example, along with the two following subsections, demonstrate that the use of flux coordinates reduce the curse of dimensionality by: (I) removing dimensions with constraints, and (II) reducing the number of parameters that influence specific metabolic processes.

3.4.1 *Reduction of the parameter space: SVD versus GJE*

In the example system shown in Figure 1, all steady state solutions where the flux $\nu_{A\to C}$ is specified, are found in a planar linear subspace. Looking at Equation 3.2, this is clear because the specified point, $\nu_{A\to C}$, and the remaining two basis vectors, $\nu_{D\to E}$ and $\nu_{E_{out}}$, form a plane. All other restrictions on the remaining seven fluxes in the system reduce this planar linear subspace to a rectangular polygon on the same plane. In higher dimensional space this would be a bounded polytope.

Performing the same operation using the kernel matrix found using SVD is not as direct. The bounds on α, β, and γ in Equation 3.3 that define the same planar linear subspace are found by solving an additional linear system.

An equation to describe the planar linear subspace formed when $\nu_{A\to C}$ is specified is found by inverting the coloured 3×3 submatrix in Equation 3.3 and solving for one of α, β, or γ. Choosing α as the dependent variable results in an equation to calculate α when β and γ are specified:

$$\alpha = \nu_{A\to C} - 0.17\,\beta - 0.64\,\gamma. \tag{3.4}$$

Equation 3.4 provides a definition of the same planar linear subspace formed by the point $\nu_{A\to C}$ and the $\nu_{D\to E}$ and $\nu_{E_{out}}$ basis vectors in Equation 3.2. Using the SVD kernel matrix, the plane is formed by the point $\nu_{A\to C}$, and two vectors that lie on the plane, the β and γ basis vectors in Equation 3.3. In essence, GJE provides a solution to the linear subsystem in the form of the coloured identity submatrix in Equation 3.2 and makes reducing the dimension of the parameter space much easier.

3.4.2 *Selective optimization within metabolic sub-networks*

It was shown in Publication III that flux coordinates control connected sub-networks of fluxes. This property could be used to aid the optimization process used in tracer-based MFA because it allows the analyst to limit the optimizer to selected regions of the metabolism. Measurements relevant to one area of the metabolism could be optimized by manipulating the flux parameters within that region of the metabolism.

3.5 USE OF THE GJE KERNEL IN MODEL REDUCTION

The kernel of the GJE matrix is visualized in Publication III Figure 2. It is sparse and provides a direct visualization of network structure. Above the identity matrix of flux coordinates are a large number of reactions that are controlled by a single flux coordinate. These reactions belong to linear segments of metabolic pathways. It was beyond the scope of Publication III to consider model reduction techniques, however, the structure of the GJE kernel with its sparse matrix representation would aid in the creation of such routines. The simplification of linear pathways is required for efficient simulation of dynamic isotopologue models, and in addition would aid in the visualization of genome-scale networks.

3.6 ANALYZING COUPLED ENZYME MECHANISMS

The reaction environment inside biological systems usually contain metabolites at a concentration that greatly exceeds the enzymes that catalyze their interconversion. If one assumes that the distribution of enzyme states remains stationary and is determined by the availability of metabolites, individual chemical transformations in the enzyme mechanism can be treated in the same way as chemical reactions.

Coupled enzyme systems often contain hundreds of individual transformations with the steady state characterized by a sufficient number of degrees of freedom to make analytical analysis prohibitively tedious and error prone, and brute force techniques computationally prohibitive. A flux coordinate system composed of fluxes in the enzyme mechanism that are known to some extent allows one to reduce the size of the steady state flux subspace prior to functional analysis; effectively lessening the impact of the curse of dimensionality.

3.7 SUMMARY OF PUBLICATION III

The original motivation to begin Publication III was to find a method of calculating all possible steady state solutions of a metabolic network using flux parameters. In the process of developing the symbolic GJE routine we observed some properties of flux coordinate systems. While comparing the routine with state of the art implementations of SVD we found that sparse SVD did not conserve memory because the resulting kernel matrix is dense. In contrast, the kernel of the GJE matrix is sparse and provides a basis for network simplification. The sparcity property shifts the limitation of analyzing *very* large systems from the amount of memory available to the computational time considered tolerable. Considering

all of these properties, it is likely that the symbolic GJE routine developed in Publication III has applications in the study of other large linear systems.

The scope of Publication III prevented a thorough analysis of the properties and usefulness of flux coordinate systems. It is possible that an underlying canonical structure of the steady state flux subspace of metabolic systems could be found by analyzing the set of all possible flux coordinate systems.

4

FLUX OF ENERGY METABOLITES IN HEART

The dynamic tracer-based MFA modeling techniques developed in the initial phase of this research to study yeast metabolism were applied in Publication IV to study the recycling fluxes of energy metabolites in heart.

In heart, the mechanisms that ensure that the recycling fluxes of energy metabolites meets the demand of adenosine triphosphatase (ATPase) reactions over a wide range of workloads remains unclear. Fundamental to this search is an accurate understanding of the fluxes of ATP, ADP, inorganic phosphate (P_i), and phosphocreatine (PCr) between the mitochondrial intermembrane space (IMS) and the ATPases on both the myofibrils and sarcoplasmic reticulum. adenosine-5'-triphosphate (ATP) is transported directly from the IMS to the cytosol, as well as through the parallel adenylate kinase (AdK) and creatine kinase (CK) shuttles. The compartmentalized network of the recycling fluxes of energy metabolites in heart studied in Publication IV is provided in Figure 2.

4.1 MOTIVATION TO STUDY ENERGY METABOLITE FLUXES IN HEART

The regulation of energy fluxes in heart is an active area of research because the deleterious effects of various myopathies can be mitigated somewhat by manipulating these fluxes. The effects of drug intervention on the energy status of hearts has been studied using ^{13}C tracer-based MFA [41]. However, forty years of searching has not revealed any definitive mechanism of how TCA cycle flux is controlled as a function of workload.

For some time calcium (Ca^{2+}) seemed to be an interesting candidate metabolite. *In vitro* studies on TCA cycle enzymes display activation by Ca^{2+} [42], modeling results demonstrate that Ca^{2+} activation could act as a stimulator of TCA cycle flux [43], however, physiological conditions prevent Ca^{2+} from controlling enzyme rates to the extent required for the regulation of homeostasis *in vivo* [44].

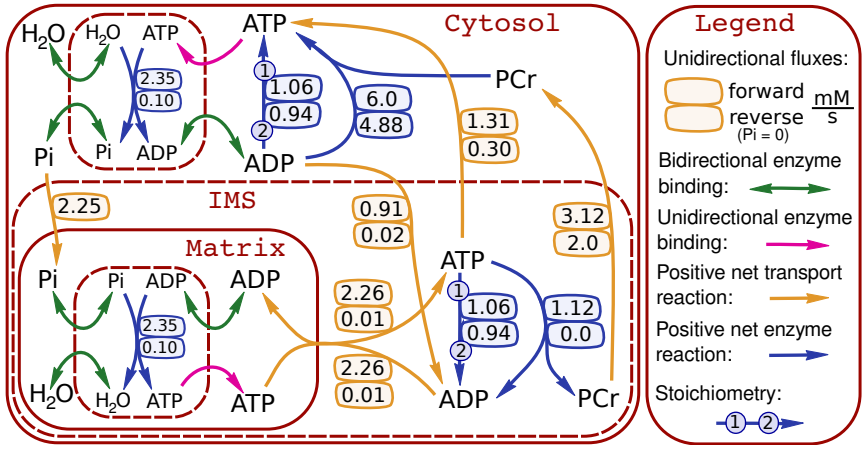

Figure 2 – Compartmentalized heart phosphotransfer network with flux distribution taken from Publication IV. The intermediate state of both ATPase and ATP synthase is reversible with respect to ^{18}O.

^{13}C tracer-based MFA is unable resolve the three parallel energy metabolite fluxes between the IMS and the cytosol in Figure 2 because the recycling fluxes of ATP, ADP, and PCr, are much faster than the incorporation of ^{13}C into these metabolites. The use of ^{13}C also prevents one from studying the recycling flux of P_i which is important in this system.

4.2 TECHNIQUES USED TO RESOLVE PARALLEL ENERGY TRANSFER IN HEART

Publication I reviews three NMR techniques that have been employed to study the flux of energy metabolites in heart: ^{31}P–NMR saturation transfer [45–53], ^{31}P–NMR inversion and saturation transfer [54], and ^{18}O–assisted ^{31}P–NMR [55–69]. At least one study combined the use of ^{13}C tracer-based MFA with ^{31}P–NMR saturation transfer [70] to study heart fluxes.

^{18}O–assisted ^{31}P–NMR uses ^{18}O as an isotopic tracer by replacing the extracellular media with one containing an elevated quantity of $H_2^{18}O$. Equation 4.1 shows how ATPase and ATP synthase move ^{18}O from $H_2^{18}O$ into P_i and the oxygen atoms attached to γ-ATP:

$$AP-\overset{\overset{\circ}{\cdot}\,i}{\underset{\underset{\circ}{\cdot}}{P}}\!\cdot\!\circ-\overset{\overset{\circ}{\cdot}\,j}{\underset{\underset{\circ}{\cdot}}{P}}\!\cdot\!\circ \;+\; H_2\!\cdot\!\overset{k}{\circ} \;\underset{\nu_r}{\overset{\nu_f}{\rightleftharpoons}}\; AP-\overset{\overset{\circ}{\cdot}\,i}{\underset{\underset{\circ}{\cdot}}{P}}\!\cdot\!\circ \;+\; \circ\!\cdot\!\overset{\overset{\circ}{\cdot}\,j+k}{\underset{\underset{\circ}{\cdot}}{P}}\!\cdot\!\circ, \tag{4.1}$$

where i, j, k are the components of the labeling system where the oxygen atoms they contain have an equal probability of being labeled with ^{18}O. The lack of positional labeling information in this system is ensured because P_i is the only metabolite that accepts ^{18}O from water and all oxygen atoms in P_i are equivalent (See Publication IV Supplemental materials 2 for the full system of equations).

Although ATP synthase is unidirectional with respect to the adenine group (A), the intermediate enzyme state exhibits multiple reversals with P_i prior to release by the enzyme complex [71].

The use of ^{18}O increases the rate of label incorporation compared with ^{13}C tracer-based techniques and was used to study the energetic fluxes in heart for just over twenty years [55–69].

4.3 WHY ARE THE FLUXES DIFFERENT?

The motivation to carry out the sensitivity analysis in Publication IV stemmed from a striking contrast:

> The fluxes calculated using the ^{18}O–assisted ^{31}P–NMR method are smaller than the same fluxes calculated using both ^{31}P–NMR saturation transfer, and ^{31}P–NMR inversion and saturation transfer.

In studies that utilize ^{18}O–assisted ^{31}P–NMR it is typically assumed that the observed labeling dynamics provide a measure of *net* flux through the AdK and CK shuttles, however, prior to Publication IV no sensitivity analysis had been performed to test this assumption. If true, this property would make the ^{18}O–assisted ^{31}P–NMR method unique because label movement occurs with the unidirectional forward and reverse fluxes in all other methods that track label movement.

Publication IV shows that the labeling state is not sensitive to net fluxes, and it is total flux that defines the labeling state.

4.4 SENSITIVITY ANALYSIS OF PHOSPHOTRANSFER FLUXES

A dynamic mass isotopologue model with bidirectional fluxes and enzymatic compartmentation was composed in Publication IV to test the sensitivity of the kinetic parameters on the labeling state of metabolites. The phosphotransfer network in Publication IV contains parallel loops with potentially rapid exchange fluxes (the CK shuttle and the AdK shuttle). It was shown that the sum of the net and exchange fluxes in each shuttle (total flux) determines the labeling state; net flux does not determine the labeling state as stated previously [55–69]. Analysis in Publication IV shows that as the total flux is increased in each shuttle, the molar fraction of the ^{18}O isotopologues of β-ATP and PCr approach a horizontal asymptote. If the unidirectional forward and reverse fluxes of the AdK and CK reactions are increased, the ^{18}O labeling state of β-ATP and PCr approach a state when they are in isotopic equilibrium with both the reactant and product pools. The rate of change of the labeling state of the reactant and product pools is determined by the rate of ^{18}O input into the system. In general, dynamic tracer-based MFA cannot be used to find exchange fluxes that are significantly higher than the rate of labeling input into the reaction.

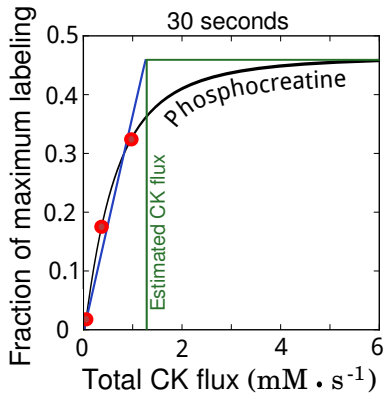

Figure 3 – "Pseudo-linear" estimation of CK flux. In [58], the CK flux was estimated by suppressing CK activity with DNFB. The red dots show the fraction of inhibition used in [58] to calculate the CK flux. The black total oxygen labeling curve is found by combining the labeling curves of the three labeled species in Figure 6, Publication IV, using the equation for total labeling used by Dzeja *et al.* [62]. The "pseudo-linear" estimated CK flux is found by the intersection of the horizontal green line and the linear blue fit to labeling data. The vertical green line provides a visual aid to show the estimated CK flux. The estimated value is close to the CK flux reported in [62] for heart. The above geometry shows that the "pseudo-linear" method underestimates total CK flux.

Because the total CK shuttle flux is more rapid than the rate of ATP synthase, Dzeja *et al.* developed the "pseudo-linear" approximation technique to estimate this flux [58]. This estimation technique continues to be applied [69] although no study has assessed the validity of applying the "pseudo-linear" technique when the assumption of unidirectional fluxes is lifted. Figure 3 shows the application of the "pseudo-linear" approximation technique to a simulated total labeling curve. The error in the "pseudo-linear" labeling technique illustrated in Figure 3 is related to an observation made in Publication IV: As the flux through the AdK and CK shuttles is increased, the labeling state becomes insensitive to changes in these fluxes. This property ensures that the "pseudo-linear" technique will provide an estimate at the low end of the range of possible CK shuttle fluxes.

The insensitivity analysis of the dynamic isotopologue model over the range of fluxes measured using ^{18}O–assisted ^{31}P–NMR, ^{31}P–NMR saturation transfer, and ^{31}P–NMR inversion and saturation transfer shows that the same kinetic model is able to explain all known measurements of the energetic fluxes in healthy normoxic heart.

4.5 IMPROVING THE SENSITIVITY OF ^{18}O–ASSISTED ^{31}P–NMR

Publication IV demonstrated that the sensitivity of the predicted labeling state to changes in pool sizes and the bidirectionality of reactions increased with the use of 100% $H_2^{18}O$. This increase in sensitivity is due to an increase in the rate of label input into the system. In general, it was found that more information about the fluxes in the system can be determined when the rate of label input into the system is increased. To this end, a number of strategies are recommended to increase the rate of label input and thus gain the greatest possible insight from ^{18}O–assisted ^{31}P–NMR experiments. In addition, the use of multiple

sampling points during different phases of the isotopic transient would aid in the analysis using a dynamic isotopologue model.

All known applications of the ^{18}O–assisted ^{31}P–NMR method [55–69] have used 30% or lower $H_2^{18}O$, introduced at lower workloads. Use of $H_2^{18}O$ with a higher enrichment at higher workloads would introduce the isotopic label into the system at the maximum possible rate.

These ^{18}O–assisted ^{31}P–NMR studies did not consider metabolite compartmentation coupled with bidirectional transport and enzyme reactions. It was mentioned in Publication IV that the original data from the above papers could be reanalyzed with an integrative kinetic model to extract more information about the fluxes in this system and should be undertaken in future ^{18}O–assisted ^{31}P–NMR studies. The original data is not available, so no such analysis was possible in Publication IV. Considering that the labeling conditions were not ideal and typically only one transient labeling state was characterized, it is likely that no new insight can be derived from historical ^{18}O–assisted ^{31}P–NMR data [55–69].

4.6 SUMMARY OF PUBLICATION IV

Publication IV was initiated to resolve a long-standing debate conducted over a number of years. The debate focused on determining why the ^{18}O–assisted ^{31}P–NMR method provides lower estimates of total CK flux than both ^{31}P–NMR saturation transfer, and ^{31}P–NMR inversion and saturation transfer. As mentioned in the introduction, it is often difficult to directly apply deductive reasoning on a complex system without the use of a mathematical model; the above debate exemplified this principle.

Upon initial analysis of the system it became clear that the analysis method applied in all ^{18}O–assisted ^{31}P–NMR studies [55–69] hinged upon the assumption that the ^{18}O–assisted ^{31}P–NMR method provides a measure of *net* flux and not *total* flux. This assumption was tested using a dynamic isotopologue model that was sufficiently complex to warrant the development of model generation software. The earliest ^{18}O–assisted ^{31}P–NMR papers were conducted at a time when the dynamic isotopologue model used in Publication IV would have pushed the limits of commonly available computational hardware. This could be the main reason why initial studies used simplified kinetic models that excluded compartmentation and bidirectional reactions [55, 56], and judiciously warned that such models should be used as a first approximation.

The above debate was resolved with the observation that the fluxes determined from ^{18}O–assisted ^{31}P–NMR, ^{31}P–NMR saturation transfer, and ^{31}P–NMR inversion and saturation transfer all lie in the insensitive region where the ^{18}O dynamic isotopologue model provides almost identical predictions of the labeling state. Other observations regarding the use of dynamic isotopologue modeling to resolve rapid bidirectional fluxes are generally valid for all applications of isotope tracer-based MFA.

4.7 SUMMARY OF PUBLICATION II

By measuring the oxygen consumption in populations of isolated cardiomyocytes, along with activity measurements, one can assess the overall rate of ATP synthesis. This technique cannot resolve fluxes in parallel pathways. However, it is widely used to assess how heart energetics change with drug treatments, genetic manipulation, pathologies, or during the process of maturation. Publication II is a critique of another Journal of Physiology paper that studied how the energetic pathways in mouse heart change during postnatal development. Our review points out that the original paper misinterpreted a change in one derived quantity, which we explained by a change in the compartmentation of adenine nucleotides during maturation. We point out that the original authors did not measure the potential contribution of ATP from glycolysis that was shown to be important in an analogous study on the maturation of rabbit heart. Publication II concludes by pointing out that interpreting the original data would have been made easier with the use of a systems biology approach using mathematical models coupled with statistical methods. Due to strict space and reference restrictions in Journal of Physiology journal club articles we were unable to expand our analysis or include additional references to stress this latter point.

SUMMARY

5

CONCLUSIONS

This dissertation focuses on the application of dynamic tracer-based MFA on the compartmentalized biological systems of yeast and the mammalian heart. The main conclusions deriving from this work are listed below, grouped according to the publication they originate from.

5.1 CONCLUSIONS FROM PUBLICATION I

Wahrheit *et al.* wrote that Publication I is the only publication they are aware of that discusses the potential of using isotopologue transients to describe compartmentation [36]. The main findings are reported below:

A. **Dynamic tracer experiments performed under the same steady metabolic state using different isotopic substrates are best analyzed together.**

Parallel solution of dynamic isotopologue simulations using different substrates may be evaluated in the same optimization loop to find the flux solution that best describes all data. This approach ensures that the properties of the metabolism revealed by each isotopic tracer are represented in the optimal flux solution.

B. **If the timing and shape of isotopic transients does not match with measured data, the discrepancy may indicate a need to add additional metabolic compartmentation to the model.**

Discrepancies between measured data and simulated isotopologue dynamics provide insight into the shortcomings of the metabolic model and may lead to further insight into the compartmentation of the underlying biology.

C. **Shortcomings in the model used to simulate the isotope dynamics are more likely to be revealed when optimizing data from multiple substrates simultaneously.**

This statement results from combining conclusions A and B. Optimization with a single labeled substrate may mask shortcomings in the compartmental structure of the model because the shape of dynamic transients are also influenced by the combined effect of bidirectional and net fluxes. An optimal set of bidirectional and net fluxes will be less likely to imitate multiple dynamic transients that result from multiple labeling experiments using different substrates.

5.2 CONCLUSIONS FROM PUBLICATION II

The following are the main points raised in the critique:

D. **The increase in $\frac{K_{mADP}}{K_{Cr}}$ during maturation of mouse cardiomyocytes is not necessarily due to increased CK coupling or activity; changes in the compartmentation of adenine nucleotides during maturation can also explain the increase.**

The original work by Piquereau *et al.* [72] potentially overemphasizes the importance of various CK isoforms in the regulation of energy metabolite fluxes. Highlighting the importance of compartmentation in the regulation of energy metabolite fluxes could influence the research goals of future studies.

E. **The regeneration of energetic metabolites by glycolysis may be significant during maturation.**

Considering that previous studies have shown that glycolysis regenerates a significant fraction of energy metabolites, future studies should consider including this system in the analysis.

F. **Mathematical models are useful in studying the properties of integrated systems.**

It was pointed out in the introduction that directly applying deductive reasoning to integrated systems can be misleading. The use of mathematical models aids in the process of excluding hypotheses.

5.3 CONCLUSIONS FROM PUBLICATION III

Publication III developed a computationally efficient method of expressing all possible steady state flux solutions of a system of chemical transformations in terms of a flux coordinate system. The main findings from this work are listed:

G. **All steady state solutions of a chemical system can be expressed using many flux coordinate systems; GJE naturally provides this convenient representation of the solution subspace.**

A definition of flux coordinate system is given in Chapter 3 Section 3.1. Some flux coordinate systems are more useful than others. The symbolic algorithm provided in Publication III allows a desired flux coordinate system to be specified by the analyst; a feature unique to this algorithm.

H. **If a flux coordinate corresponds to a known flux, the dimension of the steady state subspace is reduced by one. If a flux coordinate is known within a range of values, the steady state subspace has a reduced span.**

Limiting both the dimensions and ranges of coordinates that are used to represent all steady state solutions limits the curse of dimensionality because other representations of the steady

state solution space cannot avoid using all dimensions when scanning the space. The example provided in Publication III illustrates this point by reducing the space from 39 dimensions to 13.

I. **Inspection of the GJE kernel matrix allows for identification of sub networks within the larger metabolic network.**

The size of genome-scale metabolic networks makes them difficult to visualize and interpret. The kernel found using GJE potentially provides a way to break the larger system into subsystems. Each flux coordinate system provides a different set of subsystems, so perhaps exploring the properties of subsystems for many flux coordinate systems will enable one to find canonical properties of the steady state solution subspace and thus the biological system as a whole.

J. **The sparse kernel found from the symbolic GJE routine takes up less memory than dense SVD kernels; in practice, this shifts the limitation of analyzing *very* large systems from the amount of memory available to the computational time considered tolerable.**

The sparse symbolic routine developed in Publication III opens up the possibility of finding the steady state solutions for chemical systems with possibly millions of reactions because the final representation of the steady state solution is much more memory efficient.

5.4 CONCLUSIONS FROM PUBLICATION IV

The sensitivity analysis in Publication IV resolved a number of questions regarding the flux of energy metabolites in heart. A core set of findings is provided:

K. **The total flux through each shuttle determines the labeling state; net flux does not determine the labeling state as stated previously.**

Studies that utilize the ^{18}O–assisted ^{31}P–NMR method typically assume that the isotopic labeling state is a direct measure of *net* flux. The direct implication of this assumption is that label movement does not occur in the opposite direction to net flux. The model predictions in Publication IV (and Publication I) demonstrate that metabolites become labeled even in the case of zero net flux.

L. **If the total flux is increased in either the CK or AdK shuttles, the labeling state of the ^{18}O isotopologues approach a horizontal asymptote. The asymptote is determined by the rate of ^{18}O input into the system.**

This property limits the range of applicability of the ^{18}O–assisted ^{31}P–NMR method because the total bidirectional fluxes in the CK and AdK shuttles are known to be more rapid than the combined rate of ATPase reactions. Higher workloads and a higher enrichment of $H_2^{18}O$ extend the range of applicability.

M. **The sensitivity of the predicted labeling state to changes in pool sizes and the bidirectionality of reactions increased with the use of 100% $H_2^{18}O$ because the rate of label input into the system increased.**

In general it was found that more information about the fluxes in the system can be determined when the rate of label input into the system is increased. To this end a number of strategies are recommended in Publication IV to increase the rate of label input and thus gain the greatest possible insight from ^{18}O–assisted ^{31}P–NMR experiments.

N. **The insensitivity of the dynamic isotopologue model over the range of fluxes measured using ^{18}O–assisted ^{31}P–NMR, ^{31}P–NMR saturation transfer, and ^{31}P–NMR inversion and saturation transfer shows that a single kinetic model is able to explain all known measurements of the energetic fluxes in healthy normoxic heart.**

The predictions of the labeling state using 30% $H_2^{18}O$ display a sufficiently wide insensitive region that even the low flux predictions from the ^{18}O–assisted ^{31}P–NMR method provide almost the same labeling state of PCr as both ^{31}P–NMR saturation transfer and ^{31}P–NMR inversion and saturation transfer. Simulations using 100% $H_2^{18}O$ extend this range, but not past the flux predictions provided by ^{31}P–NMR saturation transfer and ^{31}P–NMR inversion and saturation transfer.

BIBLIOGRAPHY

BIBLIOGRAPHY

[1] S. Makin. *Aristotle: Metaphysics Theta: Translated with an Introduction and Commentary*. Oxford University Press, USA, 2006.

[2] E. Snitkin and D. Segrè. Epistatic interaction maps relative to multiple metabolic phenotypes. *PLoS Genet.*, 7(2):e1001294, 2011.

[3] C. Metallo and M. Vander Heiden. Metabolism strikes back: metabolic flux regulates cell signaling. *Genes Dev.*, 24(24):2717–2722, 2010.

[4] J. Orth, I. Thiele, and B. Palsson. What is flux balance analysis? *Nat. Biotechnol.*, 28(3):245–248, 2010.

[5] L. Blank and L. Kuepfer. Metabolic flux distributions: genetic information, computational predictions, and experimental validation. *Appl. Microbiol. Biotechnol.*, 86(5):1243–1255, 2010.

[6] M. Dauner. From fluxes and isotope labeling patterns towards in silico cells. *Curr. Opin. Biotechnol.*, 21(1):55–62, 2010.

[7] J. Niklas, K. Schneider, and E. Heinzle. Metabolic flux analysis in eukaryotes. *Curr. Opin. Biotechnol.*, 21(1):63–69, 2010.

[8] N. Zamboni. ^{13}C metabolic flux analysis in complex systems. *Curr. Opin. Biotechnol.*, 22(1):103–108, 2011.

[9] K. Nöh and W. Wiechert. The benefits of being transient: isotope-based metabolic flux analysis at the short time scale. *Appl. Microbiol. Biotechnol.*, 91(5):1247–1265, 2011.

[10] S. Wahl, K. Nöh, and W. Wiechert. ^{13}C labeling experiments at metabolic nonstationary conditions: an exploratory study. *BMC Bioinformatics*, 9:152, 2008.

[11] S. Noack, K. Nöh, M. Moch, M. Oldiges, and W. Wiechert. Stationary versus nonstationary ^{13}C-MFA: a comparison using a consistent dataset. *J. Biotechnol.*, 154(2-3):179–190, 2011.

[12] P. Anversa and J. Kajstura. Ventricular myocytes are not terminally differentiated in the adult mammalian heart. *Circ. Res.*, 83(1):1–14, 1998.

[13] B. Goldman and J. Wurzel. Evidence that human cardiac myocytes divide after myocardial infarction. *N. Engl. J. Med.*, 345(15):1131, 2001.

[14] E. Sumner and S. Avery. Phenotypic heterogeneity: differential stress resistance among individual cells of the yeast *Saccharomyces cerevisiae*. *Microbiology (Reading, Engl.)*, 148(Pt 2):345–351, 2002.

[15] S. Huang, G. Eichler, Y. Bar-Yam, and D. Ingber. Cell fates as high-dimensional attractor states of a complex gene regulatory network. *Phys. Rev. Lett.*, 94(12):128701, 2005.

[16] D. Stockholm, R. Benchaouir, J. Picot, P. Rameau, T. Neildez, G. Landini, C. Laplace-Builhé, and A. Paldi. The origin of phenotypic heterogeneity in a clonal cell population in vitro. *PLoS ONE*, 2(4):e394, 2007.

[17] A. Bishop, F. Rab, E. Sumner, and S. Avery. Phenotypic heterogeneity can enhance rare-cell survival in "stress-sensitive" yeast populations. *Mol. Microbiol.*, 63(2):507–520, 2007.

[18] M. Roussel and D. Lloyd. Observation of a chaotic multioscillatory metabolic attractor by real-time monitoring of a yeast continuous culture. *FEBS J.*, 274(4):1011–1018, 2007.

[19] A. Ghosh, B. Chance, and E. Pye. Metabolic coupling and synchronization of NADH oscillations in yeast cell populations. *Arch. Biochem. Biophys.*, 145(1):319–331, 1971.

[20] D. Murray, R. Klevecz, and D. Lloyd. Generation and maintenance of synchrony in *Saccharomyces cerevisiae* continuous culture. *Exp. Cell Res.*, 287(1):10–15, 2003.

[21] B. Tu, A. Kudlicki, M. Rowicka, and S. Mcknight. Logic of the yeast metabolic cycle: temporal compartmentalization of cellular processes. *Science*, 310(5751):1152–1158, 2005.

[22] B. Tu and S. Mcknight. Metabolic cycles as an underlying basis of biological oscillations. *Nat. Rev. Mol. Cell Biol.*, 7(9):696–701, 2006.

[23] M. Aon, S. Cortassa, and B. O'Rourke. The fundamental organization of cardiac mitochondria as a network of coupled oscillators. *Biophys. J.*, 91(11):4317–4327, 2006.

[24] M. Aon, M. Roussel, S. Cortassa, B. O'Rourke, D. Murray, M. Beckmann, and D. Lloyd. The scale-free dynamics of eukaryotic cells. *PLoS ONE*, 3(11):e3624, 2008.

[25] Z. Eelderink-Chen, G. Mazzotta, M. Sturre, J. Bosman, T. Roenneberg, and M. Merrow. A circadian clock in *Saccharomyces cerevisiae*. *Proc. Natl. Acad. Sci. U.S.A.*, 107(5):2043–2047, 2010.

[26] W. Blake, M. Kaern, C. Cantor, and J. Collins. Noise in eukaryotic gene expression. *Nature*, 422(6932):633–637, 2003.

[27] M. Boedigheimer, R. Wolfinger, M. Bass, P. Bushel, J. Chou, M. Cooper, J. Corton, J. Fostel, S. Hester, J. Lee, F. Liu, J. Liu, H. Qian, J. Quackenbush, S. Pettit, and K. Thompson. Sources of variation in baseline gene expression levels from toxicogenomics study control animals across multiple laboratories. *BMC Genomics*, 9:285, 2008.

[28] G. Lelandais, Y. Saint-Georges, C. Geneix, L. Al-Shikhley, G. Dujardin, and C. Jacq. Spatio-temporal dynamics of yeast mitochondrial biogenesis: Transcriptional and post-transcriptional mRNA oscillatory modules. *PLoS Comput. Biol.*, 5(6):e1000409, 2009.

[29] C. Des Rosiers, S. Lloyd, B. Comte, and J. Chatham. A critical perspective of the use of ^{13}C-isotopomer analysis by GCMS and NMR as applied to cardiac metabolism. *Metab. Eng.*, 6(1):44–58, 2004.

[30] M. Rühl, B. Rupp, K. Nöh, W. Wiechert, U. Sauer, and N. Zamboni. Collisional fragmentation of central carbon metabolites in LC-MS/MS increases precision of ^{13}C metabolic flux analysis. *Biotechnol. Bioeng.*, 109:763–771, 2011.

[31] E. Mori, C. Furusawa, S. Kajihata, T. Shirai, and H. Shimizu. Evaluating ^{13}C enrichment data of free amino acids for precise metabolic flux analysis. *Biotechnol J*, 6(11):1377–1387, 2011.

[32] K. Nöh, A. Wahl, and W. Wiechert. Computational tools for isotopically instationary ^{13}C labeling experiments under metabolic steady state conditions. *Metab. Eng.*, 8(6):554–577, 2006.

[33] J. Young, J. Walther, M. Antoniewicz, H. Yoo, and G. Stephanopoulos. An elementary metabolite unit (emu) based method of isotopically nonstationary flux analysis. *Biotechnol. Bioeng.*, 99(3):686–699, 2008.

[34] D. Beard and H. Qian. Relationship between thermodynamic driving force and one-way fluxes in reversible processes. *PLoS ONE*, 2(1):e144, 2007.

[35] A. Shastri and J. Morgan. A transient isotopic labeling methodology for ^{13}C metabolic flux analysis of photoautotrophic microorganisms. *Phytochemistry*, 68(16-18):2302–2312, 2007.

[36] J. Wahrheit, A. Nicolae, and E. Heinzle. Eukaryotic metabolism: measuring compartment fluxes. *Biotechnol J*, 6(9):1071–1085, 2011.

[37] L. Quek, C. Wittmann, L. Nielsen, and J. Krömer. OpenFLUX: efficient modelling software for ^{13}C-based metabolic flux analysis. *Microb. Cell Fact.*, 8:25, 2009.

[38] C. Barrett, M. Herrgard, and B. Palsson. Decomposing complex reaction networks using random sampling, principal component analysis and basis rotation. *BMC Syst. Biol.*, 3(1):30, 2009.

[39] T. Yang, O. Frick, and E. Heinzle. Hybrid optimization for ^{13}C metabolic flux analysis using systems parametrized by compactification. *BMC Syst. Biol.*, 2:29, 2008.

[40] N. Price, J. Schellenberger, and B. Palsson. Uniform sampling of steady-state flux spaces: means to design experiments and to interpret enzymopathies. *Biophys. J.*, 87(4):2172–2186, 2004.

[41] B. Lauzier, F. Vaillant, R. Gélinas, B. Bouchard, R. Brownsey, E. Thorin, J. Tardif, and C. Des Rosiers. Ivabradine reduces heart rate while preserving metabolic fluxes and energy status of healthy normoxic working hearts. *Am. J. Physiol. Heart Circ. Physiol.*, 300(3):H845–852, 2011.

[42] B. Wan, K. LaNoue, J. Cheung, and R. Scaduto. Regulation of citric acid cycle by calcium. *J. Biol. Chem.*, 264(23):13430–13439, 1989.

[43] S. Cortassa, M. Aon, E. Marbán, R. Winslow, and B. O'Rourke. An integrated model of cardiac mitochondrial energy metabolism and calcium dynamics. *Biophys. J.*, 84(4):2734–2755, 2003.

[44] K. Vinnakota, R. Dash, and D. Beard. Stimulatory effects of calcium on respiration and NAD(P)H synthesis in intact rat heart mitochondria utilizing physiological substrates cannot explain respiratory control in vivo. *J. Biol. Chem.*, 286(35):30816–30822, 2011.

[45] V. Kupriyanov, A. Ya Steinschneider, E. Ruuge, V. Kapel'Ko, M. Yu Zueva, V. Lakomkin, V. Smirnov, and V. Saks. Regulation of energy flux through the creatine kinase reaction in vitro and in perfused rat heart. ^{31}P-NMR studies. *Biochim. Biophys. Acta*, 805(4):319–331, 1984.

[46] J. Bittl and J. Ingwall. Reaction rates of creatine kinase and ATP synthesis in the isolated rat heart. a ^{31}P NMR magnetization transfer study. *J. Biol. Chem.*, 260(6):3512–3517, 1985.

[47] K. Ugurbil, M. Petein, R. Maidan, S. Michurski, and A. From. Measurement of an individual rate constant in the presence of multiple exchanges: application to myocardial creatine kinase reaction. *Biochemistry*, 25(1):100–107, 1986.

[48] R. G. Spencer, J. A. Balschi, J. S. Leigh Jr., and J. S. Ingwall. ATP synthesis and degradation rates in the perfused rat heart. ^{31}P-nuclear magnetic resonance double saturation transfer measurements. *Biophys. J.*, 54(5):921–929, 1988.

[49] S. Perry, J. Mcauliffe, J. Balschi, P. Hickey, and J. Ingwall. Velocity of the creatine kinase reaction in the neonatal rabbit heart: role of mitochondrial creatine kinase. *Biochemistry*, 27(6):2165–2172, 1988.

[50] R. Zahler and J. Ingwall. Estimation of heart mitochondrial creatine kinase flux using magnetization transfer NMR spectroscopy. *Am. J. Physiol.*, 262(4 Pt 2):H1022–1028, 1992.

[51] M. Portman and X. Ning. Maturational changes in respiratory control through creatine kinase in heart in vivo. *Am. J. Physiol.*, 263(2 Pt 1):C453–460, 1992.

[52] Y. Matsumoto, M. Kaneko, A. Kobayashi, Y. Fujise, and N. Yamazaki. Creatine kinase kinetics in diabetic cardiomyopathy. *Am. J. Physiol.*, 268(6 Pt 1):E1070–1076, 1995.

[53] R. Spencer, P. Buttrick, and J. Ingwall. Function and bioenergetics in isolated perfused trained rat hearts. *Am. J. Physiol.*, 272(1 Pt 2):H409–417, 1997.

[54] M. Vendelin, J. Hoerter, P. Mateo, S. Soboll, B. Gillet, and J. Mazet. Modulation of energy transfer pathways between mitochondria and myofibrils by changes in performance of perfused heart. *J. Biol. Chem.*, 285(48):37240–37250, 2010.

[55] R. Zeleznikar, R. Heyman, R. Graeff, T. Walseth, S. Dawis, E. Butz, and N. Goldberg. Evidence for compartmentalized adenylate kinase catalysis serving a high energy phosphoryl transfer function in rat skeletal muscle. *J. Biol. Chem.*, 265(1):300–311, 1990.

[56] R. Zeleznikar and N. Goldberg. Kinetics and compartmentation of energy metabolism in intact skeletal muscle determined from ^{18}O labeling of metabolite phosphoryls. *J. Biol. Chem.*, 266(23):15110–15119, 1991.

[57] R. Zeleznikar, P. Dzeja, and N. Goldberg. Adenylate kinase-catalyzed phosphoryl transfer couples ATP utilization with its generation by glycolysis in intact muscle. *J. Biol. Chem.*, 270(13):7311–7319, 1995.

[58] P. Dzeja, R. Zeleznikar, and N. Goldberg. Suppression of creatine kinase-catalyzed phosphotransfer results in increased phosphoryl transfer by adenylate kinase in intact skeletal muscle. *J. Biol. Chem.*, 271(22):12847–12851, 1996.

[59] P. Dzeja, R. Zeleznikar, and N. Goldberg. Adenylate kinase: kinetic behavior in intact cells indicates it is integral to multiple cellular processes. *Mol. Cell. Biochem.*, 184(1-2):169–182, 1998.

[60] P. Dzeja, K. Vitkevicius, M. Redfield, J. Burnett, and A. Terzic. Adenylate kinase-catalyzed phosphotransfer in the myocardium: Increased contribution in heart failure. *Circ. Res.*, 84(10):1137–1143, 1999.

[61] D. Pucar, E. Janssen, P. Dzeja, N. Juranic, S. Macura, B. Wieringa, and A. Terzic. Compromised energetics in the adenylate kinase AK1 gene knockout heart under metabolic stress. *J. Biol. Chem.*, 275(52):41424–41429, 2000.

[62] D. Pucar, P. Dzeja, P. Bast, N. Juranic, S. Macura, and A. Terzic. Cellular energetics in the preconditioned state: Protective role for phosphotransfer reactions captured by ^{18}O-assisted ^{31}P NMR. *J. Biol. Chem.*, 276(48):44812–44819, 2001.

[63] D. Pucar, P. Bast, R. Gumina, L. Lim, C. Drahl, N. Juranic, S. Macura, E. Janssen, B. Wieringa, A. Terzic, and P. Dzeja. Adenylate kinase AK1 knockout heart: energetics and functional performance under ischemia-reperfusion. *Am. J. Physiol. Heart Circ. Physiol.*, 283(2):H776–782, 2002.

[64] E. Janssen, A. Terzic, B. Wieringa, and P. Dzeja. Impaired intracellular energetic communication in muscles from creatine kinase and adenylate kinase (M-CK/AK1) double knock-out mice. *J. Biol. Chem.*, 278(33):30441 –30449, 2003.

[65] R. Gumina, D. Pucar, P. Bast, D. Hodgson, C. Kurtz, P. Dzeja, T. Miki, S. Seino, and A. Terzic. Knockout of Kir6.2 negates ischemic preconditioning-induced protection of myocardial energetics. *Am. J. Physiol. Heart Circ. Physiol.*, 284(6):H2106 –H2113, 2003.

[66] D. Pucar, P. Dzeja, P. Bast, R. Gumina, C. Drahl, L. Lim, N. Juranic, S. Macura, and A. Terzic. Mapping hypoxia-induced bioenergetic rearrangements and metabolic signaling by ^{18}O-assisted ^{31}P NMR and ^{1}H NMR spectroscopy. *Mol. Cell. Biochem.*, 256-257(1-2):281–289, 2004.

[67] P. Dzeja, A. Terzic, and B. Wieringa. Phosphotransfer dynamics in skeletal muscle from creatine kinase gene-deleted mice. *Mol. Cell. Biochem.*, 256-257(1-2):13–27, 2004.

[68] P. Dzeja, P. Bast, D. Pucar, B. Wieringa, and A. Terzic. Defective metabolic signaling in adenylate kinase AK1 gene knock-out hearts compromises post-ischemic coronary reflow. *J. Biol. Chem.*, 282(43):31366–31372, 2007.

[69] P. Dzeja, K. Hoyer, R. Tian, S. Zhang, E. Nemutlu, M. Spindler, and J. Ingwall. Rearrangement of energetic and substrate utilization networks compensate for chronic myocardial creatine kinase deficiency. *J. Physiology*, NA:NA, 2011.

[70] K. Neurohr and R. Shulman. Carbon-13 and phosphorus-31 nuclear magnetic resonance studies of myocardial metabolism in live guinea pigs. *Adv Myocardiol*, 6:185–193, 1985.

[71] P. D. Boyer, W. W. Luchsinger, and A. B. Falcone. ^{18}O and ^{32}P exchange reactions of mitochondria in relation to oxidative phosphorylation. *J. Biol. Chem.*, 223(1):405 –421, 1956.

[72] J. Piquereau, M. Novotova, D. Fortin, A. Garnier, R. Ventura-Clapier, V. Veksler, and F. Joubert. Postnatal development of mouse heart: formation of energetic microdomains. *J. Physiol. (Lond.)*, 588(Pt 13):2443–2454, 2010.

CURRICULUM VITAE

europass

Europass Curriculum Vitae

Personal information

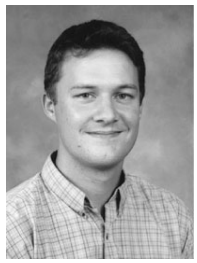

Surname(s) / First name(s)	**David William Schryer**
Email(s)	david@sysbio.ioc.ee
Nationality(-ies)	Canadian, Dutch
Date of birth	July 15th, 1975
Gender	Male

Work Experiance

Dates	April 2008 — Present
Occupation or position held	Researcher
Main activities and responsibilities	Performed the research presented within this dissertation and additional scientific duties including: Procurement of the optical components for our custom confocal microscope as well as the coils and perfusion equiptment required to perform ^{31}P NMR saturation and inversion transfer experiments on perfused hearts. Wrote sections of an FP7 proposal and an ESF proposal, and our part of a proposal to create a Marie Curie Research Training Network related to the analysis of metabolic fluxes. Produced teaching materials together with the other PhD students.
Name and address of employer	Institute of Cybernetics, Akadeemia tee 21, EE-12618 Tallinn, Republic of Estonia

Dates	April 2006 — April 2008
Occupation or position held	Researcher
Main activities and responsibilities	Developed computational tools for systems biology analysis, installed and improved the fermentation systems and new laboratory infrastructure.
Name and address of employer	Competence Center of Food and Fermentation Technologies (CCFFT), Akadeemia tee 15B, EE-12618 Tallinn, Republic of Estonia

Dates	July 2004 – July 2006
Occupation or position held	Engineer
Main activities and responsibilities	Ran a pilot plant for the industrial extraction of protein from rapeseed. Wrote an English language cirriculum document for the Department of Chemical Engineering at TUT for the purpose of external review.
Name and address of employer	Tallinn University of Technology, Ehitajate tee 5, EE-19086 Tallinn, Republic of Estonia

Work Experiance

Dates	April 2005 – June 2006
Occupation or position held	High School Teacher
Main activities and responsibilities	Developed and gave courses in Chemistry, Physics, and Computer Science. Wrote an English language cirriculum document for internal use at EBS.
Name and address of employer	Estonian Business School, Lauteri 3, EE-10114 Tallinn, Republic of Estonia

Dates	Summer 2000 and April 2002 — June 2004
Occupation or position held	Research Assistant
Main activities and responsibilities	Upgrading and repair of XPS, Mass Spectrometry, and UHV systems. Designed and built a multi-annulus flow apparatus with a constant force bellows seal thermal expansion compensator capable of sustaining 1000°C. It was used to measure the transport properties of solid oxide membranes used in SOFCs.
Name and address of employer	Laboratory of Professor C.A. Mims, Department of Chemical Engineering, 200 College st., Toronto, Ontario, Canada, M5S 3E5

Dates	September 2000 — April 2002
Occupation or position held	Research Assistant
Main activities and responsibilities	Wrote a Multimedia Fate & Transport Model to analyze the movement of Persistent Organic Pollutants (POPs) that included a novel surface compartment to account for the influence of building surfaces in urban areas. Researched and modeled the origins of a periodic water quality issue in Lake Ontario. Modeled the impact of a proposed urban development project on local water quality for use in a legal hearing.
Name and address of employer	Laboratory of Adjunct professor Miriam Diamond, Department of Chemical Engineering, 200 College st., Toronto, Ontario, Canada, M5S 3E5

Dates	April 2000 — 2003
Occupation or position held	Graduate Teaching Assistant
Main activities and responsibilities	Courses: (a) Thermodynamics laboratory instructor — Fall 2000/Winter 2001 (b) Transport phenomena/unit operations laboratory instructor — Fall 2001 (c) Process control simulation instructor (MATLAB/Simulink®) — Winter 2003 (d) Chemical plant design advisor — Fall 2003
Name and address of employer	Department of Chemical Engineering, 200 College st., Toronto, Ontario, Canada, M5S 3E5

Dates	April 2001 — 2003
Occupation or position held	GSU Executive
Main activities and responsibilities	Elected to be one of seven executive representatives for U of T's 11,000 graduate students. Graduate student representative of the Hart House Board of Stewards, and the Council of Athletics and Recreation. Founded the University of Toronto Summer Softball League (UTSSL)
Name and address of employer	Graduate Students' Union (GSU), 16 Bancroft Avenue, Toronto, Ontario, Canada, M5S 1C1

Work Experiance

Dates	May 1998 — Sept. 1999
Occupation or position held	Research Assistant
Main activities and responsibilities	Calibrated lab equipment for ISO 9002 certification and carried out standard asphalt tests.
Name and address of employer	McAsphalt Engineering Services, 8800 Sheppard Avenue East, Toronto, Ontario, Canada, M1B 5R4

Education and training

Dates	Graduation 2012
Title of qualification awarded	PhD — To be defended.
Principal subjects/occupational skills covered	Dissertation — *Metabolic Flux Analysis of Compartmentalized Systems using Dynamic Isotopologue Modeling.* Awards: (a) Archimedes Foundation Grant for PhD studies — $5904 per annum (b) DoRa travel awards for two Biophysical Society meetings — Below cost
Name and type of organisation providing education and training	Laboratory of Systems Biology, Institute of Cybernetics, Akadeemia tee 21, EE-12618 Tallinn, Republic of Estonia, Tallinn University of Technology
Level in national or international classification	ISCED 6

Dates	Graduation 2005
Title of qualification awarded	Master of Applied Science — M.A.Sc.
Principal subjects/occupational skills covered	Thesis title — *On the determination of sub-second water–cellulose sorption kinetics using mass spectrometry.* Awards: (a) Ontario Graduate Scholarship in Science and Technology (OGSST) — $15000 per annum (b) University of Toronto Fellowship — $1200 (received twice)
Name and type of organisation providing education and training	Laboratory of Professor C.A. Mims, Department of Chemical Engineering, 200 College st., Toronto, Ontario, Canada, M5S 3E5, University of Toronto
Level in national or international classification	ISCED 5A

Dates	Graduation 2000
Title of qualification awarded	Bachelor of Applied Science — B.A.Sc.
Principal subjects/occupational skills covered	Thesis title — *Measuring the ion mobility of oxygen through solid oxide membranes using transient ^{18}O exchange and SIMS depth profiling.* Awards: (a) Best Plant Design Project 2000 (b) Undergraduate Achievment Scholarship — $1500 (received twice)
Name and type of organisation providing education and training	Laboratory of Professor C.A. Mims, Department of Chemical Engineering, 200 College st., Toronto, Ontario, Canada, M5S 3E5, University of Toronto
Level in national or international classification	ISCED 5A

Personal skills and competences

Mother tongue(s) **English**

	Understanding		Speaking		Writing
Self-assessment	Listening	Reading	Spoken interaction	Spoken production	
European level $^{\Psi}$					
Estonian	B1 Independent user	B1 Independent user	B1 Independent user	B1 Independent user	B1 Independent user

$^{\Psi}$ *Common European Framework of Reference (CEF) level*

Driving licence: Estonian Class B

Social skills and competences: Considered to be a valuable team member.

Organisational skills and competences: Experience running large meetings and getting consent from participants with very different agendas.

Technical skills and competences: Electrical, plumbing, HVAC, landscaping, drafting, book binding, and construction experience.

Computer skills and competences: Highlights: (a) Experienced programmer in: Python. (b) Competent in: C, C++, FORTRAN, COBOL, Pascal. (c) Practice safe computation with version control (hg, git, svn, bzr) and unit testing. (d) Development of interactive course material using ReST, Sphinx, Django, and Beamer. (e) Have assembled and repaired many computers. (f) Avid supporter of FOSS with an emphasis on sharing my code.

Artistic skills and competences: I enjoy composing and playing songs.

Other skills and competences: Nurturing my family and watching my children develop.

Additional information

References

[1] Schryer DW, Vendelin M, Peterson P: **Symbolic flux analysis for genome-scale metabolic networks**. *BMC Systems Biology* 2011, **5**:81.

[2] Illaste A, Kalda M, Schryer DW, Sepp M: **Life of mice - development of cardiac energetics**. *The Journal of Physiology* 2010, **588**(Pt 23):4617–4619.

[3] Illaste A, Schryer DW, Birkedal R, Peterson P, Vendelin M: **Determination of regional diffusion coefficients of fluorescent ATP in rat cardiomyocytes**. *Biophysical Journal* 2010, **98**(3):749a.

[4] Schryer DW, Peterson P, Paalme T, Vendelin M: **Bidirectionality and compartmentation of metabolic fluxes are revealed in the dynamics of isotopomer networks**. *International Journal of Molecular Sciences* 2009, **10**(4):1697–1718.

[5] Schryer DW, Peterson P, Paalme T, Vendelin M: **Isotopomeric 13C labeling of amino acids reveal compartmentation in *Saccharomyces uvarum***. *Biophysical Journal* 2009, **96**(3):308a.

[6] Schryer DW, Bhavsar S, Diamond ML: **A preliminary model of the fate of geosmin & MIB2 in Lake Ontario**. In *The Canadian Association on Water Quality Annual Meeting* 2001.

[7] Schryer DW, Diamond ML, Liu Q, Stern G, McCarry B: **Multimedia Urban Model: Validation and uncertainty analysis using a dynamic Monte Carlo method**. In *22nd Annual SETAC meeting* 2001.

[8] Diamond ML, Schryer DW, Bhavsar S: **Bond Lake: Application of the Mackay–Diamond model**. Tech. rep., Ontario Municipal Board hearing on the Oak Ridges Moraine development 2001.

Publications: [1, 2, 3, 4, 5]
Invited Conference Talks: [6, 7]
Technical Report: [8]

APPENDIX

PUBLICATION I

Schryer DW, Peterson P, Paalme T, Vendelin M.

Bidirectionality and compartmentation of metabolic fluxes are revealed in the dynamics of isotopomer networks.

International Journal of Molecular Sciences, 10(4):1697-718, (2009)

Int. J. Mol. Sci. **2009**, *10*, 1697-1718; doi:10.3390/ijms10041697

OPEN ACCESS

International Journal of Molecular Sciences

ISSN 1422-0067

www.mdpi.com/journal/ijms

Review

Bidirectionality and Compartmentation of Metabolic Fluxes Are Revealed in the Dynamics of Isotopomer Networks

David W. Schryer [1], Pearu Peterson [1], Toomas Paalme [2] and Marko Vendelin [1,⋆]

[1] Laboratory of Systems Biology, Institute of Cybernetics, Tallinn University of Technology, Akadeemia 21, 12618 Tallinn, Estonia; E-Mails: david@sysbio.ioc.ee (D.W.S.); pearu@sysbio.ioc.ee (P.P.); markov@sysbio.ioc.ee (M.V.)

[2] Department of Food Processing, Tallinn University of Technology, Ehitajate 5, 19086 Tallinn, Estonia; E-Mail: tpaalme@staff.ttu.ee (T.P.)

⋆ Author to whom correspondence should be addressed; E-Mail: markov@sysbio.ioc.ee

Received: 11 March 2009; in revised form: 7 April 2009 / Accepted: 14 April 2009 / Published: 17 April 2009

Abstract: Isotope labeling is one of the few methods of revealing the *in vivo* bidirectionality and compartmentalization of metabolic fluxes within metabolic networks. We argue that a shift from steady state to dynamic isotopomer analysis is required to deal with these cellular complexities and provide a review of dynamic studies of compartmentalized energy fluxes in eukaryotic cells including cardiac muscle, plants, and astrocytes. Knowledge of complex metabolic behaviour on a molecular level is prerequisite for the intelligent design of genetically modified organisms able to realize their potential of revolutionizing food, energy, and pharmaceutical production. We describe techniques to explore the bidirectionality and compartmentalization of metabolic fluxes using information contained in the isotopic transient, and discuss the integration of kinetic models with MFA. The flux parameters of an example metabolic network were optimized to examine the compartmentalization of metabolites and and the bidirectionality of fluxes in the TCA cycle of *Saccharomyces uvarum* for steady-state respiratory growth.

Keywords: Metabolic network; isotopomer dynamics; MFA; mathematical modeling; compartmentalization; ^{13}C NMR.

1. Introduction

Isotope labeling is widely used to gain insight into the operation of metabolic networks despite the fact that neither the collection of isotopomer data, nor its simulation and analysis is considered routine. Both experimental and analytical methods enabling dynamic studies that require direct measurement of the mass and/or positional isotopomers and the pool sizes of intermediate metabolites are developing quickly [1, 2, 3]. The move from isotopomeric steady state flux analysis to studies involving dynamic enrichment is required to deal with the complexities of the eukaryotic cell and multicellularity. The compartmentalization of metabolites into organelles, often with parallel enzyme systems coupled with complex transport mechanisms makes the application of Metabolic Flux Analysis (MFA) at isotopic steady state difficult and uncertain.

MFA is an important tool for strain improvement in biotechnology [4] with a vast potential for further improvement. However it has recently been stated that "in order to truly exploit the synthetic capacity of biological systems and broaden the creation of microbial chemical factories, it is necessary to go beyond natural pathways for the synthesis of natural products towards the *de novo* design and assembly of biosynthetic pathways for both natural and unnatural compounds." [5]. Synthetic Biology, while probable in the long term, is optimistic in light of our current understanding of metabolic systems and will depend on knowledge gained from the flux analysis of natural pathways. The great potential for genetic improvement has not been realized largely due to an incomplete understanding of the metabolic operation within organisms - especially their dynamic nature.

This paper is a short review of the motivations for moving from MFA using data collected at isotopic steady state to making full use of the information contained in the isotopic transient. Examples are taken from recent studies that make good use of this information followed by a short section on performing this analysis under conditions of unstationary metabolism. An attempt is made to point towards the future of dynamic modeling of cellular systems using predictive kinetic models–The holy grail of modern biology. Simulations of isotopic transients are used to explore the information contained in the isotopic transient and examine techniques to exploit this information. Following this is a short example where the flux parameters are optimized for the TCA cycle in *Saccharomyces uvarum* for steady-state respiratory growth fed with $^{13}C_{1,2}$ acetate and unlabeled glucose.

1.1. Motivation for exploiting the dynamic transient

The majority of MFA studies have been conducted at metabolic steady state, and the majority of these involve measuring isotopomers at isotopic steady state. Recent studies conducted at the metabolic and isotopic steady state include Blank *et al.* [6] and Vo *et al.* [7]. These and other studies have contributed and will continue to contribute to our understanding of metabolic function, however MFA at metabolic and isotopic steady state is complicated by a number of factors including compartmentalization [8, 9] and makes it more difficult to study the robustness of metabolic networks [10] since a separate flux analysis is required for each metabolic perturbation. Dynamic isotopic analysis allows one to directly probe metabolic robustness and control.

A recent study demonstrates the use of MFA at metabolic steady state using isotopic transient data in the pentose phosphate pathway and citric acid cycle (TCA) of *E.coli* [11]. Their modeling was made

easier by assuming that the flux from precursor metabolites to free amino acids to protein bound amino acids was uni-directional and there was no lag in the isotopomer dynamics due to protein turnover and bi-directional transamination reactions as measured in *Saccharomyces cerevisiae* [12]. den Hollander *et al.* [13] measured this effect in 1981 using ^{13}C NMR to track metabolite dynamics. Although little is known about protein turnover rates *in vivo* prokaryotes are expected to display less protein turnover than eukaryotes [14]. Isotopic dynamics in prokaryotes avoids the most obvious types of compartmentalization, so most examples of MFA in this review are taken from eukaryotic systems.

2. Dynamic MFA in eukaryotic systems

MFA using isotopic transient data is more often applied in eukaryotic systems as it is not so easy to avoid compartmentalization and bi-directional exchange with large metabolic pools. However, since the nature of many of these dynamic processes has yet to be elucidated, MFA using isotopic transient data has been performed mostly on small linear branches of the metabolic networks without accounting for global dynamic behavior [15]. There are a few exceptions however, notably Heinzle *et al.* [16] who used a combination of kinetic network modeling and simulation to calculate metabolic fluxes in a secondary metabolic network in potato (*Solanum tuberosum*). Shastri and Morgan [17] assess the experimental needs for conducting isotopic transient MFA experiments on plants, and a few recent papers review techniques for determining fluxes in plant networks [18, 19].

Often, the organism of interest cannot be sustained in a steady metabolic state over long periods of time. To overcome this limitation one could resort to simulating the isotopic transient with a non-steady metabolism, or shorten the labeling experiment to less than one minute since the concentrations of enzymes in cells remain constant over short time spans (10 s to 1min) [20].

2.1. Flux analysis with non-steady metabolism

There has been some progress recently in MFA studies with a non-steady metabolism and a lack of kinetic structure. A few researchers have started the move towards non-stationary MFA, with Wahl *et al.* [21] and Baxter *et al.* [22] recently publishing papers that outline frameworks for performing transient isotopic experiments under a transient metabolic state. Experimental and analytical techniques have advanced to the point where it is possible to collect the data needed for studies involving non-steady metabolism, and this class of dynamic MFA should start becoming more common and will aid in excluding hypotheses regarding cellular compartmentalization and dynamic metabolic behavior.

2.2. Utilizing metabolic oscillations

It is widely accepted that metabolic systems ubiquitously display oscillations in metabolic fluxes through temporal compartmentalization, proposed to be driven by oscillating metabolic cycles [23]. By turning metabolic cycles on and off biochemical reactions can be carried out under optimal conditions and futile cycles reduced. Fluctuations in fluxes have prompted Wiechert and Noh [14] to argue that "MFA is currently reaching the biological limits of its applicability" because population inhomogeneities and flux oscillations prevent one from obtaining meaningful dynamic measurements. There are cases when these limitations can be minimized through the use of oscillations, however.

In continuous culture yeast can be enticed to grow with a stable oscillating metabolism with a period between 40 minutes to 5 hours[24]. While growing in this state the metabolic state of most cells in the fermenter are operating in synchrony, thus reducing population inhomogeneities to a minimum, although it should be noted that some inhomogeneities persist, such as that due to cells operating at different stages in the cell cycle. Tu *et al.* [25] measured the periodicities of expressed genes while yeast was growing in this state and found that over half of the ($\approx$ 3,552) yeast genes exhibited periodic expression at a confidence level of 95%. Tu *et al.* [25] conclude by arguing that metabolic oscillation may "constitute the primordial device upon which the divergent circadian and ultradian biological oscillators of modern organisms have been built".

Keeping in mind that enzyme concentrations remain constant over short time spans it is conceivable that one could use a device like the BioScope [26] to perform transient isotopic pulse experiments at different stages in the oscillating cycle (at a good approximation to metabolic steady state over the sampling period) thus avoiding metabolic inhomogeneities in the vast majority of the population and large flux oscillations. This would enable the analysis of metabolic fluxes using isotopic transient data at different metabolic states under one cultivation condition. A data set of this nature could also be used for MFA at the metabolic and isotopic steady state and could aid in the construction of a predictive large scale kinetic model of yeast metabolism with cell signaling dynamics [27].

3. Building predictive kinetic models

Predictive kinetic models can be created in systems where the *in vivo* kinetics of many enzyme systems within the metabolic network are well characterized. For many systems this information is not available, so development of kinetic models of metabolic systems is much less common than the use of phenomenological MFA to characterize metabolic activity. However, predictive kinetic models allow us to use the information content of experimental data points measured at one physiological condition to predict the dynamic behavior of the system at another physiological condition.

The modeling process involves (1) developing a theory of how the biological system operates, (2) representing the system as a set of ordinary and/or partial differential equations with direct physical meaning, (3) fitting the parameters of this system using one dataset, (4) testing the predictive qualities of the system using another related dataset, and (5) adjusting the theory and repeating the process as required. Metabolic models that have passed this kind of scrutiny allow us to predict bi-directional metabolic fluxes and system behavior under conditions where measured data is sparse. Great improvements can be achieved with the use of data gathered decades ago, which is often of high quality and fundamental in nature.

The complexity and scope of the model ought to be limited by the quality and amount of measured data used to tune it, so introduction of kinetic parameters into dynamic models must be carefully considered. It is wise to restrict the addition of kinetic parameters to enzyme systems that have been systematically studied such that the kinetic scheme is biologically relevant and the kinetic parameters are known with some level of confidence. This ensures that there is additional data available for the tuning process, and the parameters are physiologically relevant.

With this approach it is possible to maintain the structural identifiability of the model while adding more parameters. If many parameter sets can fit the available data, biological insight is severely limited if not impossible, so it is wise to always check the robustness of the solution during parameter optimization. With this in mind, it is not recommended to replace phenomenological MFA with phenomenological kinetic schemes that include more parameters since this only works to reduce the structural identifiability of the model while adding no biological insight.

Ultimately, the construction of a predictive kinetic model involves the laborious task of studying each enzyme system *in vivo* under a wide range of metabolic conditions. With the availability of additional kinetic insight and data metabolic flux analysis in the heart has progressed along a different path from the microbial and plant systems mentioned above. Predictive kinetic models in the heart are widespread since drug development is only possible with fundamental knowledge of enzyme operation, and this work is best performed in the public domain. With the future shift towards the use of cellulosic biorefineries it is predicted that there will be an increasing economic stimulus to study the fundamentals of exotic metabolisms and thus a resurgence in fundamental kinetic studies in plant and microbial systems.

With the complexity of biological systems, predictive models are useful to exclude hypotheses regarding their function. Vendelin *et al.* [28] quantified the oxygen dependence on the workload in rat cardiomyocytes using published data. By working with the kinetic assumptions in the model they refuted the assumption that the ADP concentration does not contain gradients, and found the gradients to be workload-dependent. Intra-cellular concentration gradients were not required for phosphocreatine, creatine, and ATP, whose concentrations can be assumed to be in spatial equilibrium. The change in ADP concentration taken together with changes in inorganic phosphate were found to be major components of the metabolic feedback signal to control respiration in muscle cells. Using the same modeling approach, the control of respiration was found to be dependent on the dynamics of the system [29].

Predictive kinetic models are better suited to exclude hypotheses regarding dynamic metabolism than phenomenological MFA. Selivanov *et al.* [30] and Liebermeister and Klipp [31] have published methods to make use of transient isotopic data in predictive kinetic models of dynamic cellular behavior, although the application of this technique is in its infancy due to the complexities of the underlying dynamic system including the problem of how to analyze multi-compartment labeling. The use of kinetic information coupled with isotopomer analysis will become an increasingly important tool.

3.1. Measurement of in vivo kinetics

One important tool for probing the mechanisms of complicated kinetic systems *in vivo* is the NMR saturation and inversion transfer technique developed in theory by McConnell [32] and in practice by Forsen and Hoffman [33]. Nuclei having been saturated or inverted with radio frequency radiation can retain their magnetic orientation through a chemical reaction. Thus, if the time span of the reaction is short compared to the relaxation time, the NMR spectrum may show the effects of the saturation or inversion on the corresponding, unirradiated line in the spectrum. Saturation and inversion detects only the pool of molecular species that are able to react, and gives direct insight into reaction kinetics and metabolite compartmentalization.

A number of reviews discuss techniques for using saturation and inversion transfer for studying the kinetics of complex reaction schemes [34, 35, 36]. The application of saturation and inversion transfer using ^{31}P NMR to study the energy metabolism in hearts is a good example of how compartmentalization and bi-directionality of reaction steps complicates the analysis of a small network of reactions.

Early studies observed a discrepancy between the measured forward and reverse rate in the creatine kinase reaction when the myocardium was operating at steady state. To resolve this discrepancy it was concluded that analysis of the NMR data should include either compartmentalization of substrates or enzymes, or include an exchange of ATP with other phosphorus species such as inorganic phosphate [37, 38]. In the case of compartmentalization, each compartmentalized pool will require fitting a different T_1 value [39].

Since the amount of information available from one single magnitization transfer protocol is insufficient to fit all parameters, Joubert *et al.* [40] used four different magnitization transfer protocols in one experiment and used this additional data to fit multiple possible kinetic schemes. They determined that three different creatine kinase reactions schemes should be considered and both subcellular compartmentalization and multiple exchange with inorganic phosphate are important. This work reveals insight into the spatial and temporal buffering of ATP in cardiac cells [41], which is linked with heart failure when operating in a sub-optimal mode [42].

A complimentary method for exploring *in vivo* kinetics was developed to study energy metabolism in skeletal muscle using mass spectrometry to follow the enrichment of oxygen isotopes into energy metabolites. Replacing the external cellular environment with $H_2^{18}O$ results in the incorporation of hydroxyl ions from $H_2^{18}O$ into the phosphoryl groups of energy metabolites resulting in an equilibrium distribution of phosphoryls with 1, 2, or 3 ^{18}O atoms as a function of the enrichment of ^{18}O in the water [43]. The size of metabolic pools can be calculated from the distribution of these molecular species at isotopic equilibrium, and using the time course of ^{18}O incorporation into the high-energy phosphoryls one can determine the rate of hydrolysis of the energy metabolites [43].

There are a number of technical difficulties when implementing this approach. The analytical work is very laborious and many animals are required for a statistically significant study. Each dynamic data point requires sacrificing one animal where an ^{18}O transient is induced, followed by freeze clamping in liquid nitrogen and a long preparatory procedure prior to analysis in the mass spectrometer.

The analysis of the data is also tricky since phosphotransfer dynamics contain compartmentalized metabolites and bi-directional reaction steps. To simplify the analysis of their transient experimental data on the uptake of ^{18}O in the energy metabolites of toad skeletal muscle, Dawis *et al.* [43] assumed that the fluxes through the enzymatic complexes were uni-directional and only one ^{18}O could be incorporated per molecular turnover. They judiciously discussed the issues bi-directional reaction steps within enzymatic complexes and wrote that "In practice, it will be difficult to verify a multiple-reversal model for the intact cell. Consequently, it will not be easy to choose between a multiple reversal model and a compartmentalization model." Dawis *et al.* [43] also stressed that the influence of bi-directional reaction steps "should be examined but will be difficult to prove."

A proper study of the bi-directionality of phosphotransfer networks has yet to be completed, and the amount of data collected in ^{18}O transfer studies is probably not enough to distinguish between possible

reaction networks with various combinations of compartmentalization and bi-directional fluxes. Because of these limitations the above assumption of uni-directional fluxes was applied in a series of papers that explored the kinetics and compartmentalization of energy metabolism in rat skeletal muscle [44, 45, 46, 47, 48]. However, the assumption of uni-directional fluxes is not a necessary limitation of the method and should be evaluated in future studies.

Saturation and inversion using ^{31}P NMR can be enhanced by the use of either a ^{17}O or ^{18}O induced isotope shift in the ^{31}P NMR spectra. Pucar *et al.* [49] introduced the ^{18}O assisted ^{31}P NMR method to study energetics in mouse heart. The method was employed in a series of papers exploring compartmentalized energetics [50, 51, 52] [53, Pages 178-181], with each study using the above mass spectroscopy method to determine longer time ^{18}O transfer kinetics, all with the same assumption of uni-directional fluxes. The development of improved methods utilizing NMR saturation and inversion will extend the range of applicability of this powerful technique [54, 55] while reducing the labor required.

Table 1. Metabolite abbreviations within each compartment.

Metabolite	Abbreviation	
	Cytosolic	Mitochondrial
acetate	ACo	
acetyl-CoA	AcCoAo	AcCoAm
pyruvate	PYo	PYm
PY biomass precursor	PBm	
citrate/isocitrate		CIm
oxaloacetate	OAo	OAm
succinate		SUm
malate		MAm
2-oxoglutarate		OGm

4. Simulation of isotopic transients

The isotopic transient contains information about the underlying behavior of the metabolic system. The task is to build a model of the metabolic system that can best reproduce both the isotopic transient and the steady state isotopomer distribution of all metabolites. This involves finding the sizes of metabolic pools, the bi-directional rates of exchange between compartments in the cell, and the effect of bi-directional enzyme reactions on the isotopomer distribution. Of these, only the sizes of metabolic pools do not affect the steady state labeling state of the metabolites and the biomass created from them.

4.1. Composition of the metabolic network

To aid in the discussion of extracting information from isotopic transient data, we have composed a simple example of the TCA cycle with carbon enrichment found in Figure 1. Included in the metabolic scheme are atom mappings between all species including the amino acids and their respective biomass precursors, with the carbon numbers corresponding to chemical nomenclature as in Maaheimo *et al.*

[56]. Pyruvate and acetate are inflows to the system, and carbon dioxide and biomass precursors are outflows. The metabolic system is assumed to operate at steady state and is thus simulated with net flux distributions that satisfy this criteria. There are eight degrees of freedom in this system, so eight net fluxes are specified. The remaining dependent net fluxes were calculated from equations that were generated symbolically.

Figure 1. Metabolic scheme with atom mapping and bi-directional compartmentalization between mitochondria (shaded green) and cytosol. Carbon numbers correspond to chemical nomenclature and the arrows between them indicate bi-directionality. Each reaction label is given above the red arrows that indicate the assumed net positive reaction flux. Pyruvate (PYx) derived from extracellular glucose and acetate (ACx) are inflows to the system (blue), and CO_2 and amino acids are outflows(red). Metabolite abbreviations are given in Table 1. Green carbons indicate biomass precursor metabolites with mappings to the amino acids they produce. Carbons of the same color are equivalent due to molecular symmetry.

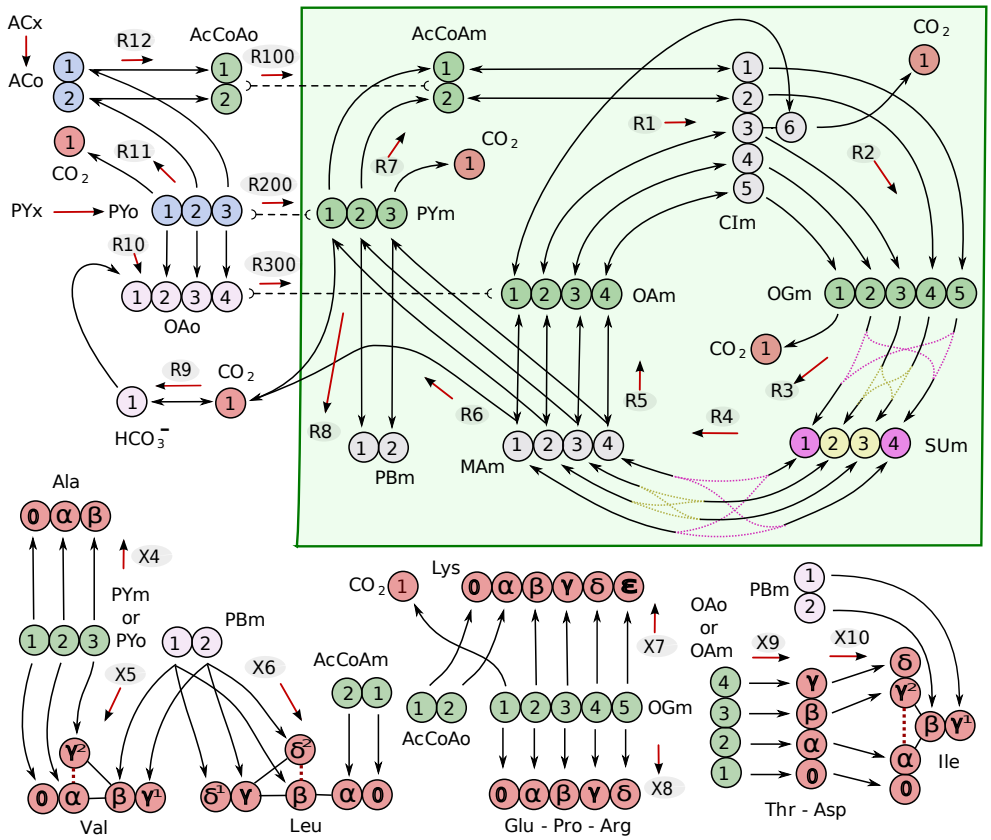

Analogous schemes can be drawn for any biological isotope including oxygen, phosphorus, and nitrogen isotopes, although the atom transitions in these networks are less well defined and functional groups

containing these elements tend to be more reactive resulting in a network with a significant number of side reactions and sinks that complicate analysis as in the above phosphotransfer network studies.

4.2. Solving for the isotopic transient state

Isotopomer balance equations can be generated from the metabolic network, and using these, an isotopic transient can be simulated. The transient is induced by a step change in any or all members of the isotopomer population distribution of all metabolites that act as inputs or outputs to the system. For isotopomers that act as outputs to the system, the bi-directionality of the exit reaction step will induce isotope labeling in reverse direction to the net flux. The isotopomer distributions of all metabolites in the system begin at the natural labeling state of 1.1% ^{13}C and end at isotopic equilibrium at an enriched ^{13}C state with steady isotopomer population distribution. Thus, the steady state isotopomer distribution for each metabolite is found from the last points of the simulation when the system has reached isotopic steady state.

We used the most direct approach to solve for the isotopic transient by numerically solving the full set of isotopomer balances. Various strategies have been devised to transform this system into an equivalent system that is computationally more efficient to solve, including the bondomer approach [57], decomposition of the network into Elementary Metabolite Units (EMU) [58], and transforming the isotopomer equations into cascaded cumomer systems [59] where lumped variables are used to represent groups of isotopomers. The 252 isotopomer balance equations in our small example network are solved in 0.4 to 6 seconds when setting the metabolic pool sizes as being equal, so use of the above methods to speed up simulation is not required in this case.

To illustrate the information one can obtain from the isotopic transient, we present two sets of simulations. Our nomenclature for isotopomers in the figures and discussion below can be summarized as follows: The carbons are numbered according to chemical nomenclature and start at the right with 0's representing ^{12}C and 1's representing ^{13}C.

The first set was obtained by continuously feeding pyruvate and acetate while performing a step change in the acetate isotopomer population from natural enrichment to 100% fully labeled $^{13}C_{1,2}$ acetate. Two simulations were made with two different sets of metabolic pool sizes (A and B). The pool sizes of all metabolites in both sets were selected at random over three orders of magnitude. All net flux and exchange flux parameters were the same in both simulations. Since only metabolic pool sizes were changed between simulations, the steady state isotopomer distribution are identical for both simulations, as expected. The isotopic transients of the most highly enriched isotopomers of mitochondrial citrate from both simulations are given in Figure 2. Comparing the transient curves for the same isotopomers between pool size set A and B, it is clear that they exhibit the same general transient shape with the main difference being the time scale of the transient. Figure 2 does not show every isotopomer, however all carbons become enriched in ^{13}C when acetate is used as the tracer illustrating the usefulness of this inexpensive tracer for studying the TCA cycle.

The second set of simulations was obtained by continuously feeding pyruvate and acetate. The three simulations were made by performing (1) a step change to fully labeled acetate as above, (2) a step change from natural enrichment to 100% fully labeled $^{13}C_{1,2,3}$ pyruvate, and (3) a step change in both

fully labeled acetate and fully labeled pyruvate together. All other parameters, including metabolic pool sizes, net fluxes, and exchange fluxes were the same in all three simulations. The citrate isotopomers from these three simulations are given in Figure 3.

Figure 2. The isotopic transient of the metabolic system given in Figure 1 was simulated with two different sets of metabolic pool sizes chosen at random over three orders of magnitude. All other parameters are the same between the two simulations. For clarity, only the isotopomers of mitochondrial citrate reaching the highest enrichment are included with their nomenclature explained in the text.

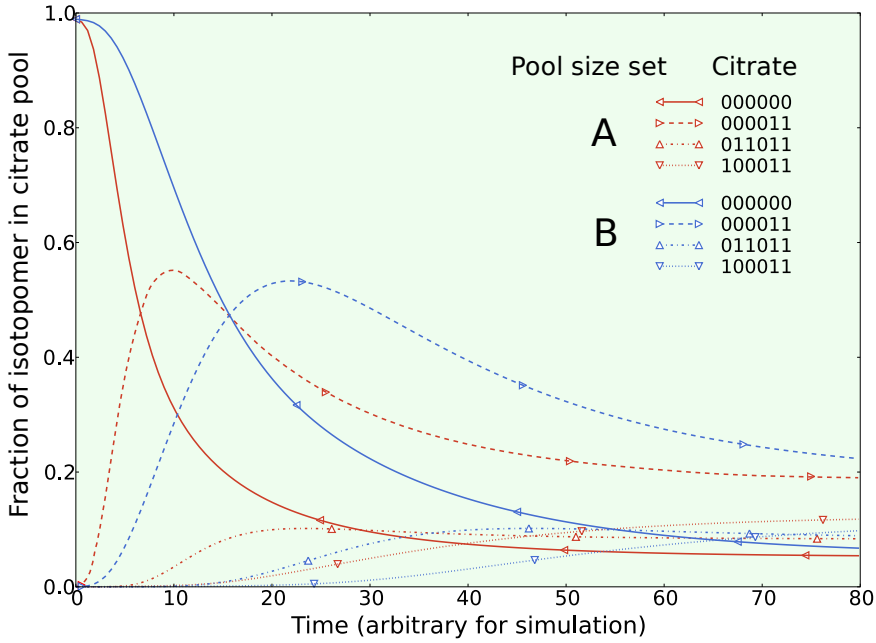

Different isotopomers from each of the three simulations display similar dynamics as the metabolic system is operating in the exact same way. Comparing the dynamics of the citrate isotopomers between the acetate and pyruvate switch, three pairs of isotopomers reach the same proportion of the steady state isotopomer population: (1) the unlabeled citrate isotopomers, (2) the 000011 and 111100 complimentary pair, and (3) the 100011 and 011100 complimentary pair. Different isotopic tracers reveal the same underlying metabolic behavior at steady state for the TCA cycle intermediates, with the dynamics revealing complimentary information.

When fully labeled acetate is fed to the metabolic system, the 000011 citrate isotopomer reveals similar dynamics as the same isotopomer when both acetate and pyruvate are fed to the metabolic system. When fully labeled pyruvate is fed to the metabolic system, the 011100 citrate isotopomer reveals similar dynamics as the 011111 citrate isotopomer when both acetate and pyruvate are fed to the system.

When both labeled acetate and labeled pyruvate enter the metabolic system, we see both types of isotopomer dynamics appear, however in this case when the isotopomer populations of pyruvate and acetate consist of 100% fully labeled compounds all information about the steady state is lost as the system becomes fully labeled. Thus the use of multiple labeling experiments on the same metabolic system under the same growth conditions is useful to study the dynamic behavior of the metabolic system, and is thus useful to gain insight into the metabolic pool sizes, compartmentalization, and the bi-directionality of metabolic fluxes.

Figure 3. Three simulations of isotopic dynamics in the metabolic system given in Figure 1 were performed with identical net flux, exchange flux, and metabolic pool sizes. Isotopic transients of mitochondrial citrate are given following a switch to: (1) fully labeled acetate, (2) fully labeled pyruvate, and (3) both fully labeled acetate and pyruvate. For clarity, only the isotopomers of mitochondrial citrate reaching the highest enrichment are included.

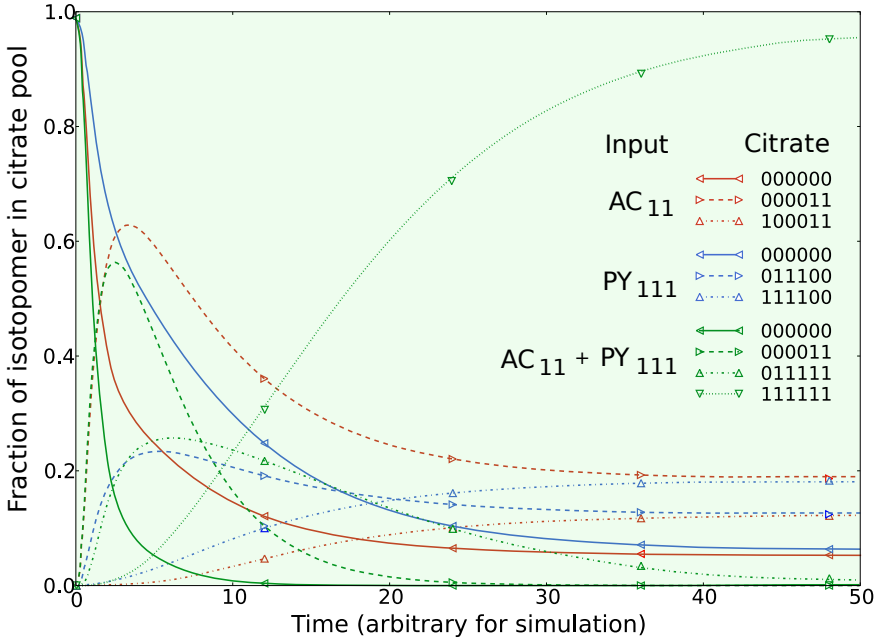

To make these two example simulations quantitative one must find the appropriate metabolite pool sizes, net fluxes, and exchange fluxes that adequately reproduce a sufficient amount of transient isotopomeric data, possibly supplemented with additional steady state isotopomeric data, measurements of metabolic pool sizes, substrate utilization rates, and biomass production rates.

5. Extracting information from isotopomeric data

Any difference between measured data and model predictions can be used in an optimization routine to find sets of net fluxes, exchange fluxes, and pool sizes that can reproduce the measured data within

experimental errors. If the optimization routine cannot obtain a realistic fit with a sufficient amount of data, the metabolic scheme must be adjusted, possibly with the inclusion of compartmentalization and the process repeated. After finding a set of model parameters that can sufficiently reproduce measured data, one can gain insight into the operation of the metabolic network.

All types of isotopomeric measurement can be compared with the output from the dynamic solver, including data collected at isotopic steady state: Mass isotopomers from mass spectrometers, NMR positional enrichments, double enrichments, triple enrichments, and beyond all contain information about the operation of the metabolic scheme. Each measurement type requires one to sum up the appropriate pool of simulated isotopomers that correspond to the measured ^{13}C enrichment probability.

It should be noted that the process of optimization is not restricted to experiments performed with one enriched substrate. Data from multiple experiments at the same metabolic state using different labeled substrates can be combined to optimize one set of parameters. In this case the optimizer must simulate the isotopomer balance equations once for every experiment with a different step change in labeled substrate using the same set of parameters, and comparing each with their respective set of experimental data. The three simulations in Figure 3 could each be matched with data collected using labeled acetate, labeled glucose or a mixture of both to optimize the single set of parameters that govern the metabolic system.

5.1. Inclusion of metabolic pool sizes

Since it is difficult to accurately measure many metabolic pools, making the transient simulation quantitative typically requires additional transient isotopic data. Using an optimization routine it is possible to find a realistic set of metabolic pool sizes that best match isotopic transient data and pool size measurements. To accomplish this, the optimizer would be allowed to manipulate all metabolic pool sizes, thus changing the isotopic transient, while attempting to minimize the difference between measured isotopomeric data and measured pool sizes. In practice one would not usually optimize only the metabolic pool sizes as one usually needs to optimize the net flux and exchange flux parameters at the same time.

Figure 2 shows a dramatic increase and then decrease in the $^{13}C_{1,2}$ isotopomer of citrate. With this in mind, transient data that is able to capture the shape and timing of major transient curves like this one are useful for constraining not only the net fluxes and bi-directionality of the metabolic network, but also metabolic pool sizes. If the pool size found by optimization does not match that measured during the experiment, it could be a clue that this metabolic pool is compartmentalized. Other clues in the shape of these transients also aid in identifying compartmentalization.

5.2. Compartmentalization is revealed in the dynamics

Information about the bi-directionality of fluxes and the compartmentalization of metabolic pools is contained in the isotopic dynamics. Compartmentalization is revealed in a number of ways. Consider a linear pathway:

$$A \rightleftharpoons B \rightleftharpoons C \quad (1)$$

If the labeling in C becomes enriched faster than B, B is compartmentalized. This means that one should optimize the flux parameters for at least two separate pools of B:

$$\begin{array}{ccccc} \mathrm{A} & \rightleftharpoons & \mathrm{B_i} & \rightleftharpoons & \mathrm{C} \\ & & \Downarrow\Uparrow & & \\ & & \mathrm{B_j} & & \end{array} \tag{2}$$

The shape of the isotopic transient depends on the exchange of B_i with B_j and their pool sizes. ATP exhibits compartmentalization in cardiomyocytes and astrocytes, as evidenced by a ^{31}P NMR saturation and inversion analysis of the creatine kinase reaction[60]:

$$\mathrm{PCr^{2-}} + \mathrm{MgADP^{-}} + \mathrm{H^{+}} \rightleftharpoons \mathrm{Cr} + \mathrm{MgATP^{2-}} \tag{3}$$

The kinetic data suggest that ATP exchanges with inorganic phosphorus and participates in other reactions via separate compartments:

$$\mathrm{PCr} \underset{k_{1r}}{\overset{k_{1f}}{\rightleftharpoons}} \gamma ATP1 \underset{k_{2r}}{\overset{k_{2f}}{\rightleftharpoons}} \mathrm{Pi} \underset{k_{3r}}{\overset{k_{3f}}{\rightleftharpoons}} \gamma ATP2 \tag{4}$$

Fitting the data to this kinetic scheme suggests the need to consider both the function of the bound enzymes and restrictions of diffusion in the system, which both may lead to localized compartmentalization. Evidence for diffusional restrictions and compartmentalization of ATP was explored by Sonnewald *et al.* [61] who observed large gradients in ATP concentration in astrocytes. Monge *et al.* [62] performed a kinetic analysis of oxidative phosphorylation in rat brain synaptosomes and mitochondria and found evidence for localized cycling of ADP and ATP between mitochondrial creatine kinase and adenine nucleotide translocase.

Localized compartmentalization of energy metabolites in cells with high energy requirements is well known [63, 64]. Kaasik *et al.* [65] studied the energy metabolism in mouse cardiomyocytes and demonstrated that this localized cycling of energy metabolites was effective enough to maintain a moderate workload even in genetically modified mice deficient in creatine kinase. These studies clearly show the functional importance of localized compartmentalization separated by diffusional barriers. Furthermore, diffusional restrictions of ADP in rat cardiomyocytes could influence the control mechanisms of oxidative phosphorylation, as shown in several modeling studies [66, 67].

Vendelin and Birkedal [68] found diffusion coefficients in rat cardiomyocytes using a fluorescently labeled ATP analogue and found them to be anisotropic. For this, raster image correlation spectroscopy (RICS) was extended to discriminate anisotropy in the diffusion tensor. Although the reason for the anisotropic diffusion is unclear, it may be related to the ordered structure of the cardiomyocytes or localized diffusional barriers. To explore these localized diffusional barriers on a cellular level using mathematical models, the accurate geometry of mitochondria within the muscle cells is required. Vendelin *et al.* [69] developed a method to analyze the two dimensional positioning of mitochondria in various muscle types, and extended this method to three dimensions in a comparative physiology study between trout and rat cardiomyocytes [70].

Compartmentalized metabolic pools may play a role in controlling shifts in metabolism. Separate cytosolic pools of pyruvate in astrocytes have been observed to switch between acting as the precursor

for energy production depending on the substrate being consumed [71]. In general compartmentalization is more complex than we have previously assumed and we may only be scratching the surface with regards to studying compartmentalized metabolism in cellular systems. With this view it is hard to avoid introducing realistic kinetic schemes into dynamic flux analysis.

5.3. Example optimization of the TCA cycle in yeast

To illustrate the process of extracting information from isotopomeric data using isotopic simulation coupled with optimization, we have included a simple example of the TCA cycle in *Saccharomyces uvarum*. This example introduces the basic process of extracting information from isotopomeric data and does not include many details in the modeling process such as sensitivity analysis and a through discussion of the flux parameters found. Judicious analysis of this system will require a separate publication.

The metabolic system is given in Figure 1 and was optimized using a non-linear constraint optimizer [72] using data collected by Paalme *et al.* [73]. We optimize a subset of their data where they performed a step change to fully labeled acetate while feeding yeast a mixture of glucose and acetate. Paalme *et al.* [73] measured ^{13}C NMR absolute and conditional enrichments from the carbon skeleton of proteinogenic amino acids harvested and hydrolyzed at isotopic steady state. This excludes the optimization of pool sizes so they have all been set to be equal to simplify simulation, and all comparisons to measured data were made at the last time point simulated after all isotopic dynamics reached steady state.

We have included measurements of the rate of biomass production from all TCA metabolites in Figure 1 to constrain the net fluxes that exit the system. These net fluxes include all biomass production, including production of amino acids, nucleic acids, and lipids, however, only amino acids are included in the metabolic scheme since it was their isotopomers that were used to constrain the isotopic steady state. By not constraining the metabolic system explicitly using the biomass production rates the optimizer is given more flexibility to find better solutions by roaming around the full flux parameter space.

The optimization was carried out with the following reactions set to be bi-directional: malate dehydrogenase (EC 1.1.1.37), fumerase (EC 4.2.1.2), citrate synthase (EC 2.3.3.1), and the three transport reactions for oxaloacetate, pyruvate, and acetyl-coenzyme A. All reactions involving carbon dioxide, except for the bi-directional production of bicarbonate via carbonic anhydrase (EC 4.2.1.1), were set to be uni-directional.

By starting at a large number of plausible starting points selected at random over the range of the free flux parameters, the optimizer always settled on one single optimal solution and occasionally stopped at a few other local optima that did not reproduce the data very well. Changing the weighting of measured data points within the optimizer and excluding one or two at random did not significantly change the optimal solution found as this solution matched all available data quite well. The optimal fit to the isotopomeric data is given in Figure 4. It is immediately seen that the fit between the NMR data and the model predictions is very good. This means that this metabolic system can adequately account for the observed labeling pattern and no important elements of the metabolic system are missing. With regards to net fluxes, the optimal fit matches that found in [73].

With respect to bi-directional reactions, malate dehydrogenase was found to be very bi-directional with $\frac{\nu_{5f}}{\nu_{5r}} = 1.3$, while the ratio for fumerase $\frac{\nu_{4f}}{\nu_{4r}} = 575.0$. The transport of pyruvate was found to be quite reversible with $\frac{\nu_{200f}}{\nu_{200r}} = 1.2$, while the transport of acetyl-coenzyme A was much less reversible with $\frac{\nu_{100f}}{\nu_{100r}} = 12.4$, and the transport of oxaloacetate was found to be essentially uni-directional.

Figure 4. Optimization of example system with absolute and conditional ^{13}C NMR data. Simulated points are marked with stars and measured data are marked with circles. Absolute enrichments are written with one carbon label, and conditional enrichments have a second carbon label. Conditional enrichment is the probability of ^{13}C enrichment in the first carbon when the second carbon is a ^{13}C.

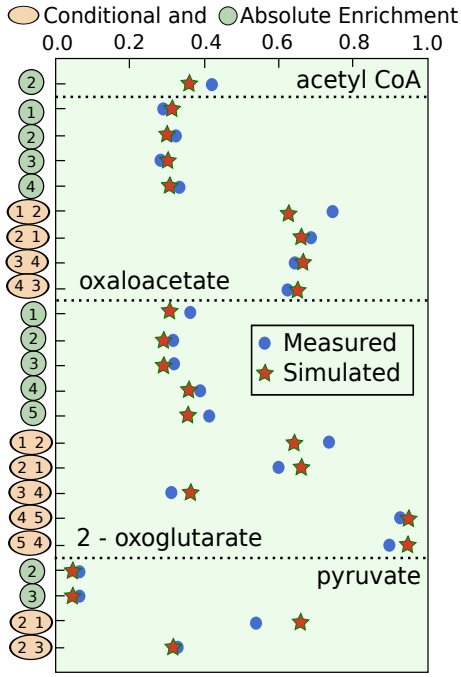

The pyruvate fit was the least perfect and the fit required the pyruvate transporter (R200) to be bidirectional. This may be telling us that the assumption that mitochondrial pyruvate is the sole precursor for Ala production is not entirely true, although at least some production of Ala from mitochondrial pyruvate is required to fit the data. Ala is produced from cytosolic pyruvate during fermentative growth so it is possible that both mitochondrial and cytosolic pyruvate act as precursors for Ala production, but this must be confirmed with additional data and future simulations possibly with the inclusion of an additional compartmentalized pool.

Pyruvate is a metabolite that participates in a large number of intersecting central metabolic pathways, typically has a low intra-cellular concentration, and has been observed to exhibit multiple cytoplasmic compartments along with mitochondrial compartmentalization [71, 74]. This hub metabolite may be

compartmentalized in a more complicated way than has been supposed and should be studied with a larger data set containing dynamic isotopic transients.

The steady state isotopomer profiles of the cytosolic and mitochondrial pools of oxaloacetate are given in Figure 5. The labeling pattern in each compartment is quite different and has important implications for the origin of Asp biosynthesis as discussed by Paalme *et al.* [73]. These simulations support the previous findings that Asp synthesis originates from mitochondrial oxaloacetate since no adequate set of net flux and exchange flux parameters could be found that give a steady state isotopomer profile for cytosolic oxaloacetate that matched with the measured enrichments in the respective carbons in Thr and Ile [73].

To make the transient of this optimization quantitative we would have to include slow bi-directional exchange with storage compounds, since this has been found to dramatically influence the time scale of isotopic dynamics. The isotopic dynamics of TCA cycle metabolites such as 2-oxoglutarate, succinate, fumerate, glutamate, and aspartate, are all influenced by reversible aminotransferase reactions that transfer amino groups from α-amino acids to α-keto acids [12]. This makes the isotopic dynamics in the TCA cycle on the same temporal order of magnitude as reaching steady-state isotopomer labeling in the biomass. Accurate simulation of short time TCA dynamics requires a long term dynamic component that can only be quantified with labeling data from a long labeling experiment. Without accurate steady state labeling data, the interpretation of short term labeling experiments is difficult [75].

Figure 5. Simulated steady state isotopomer distribution of mitochondrial and cytosolic oxaloacetate. Since the isotopomers differ between compartments comparing the simulation with measured data can help determine the functional location of biosynthesis reactions.

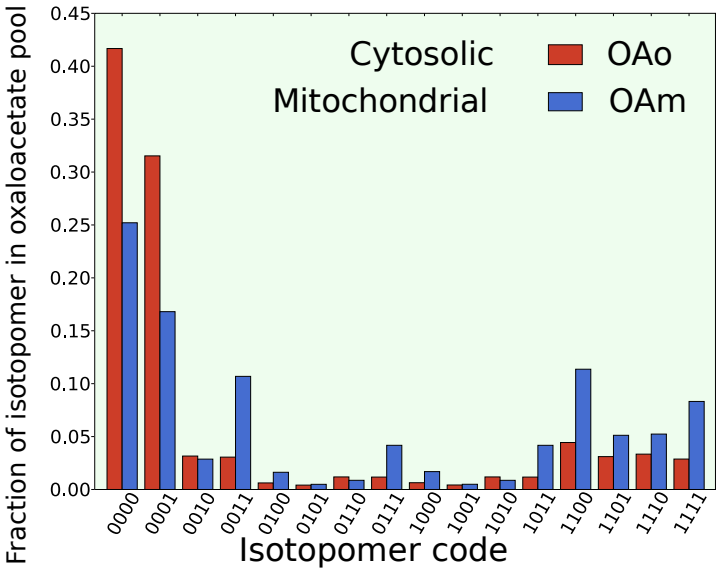

6. Conclusions

We have shown that dynamic isotopic transients reveal important insights into the operation of metabolic networks, including the bi-directionality of enzyme and transport reactions, and the compartmentalization of metabolites, including localized compartmentalization not separated by a membrane barrier and that caused by diffusional restrictions. Our optimization of the TCA cycle illustrates that using dynamic isotopic models does not complicate the analysis of steady state isotopomeric data if the transient part of the simulation is excluded, and the possibility for additional insight with the inclusion of only a small amount of transient data should not be overlooked. Models that make use of isotopic transient data are expected to become increasingly important as steady state isotopomeric models currently struggle with the realities of compartmentalization.

The predicted rise in the use of dynamic models is supported by the rapid development of analytical techniques to measure both isotopomeric transients and the kinetics of individual reactions *in vivo*. Numerical tools are also developing rapidly, however the current state of dynamic modeling continues to grapple with the difficulties of compartmentalization. Teasing out the details of compartmentalization using dynamic models involves the addition of more parameters. When introducing such parameters, the structural identifiability of the model must be preserved so that biological insight can be extracted from the measured data. This is a challenge for large metabolic systems and can only be accomplished by including as much information as possible to constrain the trajectories of the model solution. Examples include thermodynamic constraints, constraints on the pool sizes, integration of known kinetic information, and the fitting of isotopomeric data from as many experiments as possible.

Although a vast amount of kinetic detail is required to build predictive kinetic models, their use within isotopic transient models is expected to improve and expand phenomenological MFA. It is hoped that fundamental kinetic studies will once again become a funding priority and through their continuation support the use of kinetic schemes within realistically sized metabolic models, since the marriage of kinetics and MFA is predicted to become an ever increasingly important tool in systems biology.

Acknowledgments

This work was supported in part by Wellcome Trust Fellowship WT081755MA, and the Estonian Science Foundation grant ETF7344.

References and Notes

1. Henry, P.; Oz, G.; Provencher, S.; Gruetter, R. Toward dynamic isotopomer analysis in the rat brain *in vivo*: automatic quantitation of ^{13}C NMR spectra using LCModel. *NMR Biomed.* **2003**, *16*, 400-412.
2. Rodrigues, T.B.; Cerdan, S. ^{13}C MRS: an outstanding tool for metabolic studies. *Concepts Magn. Reson. Part A* **2005**, *27A*, 1-16.
3. Hellerstein, M. In vivo measurement of fluxes through metabolic pathways: The missing link in functional genomics and pharmaceutical research. *Ann. Rev. Nutr.* **2003**, *23*, 379-402.

4. Iwatani, S.; Yamada, Y.; Usuda, Y. Metabolic flux analysis in biotechnology processes. *Biotechnol. Lett.* **2008**, *30*, 791-799.
5. Prather, K. L.J.; Martin, C.H. *De novo* biosynthetic pathways: rational design of microbial chemical factories. *Curr. Opin. Biotechnol.* **2008**, *19*, 468-474.
6. Blank, L.M.; Lehmbeck, F.; Sauer, U. Metabolic-flux and network analysis in fourteen hemiascomycetous yeasts. *FEMS Yeast Res.* **2005**, *5*, 545-558.
7. Vo, T.D.; Lim, S.K.; Lee, W. N.P.; Palsson, B.O. Isotopomer analysis of cellular metabolism in tissue culture: A comparative study between the pathway and network-based methods. *Metabolomics* **2006**, *2*, 243-256.
8. Allen, D.K.; Shachar-Hill, Y.; Ohlrogge, J.B. Compartment-specific labeling information in ^{13}C metabolic flux analysis of plants. *Phytochemistry* **2007**, *68*, 2197-2210.
9. Kruger, N.J.; Lay, P.L.; Ratcliffe, R.G. Vacuolar compartmentation complicates the steady-state analysis of glucose metabolism and forces reappraisal of sucrose cycling in plants. *Phytochemistry* **2007**, *68*, 2189-2196.
10. Stelling, J.; Sauer, U.; Szallasi, Z.; Doyle, F.J., III.; Doyle, J. Robustness of cellular functions. *Cell* **2004**, *118*, 675-685.
11. Schaub, J.; Mauch, K.; Reuss, M. Metabolic flux analysis in escherichia coli by integrating isotopic dynamic and isotopic stationary ^{13}C labeling data. *Biotechnol. Bioeng.* **2008**, *99*, 1170-1185.
12. Grotkjaer, T.; Akesson, M.; Christensen, B.; Gombert, A.K.; Nielsen, J. Impact of transamination reactions and protein turnover on labeling dynamics in ^{13}C-labeling experiments. *Biotechnol. Bioeng.* **2004**, *86*, 209-216.
13. Den Hollander, J.A.; Behar, K.L.; Shulman, R.G. ^{13}C NMR study of transamination during acetate utilization by saccharomyces cerevisiae. *Proc. Natl. Acad. Sci. USA* **1981**, *78*, 2693-2697.
14. Wiechert, W.; Noh, K. From stationary to instationary metabolic flux analysis. *Adv. Biochem. Eng. Biotechnol.* **2005**, *92*, 145-172.
15. Matsuda, F.; Wakasa, K.; Miyagawa, H. Metabolic flux analysis in plants using dynamic labeling technique: Application to tryptophan biosynthesis in cultured rice cells. *Phytochemistry* **2007**, *68*, 2290-2301.
16. Heinzle, E.; Matsuda, F.; Miyagawa, H.; Wakasa, K.; Nishioka, T. Estimation of metabolic fluxes, expression levels and metabolite dynamics of a secondary metabolic pathway in potato using label pulse-feeding experiments combined with kinetic network modelling and simulation. *Plant J.* **2007**, *50*, 176-187.
17. Shastri, A.; Morgan, J. A transient isotopic labeling methodology for ^{13}C metabolic flux analysis of photo auto trophic microorganisms. *Phytochemistry* **2007**, *68*, 2302-2312.
18. Ratcliffe, R.; Shachar-Hill, Y. Measuring multiple fluxes through plant metabolic networks. *Plant J.* **2006**, *45*, 490-511.
19. Rios-Estepa, R.; Lange, B.M. Experimental and mathematical approaches to modeling plant metabolic networks. *Phytochemistry* **2007**, *68*, 2351-2374.

20. Kresnowati, M.T.A.P.; van Winden, W.A.; Almering, M.J.H.; ten Pierick, A.; Ras, C.; Knijnenburg, T.A.; Daran-Lapujade, P.; Pronk, J.T.; Heijnen, J.J.; Daran, J.M. When transcriptome meets metabolome: fast cellular responses of yeast to sudden relief of glucose limitation. *Mol. Syst. Biol.* **2006**, *2*, No. 49.
21. Wahl, S.; Noh, K.; Wiechert, W. ^{13}C labeling experiments at metabolic nonstationary conditions: An exploratory study. *BMC Bioinf.* **2008**, *9*.
22. Baxter, C.; Liu, J.; Fernie, A.; Sweetlove, L. Determination of metabolic fluxes in a non-steady-state system. *Phytochemistry* **2007**, *68*, 2313-2319.
23. Tu, B.P.; McKnight, S.L. Metabolic cycles as an underlying basis of biological oscillations. *Nat. Rev. Mol. Cell Biol.* **2006**, *7*, 696-701.
24. Murray, D.B.; Beckmann, M.; Kitano, H. Regulation of yeast oscillatory dynamics. *Proc. Natl. Acad. Sci. USA* **2007**, *104*, 2241-2246.
25. Tu, B.P.; Kudlicki, A.; Rowicka, M.; McKnight, S.L. Logic of the yeast metabolic cycle: Temporal compartmentalization of cellular processes. *Science* **2005**, *310*, 1152-1158.
26. Visser, D.; van Zuylen, G.A.; van Dam, J.C.; Oudshoorn, A.; Eman, M.R.; Ras, C.; van Gulik, W.M.; Frank, J.; van Dedem, G. W.K.; Heijnen, J.J. Rapid sampling for analysis of *in vivo* kinetics using the BioScope: a system for continuous-pulse experiments. *Biotechnol. Bioeng.* **2002**, *79*, 674-681.
27. Kholodenko, B.N. Cell-signalling dynamics in time and space. *Nat. Rev. Mol. Cell Biol.* **2006**, *7*, 165-176.
28. Vendelin, M.; Kongas, O.; Saks, V. Regulation of mitochondrial respiration in heart cells analyzed by reaction-diffusion model of energy transfer. *Am. J. Physiol. Cell. Physiol.* **2000**, *278*, C747-C764.
29. Saks, V.; Kongas, O.; Vendelin, M.; Kay, L. Role of the creatine/phosphocreatine system in the regulation of mitochondrial respiration. *Acta Physiol. Scand.* **2000**, *168*, 635-641.
30. Selivanov, V.; Sukhomlin, T.; Centelles, J.; Lee, P.; Cascante, M. Integration of enzyme kinetic models and isotopomer distribution analysis for studies of in situ cell operation. *BMC Neurosci.* **2006**, *7*, S7.
31. Liebermeister, W.; Klipp, E. Bringing metabolic networks to life: integration of kinetic, metabolic, and proteomic data. *Theor. Biol. Med. Model.* **2006**, *3*, 42.
32. McConnell, H.M. Reaction rates by nuclear magnetic resonance. *J. Chem. Phys.* **1958**, *28*, 430-431.
33. Forsen, S.; Hoffman, R.A. Study of moderately rapid chemical exchange reactions by means of nuclear magnetic double resonance. *J. Chem. Phys.* **1963**, *39*, 2892-2901.
34. Led, J.; Gesmar, H. The applicability of the magnetization transfer NMR technique to determine chemical-exchange rates in extreme cases - the importance of complementary experiments. *J. Magn. Reson.* **1982**, *49*, 444-463.
35. Ugurbil, K. Magnetization-transfer measurements of individual rate constants in the presence of multiple reactions. *J. Magn. Reson.* **1985**, *64*, 207-219.
36. Brindle, K.M. NMR methods for measuring enzyme kinetics *in vivo*. *Prog. Nucl. Magn. Reson. Spectrosc.* **1988**, *20*, 257-293.

37. Ugurbil, K.; Petein, M.; Maidan, R.; Michurski, S.; From, A. Measurement of an individual rate-constant in the presence of multiple exchanges - application to myocardial creatine-kinase reaction. *Biochemistry* **1986**, *25*, 100-107.
38. Spencer, R.G.; Balschi, J.A.; Leigh, J.S.; Ingwall, J.S. ATP synthesis and degradation rates in the perfused rat heart. ^{31}P-nuclear magnetic resonance double saturation transfer measurements. *Biophys. J.* **1988**, *54*, 921-929.
39. Koretsky, A.; Weiner, M. *^{31}Phosphorus nuclear magnetic resonance magnetization transfer measurements of exchange reactions in vivo;* Radiology Research and Education Foundation: San Francisco, CA, USA, 1984; pp. 209-230.
40. Joubert, F.; Hoerter, J.A.; Mazet, J. Discrimination of cardiac subcellular creatine kinase fluxes by NMR spectroscopy: A new method of analysis. *Biophys. J.* **2001**, *81*, 2995-3004.
41. Joubert, F.; Mazet, J.; Mateo, P.; Hoerter, J.A. ^{31}P NMR detection of subcellular creatine kinase fluxes in the perfused rat heart. contractility modifies energy transfer pathways. *J. Biol. Chem.* **2002**, *277*, 18469-18476.
42. Ventura-Clapier, R.; Garnier, A.; Veksler, V. Energy metabolism in heart failure. *J Physiol.* **2004**, *555*, 1-13.
43. Dawis, S.; Walseth, T.; Deeg, M.; Heyman, R.; Graeff, R.; Goldberg, N. Adenosine triphosphate utilization rates and metabolic pool sizes in intact cells measured by transfer of ^{18}O from water. *Biophys. J.* **1989**, *55*, 79-99.
44. Zeleznikar, R.; Heyman, R.; Graeff, R.; Walseth, T.; Dawis, S.; Butz, E.; Goldberg, N. Evidence for compartmentalized adenylate kinase catalysis serving a high energy phosphoryl transfer function in rat skeletal muscle. *J. Biol. Chem.* **1990**, *265*, 300-311.
45. Zeleznikar, R.; Goldberg, N. Kinetics and compartmentation of energy-metabolism in intact skeletal-muscle determined from ^{18}O labeling of metabolite phosphoryls. *J. Biol. Chem.* **1991**, *266*, 15110-15119.
46. Zeleznikar, R.J.; Goldberg, N.D. Adenylate kinase-catalyzed phosphoryl transfer couples ATP utilization with its generation by glycolysis in intact muscle. *J. Biol. Chem.* **1995**, *270*, 7311-7319.
47. Dzeja, P.P.; Zeleznikar, R.J.; Goldberg, N.D. Suppression of creatine kinase-catalyzed phosphotransfer results in increased phosphoryl transfer by adenylate kinase in intact skeletal muscle. *J. Biol. Chem.* **1996**, *271*, 12847-12851.
48. Dzeja, P.P.; Zeleznikar, R.J.; Goldberg, N.D. Adenylate kinase: Kinetic behavior in intact cells indicates it is integral to multiple cellular processes. *Mol. Cell. Biochem.* **1998**, *184*, 169-182.
49. Pucar, D.; Janssen, E.; Dzeja, P.P.; Juranic, N.; Macura, S.; Wieringa, B.; Terzic, A. Compromised energetics in the adenylate kinase AK1 gene knockout heart under metabolic stress. *J. Biol. Chem.* **2000**, *275*, 41424-41429.
50. Pucar, D.; Dzeja, P.P.; Bast, P.; Juranic, N.; Macura, S.; Terzic, A. Cellular energetics in the preconditioned state. protective role for phosphotransfer reactions captured by ^{18}O-assisted ^{31}P NMR. *J. Biol. Chem.* **2001**, *276*, 44812-44819.
51. Pucar, D.; Bast, P.; Gumina, R.J.; Lim, L.; Drahl, C.; Juranic, N.; Macura, S.; Janssen, E.; Wieringa, B.; Terzic, A.; Dzeja, P.P. Adenylate kinase AK1 knockout heart: energetics and functional performance under ischemia-reperfusion. *Am. J. Physiol. Heart. Circ. Physiol.* **2002**, *283*, H776-H782.

52. Pucar, D.; Dzeja, P.; Bast, P.; Gumina, R.; Drahl, C.; Lim, L.; Juranic, N.; Macura, S.; Terzic, A. Mapping hypoxia-induced bioenergetic rearrangements and metabolic signaling by ^{18}O-assisted ^{31}P NMR and ^{1}H NMR spectroscopy. *Mol. Cell. Biochem.* **2004**, *256-257*, 281-289.
53. Abstracts from the workshop: *Non invasive investigation of muscle function*. Marseille France, October 4-6, 2001, MAGMA. 2002, May; 14, 59-212.
54. Bollard, M.E.; Murray, A.J.; Clarke, K.; Nicholson, J.K.; Griffin, J.L. A study of metabolic compartmentation in the rat heart and cardiac mitochondria using high-resolution magic angle spinning ^{1}H NMR spectroscopy. *FEBS Lett.* **2003**, *553*, 73-78.
55. Thelwall, P.E. Detection of ^{17}O-tagged phosphate by ^{31}P MRS: a method with potential for *in vivo* studies of phosphorus metabolism. *Magn. Reson. Med.* **2007**, *57*, 1168-1172.
56. Maaheimo, H.; Fiaux, J.; Cakar, Z.; Bailey, J.; Sauer, U.; Szyperski, T. Central carbon metabolism of saccharomyces cerevisiae explored by biosynthetic fractional ^{13}C labeling of common amino acids. *Eur. J. Biochem.* **2001**, *268*, 2464-2479.
57. Sriram, G.; Fulton, D.B.; Shanks, J.V. Flux quantification in central carbon metabolism of catharanthus roseus hairy roots by ^{13}C labeling and comprehensive bondomer balancing. *Phytochemistry* **2007**, *68*, 2243-2257.
58. Young, J.; Walther, J.; Antoniewicz, M.; Yon, H.; Stephanopoulos, G. An elementary metabolite unit (EMU) based method of isotopically nonstationary flux analysis. *Biotechnol. Bioeng.* **2008**, *99*, 686-699.
59. Wiechert, W.; Wurzel, M. Metabolic isotopomer labeling systems - Part I: global dynamic behavior. *Math. Biosci.* **2001**, *169*, 173-205.
60. Joubert, F.; Gillet, B.; Mazet, J.; Mateo, P.; Beloeil, J.; Hoerter, J. Evidence for myocardial ATP compartmentation from NMR inversion transfer analysis of creatine kinase fluxes. *Biophys. J.* **2000**, *79*, 1-13.
61. Sonnewald, U.; Schousboe, A.; Qu, H.; Waagepetersen, H.S. Intracellular metabolic compartmentation assessed by ^{13}C magnetic resonance spectroscopy. *Neurochem. Int.* **2004**, *45*, 305-310.
62. Monge, C.; Beraud, N.; Kuznetsov, A.; Rostovtseva, T.; Sackett, D.; Schlattner, U.; Vendelin, M.; Saks, V. Regulation of respiration in brain mitochondria and synaptosomes: restrictions of ADP diffusion in situ, roles of tubulin, and mitochondrial creatine kinase. *Mol. Cell. Biochem.* **2008**, *318*, 147-165.
63. Seppet, E.K.; Kaambre, T.; Sikk, P.; Tiivel, T.; Vija, H.; Tonkonogi, M.; Sahlin, K.; Kay, L.; Appaix, F.; Braun, U.; Eimre, M.; Saks, V.A. Functional complexes of mitochondria with Ca,MgATPases of myofibrils and sarcoplasmic reticulum in muscle cells. *Biochim. Biophys. Acta* **2001**, *1504*, 379-395.
64. Saks, V.A.; Kaambre, T.; Sikk, P.; Eimre, M.; Orlova, E.; Paju, K.; Piirsoo, A.; Appaix, F.; Kay, L.; Regitz-Zagrosek, V.; Fleck, E.; Seppet, E. Intracellular energetic units in red muscle cells. *Biochem. J.* **2001**, *356*, 643657.
65. Kaasik, A.; Veksler, V.; Boehm, E.; Novotova, M.; Minajeva, A.; Ventura-Clapier, R. Energetic crosstalk between organelles: Architectural integration of energy production and utilization. *Circ. Res.* **2001**, *89*, 153-159.

66. Saks, V.; Kuznetsov, A.; Andrienko, T.; Usson, Y.; Appaix, F.; Guerrero, K.; Kaambre, T.; Sikk, P.; Lemba, M.; Vendelin, M. Heterogeneity of ADP diffusion and regulation of respiration in cardiac cells. *Biophys. J.* **2003**, *84*, 3436-3456.
67. Vendelin, M.; Eimre, M.; Seppet, E.; Peet, N.; Andrienko, T.; Lemba, M.; Engelbrecht, J.; Seppet, E.; Saks, V. Intracellular diffusion of adenosine phosphates is locally restricted in cardiac muscle. *Mol. Cell. Biochem.* **2004**, *256-257*, 229-241.
68. Vendelin, M.; Birkedal, R. Anisotropic diffusion of fluorescently labeled ATP in rat cardiomyocytes determined by raster image correlation spectroscopy. *Am. J. Physiol. Cell. Physiol.* **2008**, *295*, C1302-C1315.
69. Vendelin, M.; Beraud, N.; Guerrero, K.; Andrienko, T.; Kuznetsov, A.V.; Olivares, J.; Kay, L.; Saks, V.A. Mitochondrial regular arrangement in muscle cells: a "crystal-like" pattern. *Am. J. Physiol. Cell. Physiol.* **2005**, *288*, C757-C767.
70. Birkedal, R.; Shiels, H.A.; Vendelin, M. Three-dimensional mitochondrial arrangement in ventricular myocytes: from chaos to order. *Am. J. Physiol. Cell Physiol.* **2006**, *291*, C1148-C1158.
71. Cruz, F.; Villalba, M.; Garcia-Espinosa, M.A.; Ballesteros, P.; Bogonez, E.; Satrustegui, J.; Cerdin, S. Intracellular compartmentation of pyruvate in primary cultures of cortical neurons as detected by ^{13}C NMR spectroscopy with multiple ^{13}C labels. *J. Neurosci. Res.* **2001**, *66*, 771-781.
72. Wächter, A.; Biegler, L. On the implementation of an interior-point filter line-search algorithm for large-scale nonlinear programming. *Math. Program.* **2006**, *106*, 25-57.
73. Paalme, T.; Nisamedtinov, I.; Abner, K.; Laht, T.; Drews, M.; Pehk, T. Application of ^{13}C -[2] - and ^{13}C -[1,2] acetate in metabolic labelling studies of yeast and insect cells. *Antonie van Leeuwenhoek* **2006**, *89*, 443-457.
74. Cline, G.W.; LePine, R.L.; Papas, K.K.; Kibbey, R.G.; Shulman, G.I. ^{13}C NMR isotopomer analysis of anaplerotic pathways in INS-1 cells. *J. Biol. Chem.* **2004**, *279*, 44370-44375.
75. Noh, K.; Gronke, K.; Luo, B.; Takors, R.; Oldiges, M.; Wiechert, W. Metabolic flux analysis at ultra short time scale: Isotopically non-stationary ^{13}C labeling experiments. *J. Biotechnol.* **2007**, *129*, 249-267.

PUBLICATION II

Illaste A, Kalda M, Schryer DW, Sepp M.

Life of mice - development of cardiac energetics.

Journal of Physiology, 588(Pt 23):4617-9, (2010)

JOURNAL CLUB

Life of mice – development of cardiac energetics

Ardo Illaste, Mari Kalda, David W. Schryer and Mervi Sepp
Laboratory of Systems Biology, Institute of Cybernetics at Tallinn University of Technology, Akadeemia tee 21, 12618, Tallinn, Estonia

Email: ardo@sysbio.ioc.ee

Production and transfer of metabolites like ATP and phosphocreatine within cardiomyocytes is crucial for the robust availability of mechanical work. In mammalian cardiomyocytes, mitochondria, the main suppliers of usable chemical energy in the form of ATP, are situated adjacent to both the ATPases near the mechanical apparatus, and the sarco(endo)plasmic reticulum Ca^{2+}-ATPase (SERCA) calcium pumps. Operation of these ATPases requires a high ATP/ADP ratio, which is maintained by two parallel energy transfer systems – creatine kinase (CK) and direct adenine nucleotide channelling (DANC). Compartmentation of energy metabolites works to lessen the impact of dynamic changes in the availability of usable energy on the operation of these ATPases, and allows for a higher phosphorylation potential where it is required most.

The operational mechanism, structure and development of the barriers responsible for energetic compartmentation within cardiomyocytes have yet to be elucidated despite intensive research in this area. A recent article in *The Journal of Physiology* by Piquereau *et al.* (2010) is an extensive investigation into how the structural and energetic properties of mouse heart muscle change during postnatal development. It includes observations on structural changes and cellular morphology using electron microscopy, quantification of mitochondrial, myofibrillar and SR proteins, assessment of organelle functionality, and the quantification of the energy flux in both the CK and DANC transfer systems. SERCA function was measured via calcium mediated tension generation, while myosin ATPase function was quantified by measuring rigor tension development. Total activity of CK and mitochondrial CK (mi-CK) were estimated.

The article by Piquereau *et al.* builds upon a strong research tradition at Inserm U769, Univ. Paris-Sud, which focuses on studying how cardiac mechanisms function in response to both pathological and physiological stimuli. This includes work on contractile, sarcoplasmic reticulum (SR), and mitochondrial proteins, membrane receptors, ion channels and signalling. Their work has inspired new areas of inquiry into the function of energy compartmentation in the heart with various implications for therapeutic targets to improve both function and clinical outcomes.

As main results of their recent publication, Piquereau *et al.* concluded that the formation of energetic microdomains occurs very early in postnatal development, and that the maturation of cellular architecture plays an important role in achieving maximal flexibility in regulation of ATP production by mitochondria. They found that the development of regulatory energetic pathways does not happen simultaneously. Throughput of energy transfer between mitochondria and myosin ATPases is correlated with the changes in the cytoarchitecture in contrast to the CK supported energy transfer which seems to depend on specific localization and expression of CK. Development between days 3 and 7 is crucial in increasing the capacity of energy transfer and involves major remodelling of the contacts between organelles. The density of intracellular organelles increases at the expense of free cytosolic space. Contacts between mitochondria and longitudinally oriented myofibrils and between SR and mitochondria are established to form an effective intracellular energetic unit. After the first week (*post natum*), a different phase of hypertrophy occurs without major structural changes to the contacts between organelles. After 3 weeks, the respiratory capacity of mitochondria increases, whereas heart weight to body weight ratio decreases. The main results of the article are summarized in Fig. 1.

Considerable effort has been invested by Piquereau *et al.* in determining various changes during cardiomyocyte maturation. Several questions arise, however, when comparing the publication with previous studies. Firstly, in 3-day-old cells, based on results from electron microscopy and SR protein expression experiments, the authors deduce SR not to be present in quantities high enough to enable SR Ca^{2+} content measurement. However, volume measurements from electron microscopy are known to be very sensitive to sample preparation procedures, especially as dimensions of different organelles can change in different ratios as a result of fixation. The low level of SR protein expression in 3-day-old cells could be explained by results obtained in embryonic mouse cardiomyocytes (Takeshima *et al.* 1998), where SR Ca^{2+} release channels do not play a major role in excitation–contraction (EC) coupling but, instead, are required for cellular Ca^{2+} homoestasis. Full SR function develops rapidly in neonates, possibly explaining both the dramatic increase in SR Ca^{2+} content between day 3 and day 7 fibres, and the difficulty the authors had in conducting the experiment with fibres from 3-day-old mice.

Secondly, the authors concluded that the functional coupling of adenine nucleotide translocase (ANT) and mi-CK ('functional activity' in Piquereau *et al.* 2010) was considerably higher in adult myocytes. This conclusion, however, seems to be based on misinterpreting the K_{mADP}/K_{Cr} ratio graph (article Fig. 5*F*). As is evident from the K_m plots in the article (article Fig. 5E), K_{mCr} is constant throughout the ageing process, whereas K_{mADP} increases notably in older fibres. The increase in K_{mADP}/K_{Cr} ratio stems from the increase of K_{mADP} and is not, in this case, indicating increases in mi-CK–ANT coupling nor mi-CK activity. Rather, it can be interpreted as indication of an increase in diffusion restrictions to adenine nucleotides in the cytosol caused by changes in either mitochondrial outer membrane or myofibrillar and other cytosolic structures, or both (Vendelin & Birkedal, 2008; Sepp *et al.* 2010). In order to measure the coupling between mi-CK and ANT, different experimental techniques need to be employed, such as measuring changes in respiration in response to ATP titration.

Two observations can be made from further analysing SR calcium uptake and rigor tension sensitivity results from the article (article Figs 2 and 4). By looking at ratios of values obtained during different

DOI: 10.1113/jphysiol.2010.199901

conditions, it is possible to eliminate auxiliary effects and focus on how the role of energy supply pathways change in relation to one another as the cell matures. Two examples are given in Fig. 1 (bottom row). Firstly, from the difference in rigor tension levels ($\Delta pMgATP_{50}$) supported by CK and ATP energy supply systems (Fig. 1, line b), it is evident that myosin ATPase activity supported by CK is consistently higher than exogenous ATP throughout the growing process. On the other hand, the capacity of the CK system to load the SR increases ~2 times by day 61 (Fig. 1, line d). We suggest that this is further evidence of the role of SR transitioning from maintaining Ca^{2+} homoestasis (Takeshima *et al.* 1998) to playing an essential role in EC coupling. A possible explanation for this could be activation of SR-bound CK by day 21, whereas myofibril bound CK is already active from day three. Secondly, $pMgATP_{50}$(DANC) – $pMgATP_{50}$(ATP) (Fig. 1, line a) indicates that after an initial increase caused by changes in mitochondrial positioning, myofibrils stay constantly more sensitive to stimulation via direct channelling compared to exogenous ATP. At the same time, however, direct channelling is able to maintain an increasingly higher SR load than exogenous ATP (Fig. 1, line c). This can be explained by structural changes in the cell, whereby SR becomes more closely situated with respect to mitochondria (article Fig. 8*D*). Clearly, these interpretations should be verified through further experiments and modelling.

Building on results obtained by Piquereau *et al.* some directions could be explored in the future. One matter of interest would be how the role of glycolysis changes during maturation. It has been shown that embryonic mouse heart responds in a similar manner to inhibition of either glycolysis or oxidative phosphorylation and that in early stages of postnatal development, ATP consumed by ion pumps is preferentially supplied through glycolysis (Chen *et al.* 2007). Additionally, in 1-day-old rabbit, 44% of consumed ATP comes from glycolysis, whereas by day 7 this goes down to 7% (Lopaschuk *et al.* 1992). In the paper under discussion, the possible contribution of glycolysis to ATP supply was not directly addressed. Especially in young mouse cells, the effect from this could be considerable and might impact some of the conclusions of the article.

Another possible area to explore in the future could be to analyse these results with the aid of a computational model.

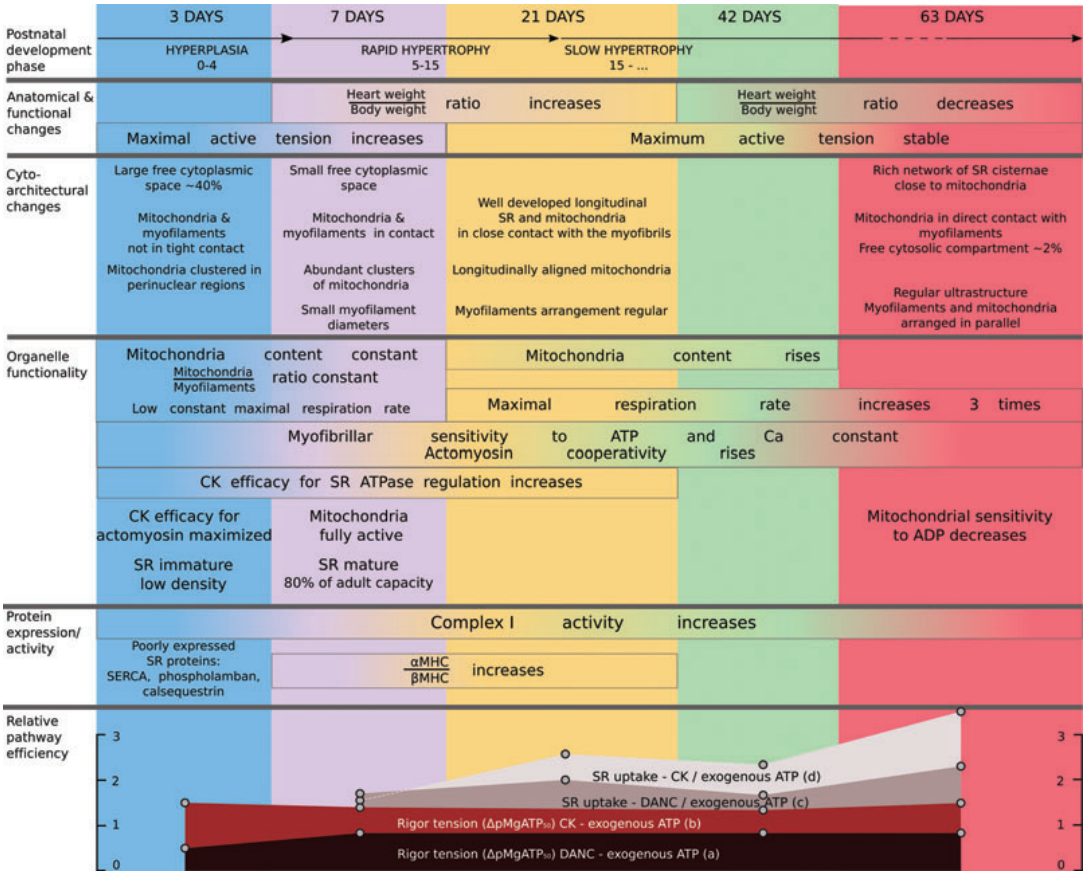

Figure 1. Summary of results from the article by Piquereau *et al*.

This would help in further unravelling the interplay between different factors during cell maturation, especially in questions where experimental methods fail to yield clear results. Different mathematical models could be compared with statistical methods in order to determine the role of various pathways and the existence of metabolite pools or spatial compartmentation in the developing cell (Sepp *et al.* 2010).

In summary, the extensive experimental work performed in the work by Piquereau *et al.* covers various aspects of energy metabolism and morphological changes in the cell during maturation. The work provides new information on postnatal development of heart energetics in mice – a popular animal model used for studying the effects of genetic manipulation.

References

Chen F, De Diego C, Xie L, Yang J, Klitzner T & Weiss J (2007). Effects of metabolic inhibition on conduction, Ca transients, and arrhythmia vulnerability in embryonic mouse hearts. *Am J Physiol Heart Circ Physiol* **293**, H2472–2478.

Lopaschuk G, Collins-Nakai R & Itoi T (1992). Developmental changes in energy substrate use by the heart. *Cardiovasc Res* **26**, 1172–1180.

Piquereau J, Novotova M, Fortin D, Garnier A, Ventura-Clapier R, Veksler V & Joubert F (2010). Postnatal development of mouse heart: formation of energetic microdomains. *J Physiol* **588**, 2443–2454.

Sepp M, Vendelin M, Vija H & Birkedal R (2010). ADP Compartmentation analysis reveals coupling between pyruvate kinase and ATPases in heart muscle. *Biophys J* **98**, 2785–2793.

Vendelin M & Birkedal R (2008). Anisotropic diffusion of fluorescently labeled ATP in rat cardiomyocytes determined by raster image correlation spectroscopy. *Am J Physiol Cell Physiol* **295**, C1302–C1315.

Takeshima H, Komazaki S, Hirose K, Nishi M, Noda T & Iino M (1998). Embryonic lethality and abnormal cardiac myocytes in mice lacking ryanodine receptor type 2. *EMBO J* **17**, 3309–3316.

Acknowledgements

We are grateful to Dr Marko Vendelin and Dr Hena R. Ramay, for fruitful discussions and review of the manuscript. This work was supported by the Wellcome Trust (Fellowship No. WT081755MA) and the Estonian Science Foundation (grant No. 7344, PhD stipends for A.I., M.S. and M.K.).

PUBLICATION III

Schryer DW, Vendelin M, Peterson P.

Symbolic flux analysis for genome-scale metabolic networks.

BMC Systems Biology, 5(1):81, (2011)

Schryer et al. BMC Systems Biology 2011, 5:81
http://www.biomedcentral.com/1752-0509/5/81

BMC Systems Biology

RESEARCH ARTICLE Open Access

Symbolic flux analysis for genome-scale metabolic networks

David W Schryer, Marko Vendelin and Pearu Peterson*

Abstract

Background: With the advent of genomic technology, the size of metabolic networks that are subject to analysis is growing. A common task when analyzing metabolic networks is to find all possible steady state regimes. There are several technical issues that have to be addressed when analyzing large metabolic networks including accumulation of numerical errors and presentation of the solution to the researcher. One way to resolve those technical issues is to analyze the network using symbolic methods. The aim of this paper is to develop a routine that symbolically finds the steady state solutions of large metabolic networks.

Results: A symbolic Gauss-Jordan elimination routine was developed for analyzing large metabolic networks. This routine was tested by finding the steady state solutions for a number of curated stoichiometric matrices with the largest having about 4000 reactions. The routine was able to find the solution with a computational time similar to the time used by a numerical singular value decomposition routine. As an advantage of symbolic solution, a set of independent fluxes can be suggested by the researcher leading to the formation of a desired flux basis describing the steady state solution of the network. These independent fluxes can be constrained using experimental data. We demonstrate the application of constraints by calculating a flux distribution for the central metabolic and amino acid biosynthesis pathways of yeast.

Conclusions: We were able to find symbolic solutions for the steady state flux distribution of large metabolic networks. The ability to choose a flux basis was found to be useful in the constraint process and provides a strong argument for using symbolic Gauss-Jordan elimination in place of singular value decomposition.

Background

The explosion of tools available to simulate the systems level properties of biological systems is indicative of the wide scale uptake of integrative biology. The Systems Biology Markup Language (SBML) Web site [1] now lists over 200 packages that make use of their library. This large number of tools reflects both the wide variety and abundance of biological data now available to constrain biological models as well as the large variety of simplifying assumptions made to gain insight from this plethora of data.

At the core of many of these analytical tools is the strict requirement of conservation of mass for each biological transformation. Because models of metabolic systems are typically under-determined, a common task when analyzing them is to find all possible steady state regimes when the concentrations of each metabolite do not change appreciably with time.

With the advent of genomic technology, the size of networks that are subject to conservation analysis is growing. This is true also of the amount of data that constrains biological function, forcing the analysis procedure to become more involved. This is especially true when faced with the realities of compartmentation in large biological systems.

The analysis of systems of chemical reactions can be traced back to 1921 when Jouguet established the notion of independence of reactions and the invariants of a system of reactions [2]. In the 1960s, with the advent of computers, routines were written for solving systems of chemical equations [3]. These were made accessible to biologists and opened up the possibility for simulating complex biological systems [4].

It may come as a surprise to many biologists that the mathematically simple operation of finding a set of

* Correspondence: pearu@sysbio.ioc.ee
Laboratory of Systems Biology, Institute of Cybernetics at Tallinn University of Technology, Akadeemia tee 21, 12618 Tallinn, Estonia

parameters that describe the steady state solution of large chemical systems continues to challenge the limits of widely used numerical libraries used to perform this task, and the development of robust computational routines for this purpose continues to be an active research area [5]. Sauro and Ingalls reviewed a number of technical issues related to the analysis of large biochemical networks and mention the attractiveness of using rational arithmetic routines that avoid the accumulation of errors [6]. They point out that this symbolic approach requires a complete rewrite of the algorithms used to solve these systems. Programs that perform conservation analysis exist. A review [6] discusses 13 software packages that perform stoichiometric conservation analysis. However, only one of these (emPath by John Woods) uses rational arithmetic. For analyzing large metabolic networks the use of numerical algorithms with floating point arithmetics seems to be considered the only practical approach, especially because of the numerical robustness of singular value decomposition (SVD) algorithm that is an integral part of many analysis tools. A more recent study uses a Computer Algebra System for symbolic Metabolic Control Analysis [7]. The author notes that the most pertinent issue with symbolic computation is its inefficiency and for the analysis of very large systems more efficient methods and software need to be developed. Other methods exists to avoid floating point operations, for example, de Figueiredo et al use a linear integer programming approach to find the shortest elementary flux modes in genome scale networks [8]. Linear programming was also used to avoid exhaustive identification of elementary flux modes as well as problems in computing null-space matrices for large metabolic networks [9].

It is notable that existing software packages do not take into account the inherit sparsity of large metabolic networks [6]. This is most likely because the result of SVD is generally non-sparse and further analysis would require non-sparse data structures. So, the use of SVD based algorithms for large metabolic networks will be limited by the size of available computer memory. For example, creating a dense stoichiometric matrix with 4000 reactions takes approximately 100MB of computer memory and various matrix operations may increase the actual memory need by a factor of ten. Holding the same stoichiometric matrix in a sparse data structure is almost one thousand times more memory efficient (Recon 1 [10] has a sparsity of 99%, for instance).

To our knowledge, no software package is available that both makes use of rational arithmetic and accounts for the inherit sparsity of large metabolic networks. To use sparse representations of metabolic networks, SVD based algorithms need to be replaced with alternative algorithms that would preserve the sparsity property in their results. To achieve the same numerical robustness of these algorithms as SVD provides, rational arithmetics can be used. The decrease of performance due to the use of rational arithmetics ought to be balanced by the sparsity of matrices as the number of numerical operations is reduced considerably. The aim of this paper is to develop a routine that symbolically finds the steady state solutions of large chemical systems.

Specifically, we have developed a routine that solves for the kernel of large stoichiometric matrices using a symbolic Gauss-Jordan Elimination (GJE) routine. For a given metabolic network the routine computes steady state solutions in a form of steady state flux relations that define how certain fluxes termed as dependent fluxes vary when the rest of fluxes termed as independent fluxes are changed. The list of dependent and independent flux variables can be either computed by the routine or specified by the researcher. The performance of this method is compared with Singular Value Decomposition (SVD) implemented in a widely used numerical routine. In addition, we demonstrate that the usefulness of solving for the stoichiometric matrix kernel symbolically goes beyond the avoidance of numerical errors. Specifically, the kernel arrived at using GJE consists of flux vectors that align with actual metabolic processes which is useful for applying constraints on steady state metabolism.

Results

A symbolic GJE routine was developed within SympyCore [11] during the course of this research. This routine was tested by finding the kernels for a number of curated metabolic models, and then utilized to calculate a metabolic flux distribution for the central metabolic and amino acid biosynthesis pathways of yeast.

Comparison of GJE and SVD

Five large metabolic networks of increasing complexity were selected to test the performance of symbolic GJE to that of numerical SVD. These metabolic networks were formulated in a closed form as described by Famili and Palsson [12]. To obtain non-trivial solutions to the steady state equations, the metabolic networks need to be converted to open form where the boundary conditions are specified via transport fluxes into the network rather than via external metabolites. For simplicity, we convert the metabolic networks to open form by introducing transport fluxes across the network boundary to metabolites that either appear in exactly one reaction or are products of polymerization reactions (see Methods).

The kernel of five stoichiometric matrices were solved for using both numerical SVD and the symbolic GJE routine with the results given in Table 1. The computation time for both methods was found to be almost the

Table 1 Performance of GJE versus SVD

Model	Publ.	Species	Reactions		Flux variables		CPU time (s)		εSVD $\times 10^{-12}$	Condition number
			Orig.	Open	Dep.	Indep.	SVD	GJE		
Example		118	129	156	118	39	0.02	0.03	0.003	15
iPS189	[15]	433	350	482	413	69	0.3	0.4	0.07	31000
iND750	[16]	1177	1266	1561	1162	399	6.2	8.0	6.37	68000
AraGEM	[17]	1767	1625	2361	1720	641	19.7	34.2	12.65	3000
iAF1260	[18]	1972	2382	2773	1960	813	30.5	34.3	1.43	2800
Recon 1	[10]	3188	3742	4480	3169	1311	123.5	145.6	32.63	71000

Kernel computation times for numerical SVD and symbolic GJE for the example yeast network given in Figure 3 and five genome-scale metabolic networks. All techniques are described in Methods. The condition number was calculated for V_{indep} from Equation (9). The inversion of V_{indep} is required to directly compare SVD results with the solution found from GJE. The difference between the results is given by ε_{SVD} in Equation (11).

same with SVD being slightly faster. However, we noted that the numerical SVD routine used effectively two CPUs (see Methods for details about the test computer system) while the symbolic GJE routine used only one. Hence for a number of parallel kernel calculations that would consume all computer CPUs, the symbolic GJE routine would be more productive. Figure 1 (top) illustrates how the kernel computation time depends on the size of the network. The computational time increases exponentially with the size. It should be noted that the ratio of these exponents depends on a computer system and underlying computational libraries. Also note that the complexity of both SVD and GJE algorithms are $O(mn^2)$, that is, increasing the network size by a factor of 10, the complexity should increase by 1000 times. The actual complexity increase (about 400 for SVD and 640 for GJE) is smaller because of using threaded libraries for the SVD routine and because of computing with high sparsity for the GJE routine. The numerical errors introduced when using SVD were found to be insignificant for the purpose of biological flux calculations and confirm the fact of numerical robustness of the SVD routine. This assessment was made by calculating the maximum relative flux error $\varepsilon_{\mathrm{SVD}}$ using Equation (11). Note that this loss of accuracy is in agreement with the condition number calculated for $\mathbf{V}_{\mathrm{indep}}$ in Equation (9); the number of inaccurate digits is approximately equal to the order of magnitude of $\varepsilon_{\mathrm{SVD}}$.

With our test computer system both numerical SVD and symbolic GJE routines can easily cope with 4000+ reaction networks. To test the limits of these routines, we repeatedly doubled the sizes of considered networks by repeating given stoichiometric matrix diagonally within a doubled stoichiometric matrix and then randomly shuffling the columns. The doubled stoichiometric matrix would then correspond to two independent but identical metabolic networks. The shuffling is needed for modeling the structure of actual metabolic network models where the order of columns is arbitrary. The process of increasing the sizes of networks was repeated with doubled stoichiometric matrices until applying our routines were close to exceeding the resources of our computer system. Figure 1 (bottom) shows the dependence of the memory usage on the size of the network. The memory usage for computing the kernels increases exponentially with the size. The two times smaller memory increase when using the symbolic GJE routine compared to the numerical SVD routine is explained by the fact that symbolic GJE routine preserves sparsity while the result of numerical SVD routine is generally non-sparse. This is illustrated in Figure 2 where the corresponding kernels from SVD and GJE algorithms are shown for the example yeast network (see next Section). For other tested networks the sparsity of GJE kernels varied in the range 95-99.9% and the sparsity of SVD kernels in 1-25%.

Application of constraints to the example yeast network

Often one needs to constrain the flux values that are physiologically meaningful, that is, either they have been experimentally measured or they must be non-negative due to the irreversibility of some reactions. We demonstrate the application of constraints by calculating a flux distribution for an example yeast network. The metabolic network is given as an SBML file in additional file 1: yeast_example.xml, and is laid out in Figure 3. This network contains 129 reactions and 118 metabolites, including 62 metabolites in the cytosol, 29 metabolites in mitochondria, and 27 metabolites that are external to the network. Because the list of external metabolites is known in this example then the system can be converted to open form by removing those rows from the stoichiometric matrix that correspond to external metabolites. Note that this is our alternative method of opening metabolic networks (see Methods).

The symbolic GJE of the stoichiometric matrix for the open system provides 91 relations for the dependent fluxes expressed in terms of 39 independent fluxes. A full list of reactions, metabolites, and steady state flux relations is given in additional file 2: yeast_example.pdf. The corresponding kernel matrix is shown in Figure 2. The relations are formed from the rows of this matrix.

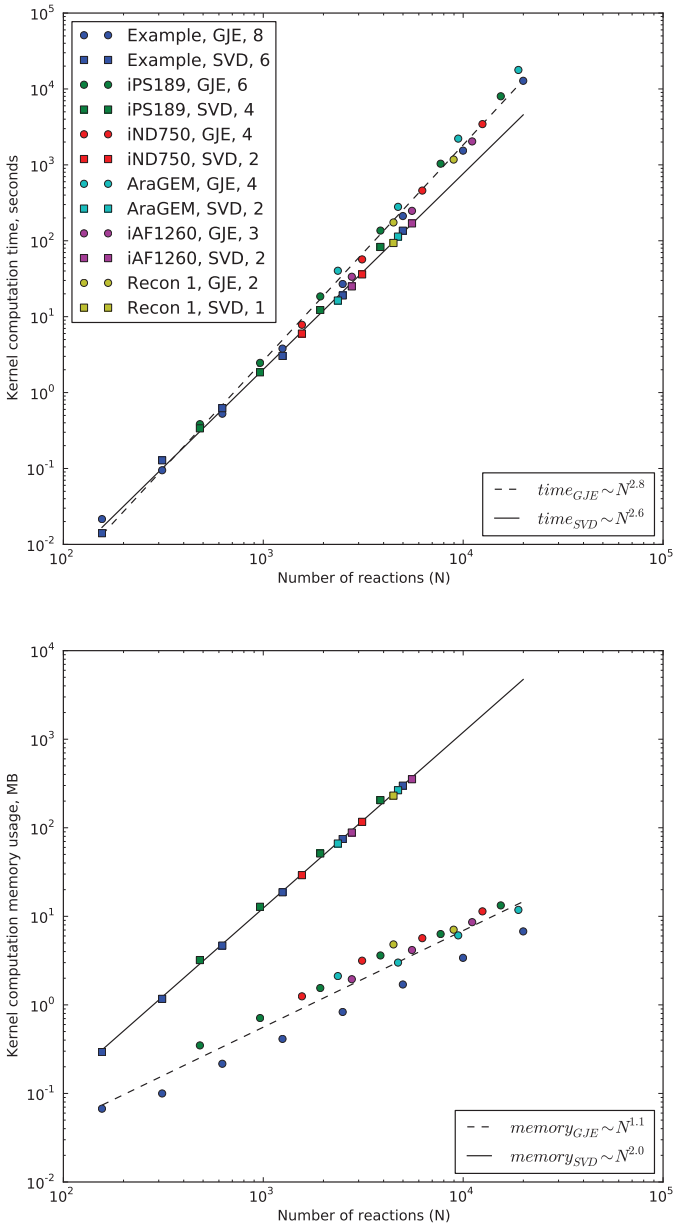

Figure 1 Computational resources for computing kernels. The computational time (upper) and memory usage (lower) for computing kernels of stoichiometric matrices using SVD and GJE algorithms for curated genome-scale networks. The system names correspond to those from Table 1. The squares correspond to SVD while circles to GJE. Numbers in upper legend denote the number of duplicated versions of the same network (see Results). Note that the computational time increases with increasing network size and the growth rate is roughly the same for both methods. However, SVD memory usage increases at twice the rate of GJE memory usage.

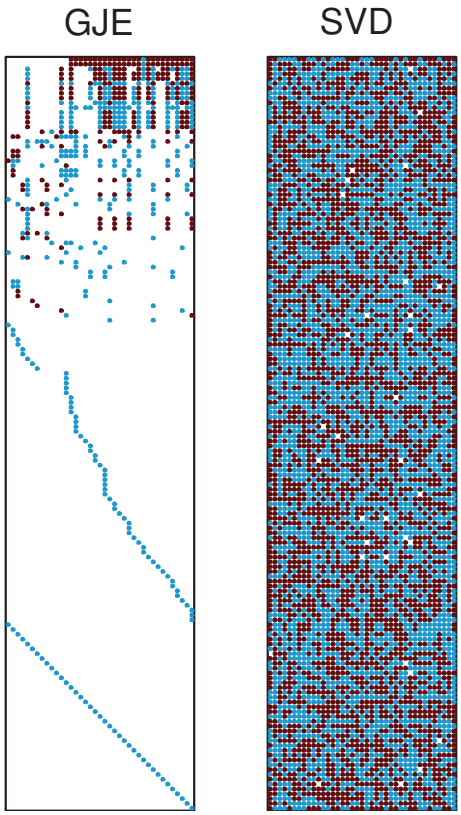

Figure 2 Kernels for the example yeast network. Two kernels of the stoichiometric matrix of the example yeast network obtained with SVD (left) and GJE (right) algorithms, respectively. The kernels define the same steady state solutions but the sparsity of the GJE kernel allows easier interpretation of these solutions.

The independent fluxes can be selected prior to performing GJE. We compose the set of independent fluxes from biomass production rates that have been experimentally measured. In total, 26 measured biomass fluxes taken from Cortassa et al [13] were used to constrain this network. The table of such exchange fluxes and their values is given in additional file 2: yeast_example.pdf. The remaining 13 independent flux variables are left unspecified which means that the symbolic GJE routine will choose a viable set of independent fluxes. In this example these are all internal to the network.

After substituting the biomass production values into the steady state flux relations, 27 dependent fluxes become fully specified with 64 relations described by the 13 internal variables. Inspection of this system of equations (also given in additional file 2: yeast_example.pdf) immediately reveals which part of the metabolism each of these 13 variables controls. Each internal variable is connected to dependent variables via nonzero entries in the corresponding column of the kernel matrix. The set of these dependent variables share metabolites and thus can be considered as one connected sub-network of the original system. Five of these sub-networks determine the split between cytosolic and mitochondrial valine, leucine, alanine, and aspartate biosynthesis via *BAT1* and *BAT2*, the split between *LEU4* and *LEU9*, *ALT1* and *ALT2*, and *AAT1* and *AAT2*. Two determine the interconversion and transport of glutamine, glutamate, and oxoglutarate via the split between *GLT* and *GDH*. The remaining six determine: (1) urea cycle flux, (2) relative production of glycine from either serine or threonine, (3) the flux of D-Glucose 6-phosphate directed towards D-Ribulose 5-phosphate, (4) production of pyruvate by the malic enzyme *MAE*1, (5) the production of phosphoenolpyruvate by *PCK*1, and (6) the relative production of acetaldehyde to acetyl-CoA from pyruvate. Figure 3 gives one flux distribution calculated by specifying the values for the 26 biomass fluxes and 13 internal fluxes. The values chosen to substitute into the flux relations are highlighted on the figure.

In addition to constraining the measured independent variables directly, knowledge about the dependent fluxes in the example yeast network was used to constrain the network. We specified the net flux direction for reactions that involved the production of carbon dioxide. The constraints of measured flux values and the specified net flux direction of reactions, can be written as a system of 91 flux relations, 26 measured independent fluxes, and 17 inequalities. Following this all redundancies were removed using computational geometry techniques described in Methods. The result is a set of five upper and lower bound conditions for 5 independent fluxes, given in additional file 2: yeast_example.pdf.

Discussion

It is now computationally practical to find the kernel of large stoichiometric matrices symbolically. The computational expense of symbolic GJE was not found to be overly restrictive with SympyCore [11], the package we used for analyzing genome-scale metabolic networks. The kernel obtained using the symbolic approach avoids numerical errors that may occur when applying numerical methods. The numerical errors result from the multitude of row operations that are needed to decompose large stoichiometric matrices [6]. The maximum relative flux error presented in Table 1 was found to be insignificant for biological flux calculations. However, symbolic GJE was found to be useful in more ways than avoiding numerical errors.

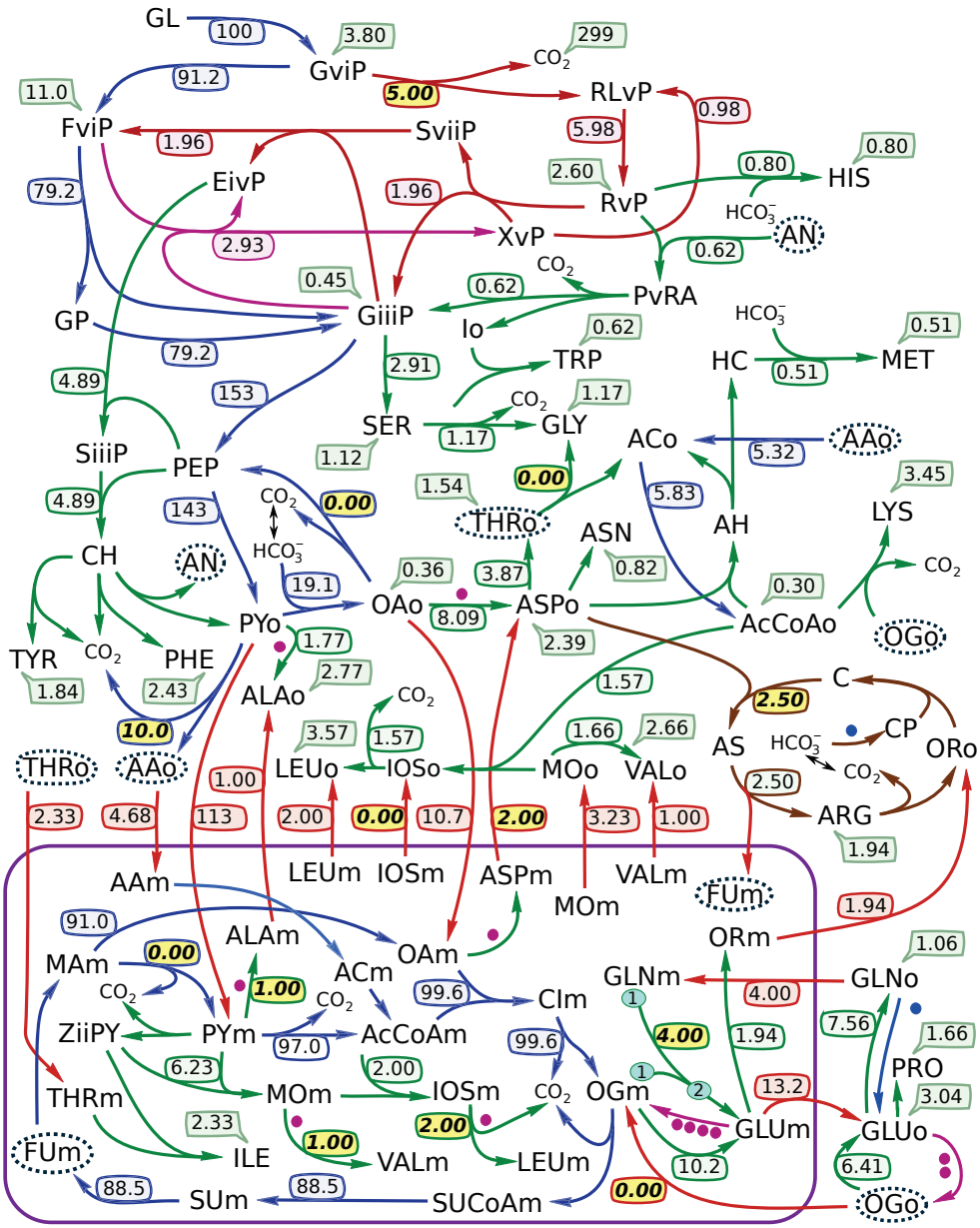

Figure 3 Example yeast network. One flux distribution for the central metabolic and amino acid biosynthesis pathways of yeast. Metabolite abbreviations, reaction details, and the symbolic flux relations used to calculate this steady state are provided in additional file 2: yeast_example.pdf. The values of the independent flux variables substituted into the flux relations are set in italic font. The mitochondrial compartment is separated with a purple boarder and all inter-compartmental transport reactions are given as orange arrows. Amino acid synthesis reactions are green, and all transport fluxes out of the system are depicted with green cartoon bubbles. The pentose phosphate pathway reactions are given in red and the urea cycle is shown in brown. Dots are placed next to reactions that are coupled; pink dots indicate the transformation of glutamate to oxoglutarate, and the blue dot shows the transformation of glutamine to glutamate. Species that occur in more than one place within one compartment are circled with a dotted blue line.

Symbolic relationships give an informative representation of metabolic network structure

There are several technical issues that complicate analysis of large metabolic networks. Among them are numerical robustness of the algorithm and presentation of solution to the researcher [5,6]. Those problems are resolved when using symbolic GJE presented in this work. While GJE and SVD provide mathematically equivalent methods of solving for the steady state flux relations of metabolic networks, there is a difference in how the solutions are formed. In SVD, steady state solution is given through a combination of eigenvectors that often span the entire metabolic network [12]. Those eigenvectors contain information about the metabolic network, however extracting and interpreting this information is not always trivial and has inspired the creation of a diverse set of tools and techniques [14]. In contrast, symbolic GJE gives the researcher an opportunity to find the set of independent fluxes and relationships between independent and dependent fluxes. Through such relationships it is easy to see which dependent fluxes are influenced by any particular independent flux and gain insight into the operation of the metabolic network.

In the example yeast network given in Figure 3, many different sets of independent fluxes can be used to find a steady state solution. The GJE routine allows the researcher to specify which independent fluxes will be used to form the solution. By choosing biomass production rates, one can constrain the operation of the metabolic network to any given set of biomass measurements.

In our example, application of biomass constraints leaves 13 independent variables that are internal to the network and define all steady state flux distributions. We found that these 13 independent fluxes influence only a specific portion of the metabolism. Each independent variable only influences those dependent fluxes that have non-zero values in its column of the GJE kernel matrix. This property has potentially far reaching implications for the physical interpretation of steady state metabolism in large networks. All nonzero entries in each column of the GJE kernel define a set of dependent variables. These variables share metabolites and thus form a sub-network. Sub-networks that share common dependent variables can be combined into a larger sub-network. For example, it allows one to identify sub-networks within the metabolic network that are linked with shared metabolites and are controlled by sets of independent fluxes. In the example yeast network two fluxes are needed to describe glutamine, glutamate, and oxoglutarate transport and interconversion while five fluxes control the split between cytosolic and mitochondrial production of valine, leucine, alanine, and aspartate. The loops within these sub-networks are determined solely by independent fluxes that occur within each sub-network.

Applicability of symbolic GJE and technical issues

We found that the computational time of applying symbolic GJE and numerical SVD routines to be similar for all networks considered. The memory usage of numerical SVD routine for networks with 6000+ reactions became close to exceeding memory resources of our test computer system. With the same memory usage level GJE routine would be able to analyze a network with 10^6 reactions, however, this calculation is estimated to take one year. Even when memory usage will be optimized in the SVD routine, the doubling network size will quadruple SVD memory usage while GJE memory usage would only double. This is because GJE algorithm preserves sparsity.

We did not observe the phenomena of coefficient explosion that would be typical for GJE algorithm using rational arithmetics on large matrices. This is explained because genome-scale stoichiometric matrices are inherently sparse and majority of elements are small integers such as 1 or -1. In addition, SympyCore [11] minimizes the number of operations by its pivot element selection rule (see Methods) to reduce computational time and this has added benefit of reducing the chance of coefficient explosion.

The reduced row echelon form of the stoichiometric matrix is formed by elementary row operations. The sequence of elementary row operations typically depends on the original ordering of the rows and columns, which is arbitrary. However, if one chooses the set of independent flux variables, i.e. columns to be skipped in the reduction process, the same reduced row echelon form of the matrix is found irregardless of the original ordering of the rows and columns. For this to be true, the columns corresponding to the chosen set must be linearly independent. When a viable set of independent flux variables is unknown or only partially known beforehand, the GJE routine implemented in SympyCore will choose the remaining independent flux variables to complete the matrix reduction process.

Flux analysis in vivo

One of the most challenging tasks for the analysis of fluxes *in vivo* is intracellular compartmentation. There are several levels of compartmentation that ought to be taken into account in a large scale metabolic model. They range from the organ level to the sub-cellular level. The genome-scale metabolic models used in this text [10] are typical in that they are compartmentalized into standard intracellular compartments separated by membrane barriers, such as mitochondria. However, even smaller compartmental units exist such as

submembrane space leading to the coupling between the K-ATP sensitive channel and creatine kinase [19], or intracellular diffusion barriers grouping ATPases and mitochondrial oxidative phosphorylation in cardiomyocytes [20-23], and the compartmentation of metabolites within enzyme systems [24]. These forms of compartmentation are often excluded from metabolic models. A genome-scale model that includes all such smaller compartmental units has yet to be formulated and will be larger. The symbolic GJE routine developed in this paper would be a suitable tool to analyze such large networks due to its efficiency.

Frequently, compartmentation can be analyzed by fully or partially decoupling the links between metabolites and reactions in the stoichiometric matrix. However, concentration gradients within the cell cannot be incorporated into a stoichiometric model. This form of compartmentation requires the use of reaction-diffusion models that take into account the three dimensional organization of the cell [25,26], and the development and application of specialized techniques such as the measurement of diffusion coefficient in the cell [27] and the use of kinetic measurements to estimate the diffusion restrictions partitioning the cell into compartments [22]. Thus the concentration gradients limit the application of stoichiometric modeling to the thermodynamic level.

Even without resorting to spatial modeling, the analysis of compartmentation remains challenging since more data is required to constrain the extra degrees of freedom introduced when splitting up metabolic pools. A recent organ level study of human brain [28] discusses the challenges of both composing an organ level compartmentalized model and obtaining the data required to constrain it. Our analysis of the example yeast network shows that each degree of freedom controls a local sub-networks of fluxes. By specifying intercompartmental fluxes to be part of the set of independent fluxes the influence of compartmentation may be characterized by a subset of variables making the analysis of compartmentation more straight forward.

Functional coupling within enzyme systems is often neglected in large scale metabolic models. When studying enzyme kinetics, it is often assumed that the distribution of the states of the enzyme remains stationary and is determined by the availability of metabolites. This assumption has been applied to study coupled enzyme systems [29] whose steady state is non-trivial since they may contain hundreds of transformations. When this assumption is made, individual mechanistic transformations can be treated in the same way as chemical reactions. The ability to choose some of these mechanistic transformations to be part of the set of independent fluxes would aid in the constraint process. It would also help one to incorporate enzyme mechanisms into larger stoichiometric models since the fluxes through the branches in the enzyme mechanism would be controlled by a subset of the independent variables and this subset would not influence remote regions of the metabolism.

Several approaches have been developed to study flux distributions *in vivo* without perturbing enzyme function. Notably, isotope labeling [30] and magnetization transfer [31]. The dynamic component of the labeling can be used to reveal compartmental effects such as the identification of barriers to metabolite transport. However this approach requires the use of optimization tools that must scan a high-dimensional space [30]. Recently, an improved optimization approach was developed that makes use of a flux coordinate system found using GJE [32]. Our GJE routine allows for the pre-selection of the independent variables, and it is anticipated that a well chosen flux coordinate system would further improve the application of this optimization procedure.

Different representations of steady state solutions

The goals of constraint based flux analysis are currently pursued using an increasing number of complimentary approaches including extreme currents [33], extreme pathways [34], elementary modes [35,36], minimal generators [37], minimal metabolic behaviors [38], and other techniques [39]. In this paper we only applied symbolic GJE algorithm to carry out Metabolic Flux Analysis (MFA).

SympyCore can be extended by implementing the double description method [40] which is an integral part of Elementary Flux Mode Analysis (EFMA).

Although both MFA and EFMA provide solutions to the same steady state problem, comparing these solutions must take into account differences in the representations of the solutions and underlying assumptions in these methods. While MFA defines a subspace of steady state flux distributions then EFMA restricts this subspace by taking into account of irreversibility of certain reactions.

Within MFA, to represent a point in such a flux subspace, it is convenient to use a linear combination of the columns of the kernel of the stoichiometric matrix. Note that such a kernel is not unique: in the SVD approach the kernel depends on the ordering of reactions as they are used to compose the stoichiometric matrix; and in the symbolic GJE approach, the kernel depends on the initial choice of independent and dependent flux variables. Reaction irreversibilities convert to constraints on the coefficients of the linear combination. In the case of the SVD kernel, these constraints are difficult to interpret because of the convolved nature of the SVD coefficients: change of one coefficient will have effect to all fluxes. In the case of the GJE kernel, the

coefficients are fluxes themselves (independent fluxes) and hence the constraints on the coefficients have a straightforward interpretation.

Within EFMA, it is mathematically more convenient to use convex polytope to represent the restricted part of the flux subspace because the conditions of reaction irreversibilities directly define the representation. This approach has given rise to the now widely used notation of elementary flux modes [41] and extreme pathways [34] that mathematically speaking are extreme rays of the convex polytope of thermodynamically feasible steady state flux distributions. It is interesting to note that in the case of pointed polytope the steady state flux distribution can be represented as a conical combination of elementary flux modes. While the elementary flux modes are uniquely determined then different combinations of elementary flux modes may define the same steady state solutions. This is orthogonal to kernel based representations: steady state solutions can be represented via different kernels but when fixing a kernel then the linear combination of its columns uniquely defines the flux distribution.

Conclusions

A symbolic GJE routine was developed within SympyCore [11] to efficiently calculate the steady state flux distribution of genome-scale metabolic networks.

Constraints can be applied directly to each independent flux. The independent flux variables can be specified in the symbolic GJE routine to match the measured data available. In addition, it was demonstrated that knowledge regarding dependent flux variables can be used to find limits on the possible ranges of independent flux variables.

We found that independent fluxes influence only specific portions of the metabolism and sub-networks can be identified from the GJE kernel matrix. This property has potentially far reaching implications for the physical interpretation of steady metabolism in genome-scale metabolic networks.

Note that usage of the symbolic GJE routine does not introduce numerical errors while numerical SVD routines do. We estimated the relative flux error introduced by the numerical SVD routine and concluded that the numerical errors are insignificant for biological applications and confirm the numerical robustness of the SVD routine. Both numerical SVD and symbolic GJE routines are equivalent with respect to computation time, however, the memory consumed by numerical SVD routine increases two times faster than that of the symbolic GJE routine using sparse data structures.

The main arguments for using symbolic GJE routine for analyzing large metabolic networks are memory efficiency, numerical robustness, freedom of choosing different sets of independent fluxes, and the ability to define sub-networks.

Our results show that symbolic implementation of relevant algorithms are competitive with highly efficient numerical algorithms when taking into account the inherit sparsity of genome-scale metabolic networks.

Methods

In this section we present two alternative procedures to obtain steady state solutions of possibly large underdetermined metabolic networks. The first approach uses a symbolic GJE algorithm that guarantees exact solutions and the second approach uses SVD implemented in a numerical algorithm that ought to give better performance. In addition, we describe a method for applying constraints to the steady state solution.

Statement of the steady state problem

Every chemical reaction and thus reaction system has the strict requirement of conservation of mass. A system of mass balances around each species has the form:

$$\dot{\mathbf{x}} = \mathbf{N}\boldsymbol{v}, \tag{1}$$

where $\dot{\mathbf{x}}$ is a length m vector of the time derivative for each mass density of metabolic species, $\mathbf{N}$ is the m × n stoichiometric matrix that links metabolites to their reactions via stoichiometry, and $\boldsymbol{v}$ is a length n vector that describes the flux through each reaction. For a system at steady state with n reactions and m species, the system of chemical reactions becomes:

$$\mathbf{N}\boldsymbol{v} = \mathbf{0}. \tag{2}$$

The number of flux variables that need to be specified to calculate a viable steady state is f = n - r where r is the rank of $\mathbf{N}$. Let us denote the vectors of dependent and independent flux variables as $\boldsymbol{v}_{\mathrm{dep}}$ and $\boldsymbol{v}_{\mathrm{indep}}$ of length r and f, respectively. Then with a n × n permutation matrix $\mathbf{P}$ that reorders the columns of $\mathbf{N}$ such that columns corresponding to dependent flux variables appear earliest, the steady state Equation (2) reads

$$\mathbf{N}_1\boldsymbol{v}_{\mathrm{dep}} + \mathbf{N}_2\boldsymbol{v}_{\mathrm{indep}} = \mathbf{0}, \tag{3}$$

where $\boldsymbol{v} = \mathbf{P}\begin{bmatrix}\boldsymbol{v}_{\mathrm{dep}}\\ \boldsymbol{v}_{\mathrm{indep}}\end{bmatrix}$ and $\mathbf{N} = [\mathbf{N}_1\ \mathbf{N}_2]\ \mathbf{P}^{\mathrm{T}}$. Clearly, when the m × r matrix $\mathbf{N}_1$ is regular (m = r and $\det \mathbf{N}_1 \neq 0$), the relation between $\boldsymbol{v}_{\mathrm{dep}}$ and $\boldsymbol{v}_{\mathrm{indep}}$ vectors can be computed directly:

$$\boldsymbol{v}_{\mathrm{dep}} = -\mathbf{N}_1^{-1}\mathbf{N}_2\boldsymbol{v}_{\mathrm{indep}}. \tag{4}$$

However, for many metabolic networks the stoichiometric matrix $\mathbf{N}$ may contain linearly dependent rows (r < m). In addition, $\boldsymbol{v}_{\mathrm{indep}}$ or $\mathbf{P}$ are not known in advance.

In the following we consider two methods based on GJE and SVD procedures that solve Equation (2) for the relation between dependent and independent flux variables: The general solution is written as:

$$\boldsymbol{v} = \mathbf{P}\begin{bmatrix} \boldsymbol{v}_{\mathrm{dep}} \\ \boldsymbol{v}_{\mathrm{indep}} \end{bmatrix}, \tag{5a}$$

$$\boldsymbol{v}_{\mathrm{dep}} = \mathbf{R}\boldsymbol{v}_{\mathrm{indep}}. \tag{5b}$$

We identify $\mathbf{R}$ as a kernel of the steady state solution where the columns are flux basis vectors and $\boldsymbol{v}_{\mathrm{indep}}$ are flux coordinates.

Solving the steady state problem via GJE

Solving the steady state problem via GJE is based on transforming the stoichiometric matrix $\mathbf{N}$ to a row-echelon form $\mathbf{N}^{\mathrm{GJE}}$ where all columns corresponding to dependent flux variables would have exactly one nonzero element and Equation (5) can be easily composed ($\mathbf{N}_1^{\mathrm{GJE}}$ is identity matrix and hence $\mathbf{R} = -\mathbf{N}_2^{\mathrm{GJE}}$). The column permutation matrix $\mathbf{P}$ is constructed during the GJE process while applying the leading row and column selection rules (pivot element selection). One of the advantage of using GJE is that it allows one to influence the pivot element selection rules so that a preferred flux basis for the system will be obtained. If the selected flux variables cannot form a basis, the routine will move one or more of the preselected independent variables to become dependent.

Note that in numerical GJE algorithms the typical leading row and column selection rule consists of choosing a pivot element with largest absolute value for maximal numerical stability. Symbolic GJE algorithms that calculate in fractions avoid numerical rounding errors and can implement more optimal selection rules that take into account the sparsity of the system. In SympyCore [11] the leading row and column selection rule consists of choosing such a pivot element that minimizes the number of row operations for minimal computation time.

Solving the steady state problem via SVD

Solving the steady state problem via SVD is based on decomposing the stoichiometric matrix $\mathbf{N}$ into a dot product of three matrices:

$$\mathbf{N} = \mathbf{U}_{\mathrm{m\times m}}\begin{bmatrix} \boldsymbol{\sigma}_{\mathrm{r\times r}} & \mathbf{0}_{\mathrm{r\times f}} \\ \mathbf{0}_{\mathrm{(m-r)\times r}} & \mathbf{0}_{\mathrm{(m-r)\times f}} \end{bmatrix}\begin{bmatrix} \mathbf{V}^{\mathrm{T}}_{\mathrm{im\ f\times n}} \\ \mathbf{V}^{\mathrm{T}}_{\mathrm{ker\ r\times n}} \end{bmatrix}, \tag{6}$$

where $\mathbf{u}$, $\mathbf{v} = [\mathbf{V}_{\mathrm{im}}\ \mathbf{V}_{\mathrm{ker}}]$ are orthogonal matrices and $\boldsymbol{\sigma}$ is a diagonal matrix with nonzero values on the diagonal. The solution to the steady state Equation (2) is

$$\boldsymbol{v} = \mathbf{V}_{\mathrm{ker}}\boldsymbol{\alpha}, \tag{7}$$

where $\boldsymbol{\alpha}$ is a f vector of arbitrary parameters. Note that the SVD approach does not provide a numerically reliable and efficient way to determine the vectors of dependent and independent flux variables and in the following we use these in the form of the permutation matrix $\mathbf{P}$ found from the GJE approach:

$$\begin{bmatrix} \boldsymbol{v}_{\mathrm{dep}} \\ \boldsymbol{v}_{\mathrm{indep}} \end{bmatrix} = \mathbf{P}^{\mathrm{T}}\mathbf{V}_{\mathrm{ker}}\boldsymbol{\alpha} = \begin{bmatrix} \mathbf{V}_{\mathrm{dep}} \\ \mathbf{V}_{\mathrm{indep}} \end{bmatrix}\boldsymbol{\alpha}, \tag{8}$$

which gives Equation (5b):

$$\boldsymbol{v}_{\mathrm{dep}} = \mathbf{V}_{\mathrm{dep}}\mathbf{V}^{-1}_{\mathrm{indep}}\boldsymbol{v}_{\mathrm{indep}}, \tag{9}$$

where $\mathbf{V}_{\mathrm{indep}}$ is a regular f × f matrix.

Processing and analysis of metabolic networks

SBML models of metabolic networks were obtained from the BiGG database [42]. During the parsing all floating point numbers were converted to fractional numbers. All species that did not participate in any reactions were excluded. Species that are appear as both a reactant and product, i.e. in polymerization reactions, were removed from the list of reactants, and an additional reaction transporting this species across the system boundary was added.

Each metabolic network was transformed into open form using the following rule: if a species participated in exactly one reaction, a reaction transporting this species across the system boundary was added. As an alternative rule used in the example yeast network, if all transport reactions out of the system are known, then transformation to open form is accomplished by removing rows for the species that are external to the system.

Both of these approaches result in equivalent steady state solutions because adding extra reactions extends linear pathways that each contain a species that exits the system. Both approaches were applied to the example yeast network: external species were removed to calculate the flux distribution in Figure 3 and additional file 2: yeast_example.pdf while the algorithm to add extra transport reactions was used to calculate the values in Table 1.

Composing the example yeast network

The example yeast network given in Figure 3 was manually composed for analyzing carbon isotope dynamics, and thus excludes metabolites that do not participate in carbon rearrangement, i.e. cofactors. To simplify the model, Carbon 3 of histidine (by InChI carbon number) was assumed to come from bicarbonate, and not Carbon 2 of ATP. Similarly, Carbon 1 of methionine was also assumed to come from bicarbonate, and not 5-Methyltetrahydropteroyltri-L-glutamate. In addition, the glyoxylate cycle and thus the third pathway for producing glycine was removed.

All relevant details of the network including metabolite abbreviations, reaction definitions, the steady state solution, and substituted flux values used to constrain the system are given in additional file 2: yeast_example.pdf.

The example yeast network makes use of fictitious metabolites that link the stoichiometry of coupled reactions. The three pentose phosphate pathway reactions are broken into two parts each linked with a fictitious metabolite that represents the carbon skeleton that is broken off of one metabolite in the first step and transferred to the next. In the additional file 2: yeast_example.pdf fictitious metabolite names start with either a capital X, Y, or Z, followed by a lower case Greek number indicating the number of carbons they contain followed by a section indicating their use. This latter section is either the yeast enzyme they participate in, the code for the metabolite they are derived from, or GOG indicating the transfer of glutamate to 2-Oxoglutarate.

Applying constraints to the steady state solution

The GJE routine provides a flux based coordinate system to describe the steady state flux space while SVD provides an orthogonal coordinate system. When specifying a flux value that is part of a flux coordinate system, one dimension from the steady state flux space is removed.

Many different sets of independent flux variables can form a coordinate system for the steady state flux space. The GJE routine allows the researcher to specify which flux variables forms a flux coordinate system and thus can match the choice of coordinate system with the experimental data available. The basis vectors formed from a flux coordinate system are often sparse and tend to span connected portions of the metabolism.

Let us assume a relation between dependent and independent flux variables as given in Equation (5). In addition to that, let us assume some constraining knowledge about the dependent variables, for example, the flux positivity for irreversible reactions: $\boldsymbol{v}_{\mathrm{dep}_i} \geq 0$ for some $i \in [1; r]$. The problem being solved is how the constraints on $\boldsymbol{v}_{\mathrm{dep}}$ constrain the independent flux variables $\boldsymbol{v}_{\mathrm{indep}}$. The goal is to determine how the steady state flux space is bounded. This is useful for many techniques used to analyze the properties of metabolic networks, for example in optimization procedures that must scan the steady state flux space while avoiding regions that are not feasible [32].

To find the constraints for $\boldsymbol{v}_{\mathrm{indep}}$, we set up the following system:

$$\boldsymbol{v}_{\mathrm{dep}} = \mathbf{R}\boldsymbol{v}_{\mathrm{indep}}, \tag{10a}$$

$$\mathbf{G}\boldsymbol{v}_{\mathrm{indep}} = \mathbf{b}, \tag{10b}$$

$$\mathbf{Q}\boldsymbol{v}_{\mathrm{dep}} \geq 0, \tag{10c}$$

where g × f matrix $\mathbf{G}$ and g vector $\mathbf{b}$ define g measured data constraints for $\boldsymbol{v}_{\mathrm{indep}}$; q × r matrix $\mathbf{Q}$ that defines q positivity constraints for $\boldsymbol{v}_{\mathrm{dep}}$. The system in Equation (10) defines a convex polytope and due to the constraining parts it is redundant. The redundancy can be removed by using the following geometric computation algorithm: solve the vertex enumeration problem for the convex polytope defined by Equation (10) and then using the obtained vertexes and rays solve the facet enumeration problem. The solution to the facet enumeration problem is a set of inequalities that has no redundancies and defines the same convex polytope as Equation (10). Note that the intermediate result of the vertex enumeration problem (polytope vertexes and rays) provides convenient information to volume scanning applications.

Computational software and error analysis

The GJE results of this paper are obtained using a Python package SympyCore [11] that implements both memory and processor efficient sparse matrix structures and manipulation algorithms. For solving the steady state problem we are using the symbolic matrix object method `get_gauss_jordan_elimination_operations` that allows one to specify the list of preferred leading columns (that is, the preferred list of dependent flux variables) for the GJE algorithm and after applying the GJE process the method returns a matrix object that is in row-echelon form. In addition to that, the method returns also a list of all applied row operations that can be later efficiently applied to other matrix objects. This feature is especially useful for adding extra columns to a stoichiometric matrix and then applying GJE process without the need to recompute the row-echelon form of the original matrix. One could use this to add transport reactions to a metabolic network during the constraint process.

The SVD results of this paper were obtained using a Python package NumPy [43] that provides a function numpy.linalg.svd for computing SVD of an array object. NumPy was built with LAPACK and ATLAS (version 3.8.3) libraries that provide a state-of-the-art routine (dgesdd) for computing SVD.

Since the results obtained with the symbolic GJE routine are correct and the results of the numerical SVD routine contain numerical rounding errors then in the error analysis we are using maximal relative flux error

$$\varepsilon_{\mathrm{SVD}} = \max_{i \in [1,r]} \frac{\sum_{j=1}^{\mathrm{f}} |R_{ij}^{\mathrm{GJE}} - R_{ij}^{\mathrm{SVD}}|}{\sum_{j=1}^{\mathrm{f}} \max(1, |R_{ij}^{\mathrm{GJE}}|, |R_{ij}^{\mathrm{SVD}}|)}, \tag{11}$$

where R_{ij}^{GJE} and R_{ij}^{SVD} are matrix elements in Equation (5) obtained with GJE and SVD routines, respectively.

Note that ε_{SVD} characterizes relative errors in dependent flux variables introduced by the numerical SVD routine.

For solving vertex and facet enumeration problems we use a Python package pycddlib [44], a wrapper of the cddlib (version 094g) that implements the double description method [40].

The Python scripts used for computing the results are available in SympyCore [45]. The performance timings were obtained on a Ubuntu Linux dual-core (AMD Phenom(tm) II X2 550) computer with 4GB RAM.

Additional material

Additional file 1: SBML model of the example yeast network. This file is marked up in SBML and contains all of the reactions of the example yeast network.

Additional file 2: SBML model details. This is a PDF file that summarizes the details of the model given in additional file 1: yeast_example.xml and presents all calculated results.

Acknowledgements
This work was supported in part by the Wellcome Trust (Fellowship No. WT081755MA). SympyCore development was supported by a Center of Excellence grant from the Norwegian Research Council to the Center for Biomedical Computing at Simula Research Laboratory http://www.simula.no/.

Authors' contributions
DS and PP developed the GJE technique with DS providing chemical insight and PP providing mathematical insight. DS composed the example yeast network and analyzed constraints. All authors contributed to the text and approved the content of the final manuscript.

Received: 4 February 2011 Accepted: 23 May 2011
Published: 23 May 2011

References

1. SBML Software Guide - SBML.org. [http://sbml.org/SBML_Software_Guide].
2. Jouguet M: **Observations sur les principes et les theoremes generaux de la statique chimique.** *J de L'Ecole polytechnique* 1921, **21**:62-180.
3. Garfinkel D, Rutledge JD, Higgins JJ: **Simulation and analysis of biochemical systems: I. representation of chemical kinetics.** *Commun ACM* 1961, **4(12)**:559-562.
4. Garfinkel D: **A machine-independent language for the simulation of complex chemical and biochemical systems.** *Comput Biomed Res* 1968, **2**:31-44.
5. Vallabhajosyula RR, Chickarmane V, Sauro HM: **Conservation analysis of large biochemical networks.** *Bioinf* 2006, **22(3)**:346-353.
6. Sauro HM, Ingalls B: **Conservation analysis in biochemical networks: computational issues for software writers.** *Biophys Chem* 2004, **109**:1-15.
7. Akhurst T: **Symbolic control analysis of cellular systems.** *PhD thesis* Stellenbosch University, Faculty of Science, Department of Biochemistry; 2011.
8. de Figueiredo LF, Podhorski A, Rubio A, Kaleta C, Beasley JE, Schuster S, Planes FJ: **Computing the shortest elementary flux modes in genome-scale metabolic networks.** *Bioinformatics (Oxford, England)* 2009, **25(23)**:3158-3165.
9. Burgard AP, Nikolaev EV, Schilling CH, Maranas CD: **Flux coupling analysis of genome-scale metabolic network reconstructions.** *Genome Research* 2004, **14(2)**:301-312.
10. Duarte NC, Becker SA, Jamshidi N, Thiele I, Mo ML, Vo TD, Srivas R, Palsson BO: **Global reconstruction of the human metabolic network based on genomic and bibliomic data.** *Proc Natl Acad Sci USA* 2007, **104(6)**:1777-1782.
11. Peterson P, Johansson F: **SympyCore - an efficient pure Python Computer Algebra System.**[http://code.google.com/p/sympycore/].
12. Famili I, Palsson BO: **The convex basis of the left null space of the stoichiometric matrix leads to the definition of metabolically meaningful pools.** *Biophys J* 2003, **85**:16-26.
13. Cortassa S, Aon JC, Aon MA: **Fluxes of carbon, phosphorylation, and redox intermediates during growth of Saccharomyces cerevisiae on different carbon sources.** *Biotechnol Bioeng* 1995, **47(2)**:193-208.
14. Llaneras F, Picó J: **Which metabolic pathways generate and characterize the flux space? A comparison among elementary modes, extreme pathways and minimal generators.** *J Biomed Biotechnol* 2010, **2010.**
15. Suthers PF, Dasika MS, Kumar VS, Denisov G, Glass JI, Maranas CD: **A genome-scale metabolic reconstruction of mycoplasma genitalium, iPS189.** *PLoS Comput Biol* 2009, **5(2)**:e1000285.
16. Duarte NC, Herrgard MJ, Palsson BO: **Reconstruction and validation of Saccharomyces cerevisiae iND750, a fully compartmentalized genome-scale metabolic model.** *Genome Res* 2004, **14(7)**:1298-1309.
17. de Oliveira Dal'Molin CG, Quek L, Palfreyman RW, Brumbley SM, Nielsen LK: **AraGEM, a genome-scale reconstruction of the primary metabolic network in arabidopsis.** *Plant Physiol* 2010, **152(2)**:579-589.
18. Feist AM, Henry CS, Reed JL, Krummenacker M, Joyce AR, Karp PD, Broadbelt LJ, Hatzimanikatis V, Palsson BO: **A genome-scale metabolic reconstruction for Escherichia coli K-12 MG1655 that accounts for 1260 ORFs and thermodynamic information.** *Mol Syst Biol* 2007, **3.**
19. Abraham MR, Selivanov VA, Hodgson DM, Pucar D, Zingman LV, Wieringa B, Dzeja PP, Alekseev AE, Terzic A: **Coupling of cell energetics with membrane metabolic sensing.** *J Biol Chem* 2002, **277(27)**:24427-24434.
20. Kaasik A, Veksler V, Boehm E, Novotova M, Minajeva A, Ventura-Clapier R: **Energetic crosstalk between organelles: architectural integration of energy production and utilization.** *Circ Res* 2001, **89(2)**:153-159.
21. Vendelin M, Eimre M, Seppet E, Peet N, Andrienko T, Lemba M, Engelbrecht J, Seppet EK, Saks VA: **Intracellular diffusion of adenosine phosphates is locally restricted in cardiac muscle.** *Mol Cell Biochem* 2004, **256-257(1-2)**:229-241.
22. Sepp M, Vendelin M, Vija H, Birkedal R: **ADP compartmentation analysis reveals coupling between pyruvate kinase and ATPases in heart muscle.** *Biophys J* 2010, **98(12)**:2785-2793.
23. Sokolova N, Vendelin M, Birkedal R: **Intracellular diffusion restrictions in isolated cardiomyocytes from rainbow trout.** *BMC Cell Biol* 2009, **10**:90.
24. Huang X, Holden HM, Raushel FM: **Channeling of substrates and intermediates in enzyme-catalyzed reactions.** *Annu Rev Biochem* 2001, **70**:149-180.
25. Ramay HR, Vendelin M: **Diffusion restrictions surrounding mitochondria: A mathematical model of heart muscle fibers.** *Biophys J* 2009, **97(2)**:443-452.
26. Shorten P, Sneyd J: **A mathematical analysis of obstructed diffusion within skeletal muscle.** *Biophys J* 2009, **96**:4764-4778.
27. Vendelin M, Birkedal R: **Anisotropic diffusion of fluorescently labeled ATP in rat cardiomyocytes determined by raster image correlation spectroscopy.** *Am J Physiol Cell Physiol* 2008, **295(5)**:C1302-1315.
28. Lewis NE, Schramm G, Bordbar A, Schellenberger J, Andersen MP, Cheng JK, Patel N, Yee A, Lewis RA, Eils R, Konig R, Palsson BO: **Large-scale in silico modeling of metabolic interactions between cell types in the human brain.** *Nat Biotech* 2010, **28(12)**:1279-1285.
29. Vendelin M, Lemba M, Saks VA: **Analysis of functional coupling: Mitochondrial creatine kinase and adenine nucleotide translocase.** *Biophys J* 2004, **87**:696-713.
30. Schryer DW, Peterson P, Paalme T, Vendelin M: **Bidirectionality and compartmentation of metabolic fluxes are revealed in the dynamics of isotopomer networks.** *Int J Mol Sci* 2009, **10(4)**:1697-1718.
31. Vendelin M, Hoerter JA, Mateo P, Soboll S, Gillet B, Mazet J: **Modulation of energy transfer pathways between mitochondria and myofibrils by changes in performance of perfused heart.** *J Biol Chem* 2010, **285(48)**:37240-37250.
32. Yang TH, Frick O, Heinzle E: **Hybrid optimization for 13C metabolic flux analysis using systems parametrized by compactification.** *BMC Systems Biology* 2008, **2**:29.
33. Clarke BL: **Stoichiometric network analysis.** *Cell Biophysics* 1988, **12**:237-253.
34. Schilling CH, Letscher D, Palsson BO: **Theory for the systemic definition of metabolic pathways and their use in interpreting metabolic function from a pathway-oriented perspective.** *Journal of Theoretical Biology* 2000, **203(3)**:229-248.

35. Schuster S, Fell DA, Dandekar T: **A general definition of metabolic pathways useful for systematic organization and analysis of complex metabolic networks.** *Nat Biotech* 2000, **18(3)**:326-332.
36. Wagner C: **Nullspace Approach to Determine the Elementary Modes of Chemical Reaction Systems.** *The Journal of Physical Chemistry B* 2004, **108(7)**:2425-2431.
37. Urbanczik R, Wagner C: **An improved algorithm for stoichiometric network analysis: theory and applications.** *Bioinformatics (Oxford, England)* 2005, **21(7)**:1203-1210.
38. Larhlimi A, Bockmayr A: **A new constraint-based description of the steady-state flux cone of metabolic networks.** *Discrete Applied Mathematics* 2009, **157(10)**:2257-2266.
39. Barrett C, Herrgard M, Palsson B: **Decomposing complex reaction networks using random sampling, principal component analysis and basis rotation.** *BMC Syst Biol* 2009, **3**:30.
40. Fukuda K, Prodon A: **Double description method revisited.** In *Combinatorics and Computer Science, Volume 1120 of Lecture Notes in Computer Science.* Edited by: Deza M, Euler R, Manoussakis I. London, UK: Springer; 1996:91-111.
41. Schuster S, Hilgetag C: **On elementary flux modes in biochemical reaction systems at steady state.** *Journal of Biological Systems* 1994, **2(2)**:165-182.
42. Schellenberger J, Park J, Conrad T, Palsson B: **BiGG: a biochemical genetic and genomic knowledgebase of large scale metabolic reconstructions.** *BMC Bioinf* 2010, **11**:213.
43. Oliphant TE: **Python for scientific computing.** *Comput Sci Eng* 2007, **9(3)**:10-20.
44. Troffaes M: **pycddlib - a Python wrapper for Komei Fukuda's cddlib.** [http://pypi.python.org/pypi/pycddlib].
45. Peterson P: **SympyCore subpackage for steady state flux analysis.**[http://code.google.com/p/sympycore/wiki/SteadyStateFluxAnalysis].

doi:10.1186/1752-0509-5-81
Cite this article as: Schryer *et al.*: Symbolic flux analysis for genome-scale metabolic networks. *BMC Systems Biology* 2011 **5**:81.

PUBLICATION IV

Schryer DW, Peterson P, Illaste A, Vendelin M.

Sensitivity analysis of flux determination in heart by $H_2^{18}O$-provided labeling using a dynamic isotopologue model of energy transfer pathways

Submitted, (2012)

The rules of the publisher prevent publication of the manuscript of Publication IV prior to acceptance. Official committee members and opponents will be given a copy of the submitted manuscript to enable them to carry out a judicious review of this dissertation.

DISSERTATIONS DEFENDED AT TUT IN NATURAL AND EXACT SCIENCES

1. **Olav Kongas**. *Nonlinear Dynamics in Modeling Cardiac Arrhytmias.* 1998.
2. **Kalju Vanatalu**. *Optimization of Processes of Microbial Biosynthesis of Isotopically Labeled Biomolecules and Their Complexes.* 1999.
3. **Ahto Buldas**. *An Algebraic Approach to the Structure of Graphs.* 1999.
4. **Monika Drews**. *A Metabolic Study of Insect Cells in Batch and Continuous Culture: Application of Chemostat and Turbidostat to the Production of Recombinant Proteins.* 1999.
5. **Eola Valdre**. *Endothelial-Specific Regulation of Vessel Formation: Role of Receptor Tyrosine Kinases.* 2000.
6. **Kalju Lott**. *Doping and Defect Thermodynamic Equilibrium in ZnS.* 2000.
7. **Reet Koljak**. *Novel Fatty Acid Dioxygenases from the Corals Plexaura homomalla and Gersemia fruticosa.* 2001.
8. **Anne Paju**. *Asymmetric oxidation of Prochiral and Racemic Ketones by Using Sharpless Catalyst.* 2001.
9. **Marko Vendelin**. *Cardiac Mechanoenergetics in silico.* 2001.
10. **Pearu Peterson**. *Multi-Soliton Interactions and the Inverse Problem of Wave Crest.* 2001.
11. **Anne Menert**. *Microcalorimetry of Anaerobic Digestion.* 2001.
12. **Toomas Tiivel**. *The Role of the Mitochondrial Outer Membrane in in vivo Regulation of Respiration in Normal Heart and Skeletal Muscle Cell.* 2002.
13. **Olle Hints**. *Ordovician Scolecodonts of Estonia and Neighbouring Areas: Taxonomy, Distribution, Palaeoecology, and Application.* 2002.
14. **Jaak Nõlvak**. *Chitinozoan Biostratigrapy in the Ordovician of Baltoscandia.* 2002.
15. **Liivi Kluge**. *On Algebraic Structure of Pre-Operad.* 2002.
16. **Jaanus Lass**. *Biosignal Interpretation: Study of Cardiac Arrhytmias and Electromagnetic Field Effects on Human Nervous System.* 2002.
17. **Janek Peterson**. *Synthesis, Structural Characterization and Modification of PAMAM Dendrimers.* 2002.
18. **Merike Vaher**. *Room Temperature Ionic Liquids as Background Electrolyte Additives in Capillary Electrophoresis.* 2002.
19. **Valdek Mikli**. *Electron Microscopy and Image Analysis Study of Powdered Hardmetal Materials and Optoelectronic Thin Films.* 2003.
20. **Mart Viljus**. *The Microstructure and Properties of Fine-Grained Cermets.* 2003.
21. **Signe Kask**. *Identification and Characterization of Dairy-Related Lactobacillus.* 2003
22. **Tiiu-Mai Laht**. *Influence of Microstructure of the Curd on Enzymatic and Microbiological Processes in Swiss-Type Cheese.* 2003.
23. **Anne Kuusksalu**. *2–5A Synthetase in the Marine Sponge Geodia cydonium.* 2003.
24. **Sergei Bereznev**. *Solar Cells Based on Polycristalline Copper-Indium Chalcogenides and Conductive Polymers.* 2003.
25. **Kadri Kriis**. *Asymmetric Synthesis of C2-Symmetric Bimorpholines and Their Application as Chiral Ligands in the Transfer Hydrogenation of Aromatic Ketones.* 2004.
26. **Jekaterina Reut**. *Polypyrrole Coatings on Conducting and Insulating Substracts.* 2004.
27. **Sven Nõmm**. *Realization and Identification of Discrete-Time Nonlinear Systems.* 2004.
28. **Olga Kijatkina**. *Deposition of Copper Indium Disulphide Films by Chemical Spray Pyrolysis.* 2004.
29. **Gert Tamberg**. *On Sampling Operators Defined by Rogosinski, Hann and Blackman Windows.* 2004.
30. **Monika Übner**. *Interaction of Humic Substances with Metal Cations.* 2004.
31. **Kaarel Adamberg**. *Growth Characteristics of Non-Starter Lactic Acid Bacteria from Cheese.* 2004.
32. **Imre Vallikivi**. *Lipase-Catalysed Reactions of Prostaglandins.* 2004.
33. **Merike Peld**. *Substituted Apatites as Sorbents for Heavy Metals.* 2005.
34. **Vitali Syritski**. *Study of Synthesis and Redox Switching of Polypyrrole and Poly(3,4-ethylenedioxythiophene) by Using in-situ Techniques.* 2004.
35. **Lee Põllumaa**. *Evaluation of Ecotoxicological Effects Related to Oil Shale Industry.* 2004.
36. **Riina Aav**. *Synthesis of 9,11-Secosterols Intermediates.* 2005.
37. **Andres Braunbrück**. *Wave Interaction in Weakly Inhomogeneous Materials.* 2005.

38. **Robert Kitt**. *Generalised Scale-Invariance in Financial Time Series.* 2005.
39. **Juss Pavelson**. *Mesoscale Physical Processes and the Related Impact on the Summer Nutrient Fields and Phytoplankton Blooms in the Western Gulf of Finland.* 2005.
40. **Olari Ilison**. *Solitons and Solitary Waves in Media with Higher Order Dispersive and Nonlinear Effects.* 2005.
41. **Maksim Säkki**. *Intermittency and Long-Range Structurization of Heart Rate.* 2005.
42. **Enli Kiipli**. *Modelling Seawater Chemistry of the East Baltic Basin in the Late Ordovician–Early Silurian.* 2005.
43. **Igor Golovtsov**. *Modification of Conductive Properties and Processability of Polyparaphenylene, Polypyrrole and polyaniline.* 2005.
44. **Katrin Laos**. *Interaction Between Furcellaran and the Globular Proteins (Bovine Serum Albumin β -Lactoglobulin).* 2005.
45. **Arvo Mere**. *Structural and Electrical Properties of Spray Deposited Copper Indium Disulphide Films for Solar Cells.* 2006.
46. **Sille Ehala**. *Development and Application of Various On- and Off-Line Analytical Methods for the Analysis of Bioactive Compounds.* 2006.
47. **Maria Kulp**. *Capillary Electrophoretic Monitoring of Biochemical Reaction Kinetics.* 2006.
48. **Anu Aaspõllu**. *Proteinases from Vipera lebetina Snake Venom Affecting Hemostasis.* 2006.
49. **Lyudmila Chekulayeva**. *Photosensitized Inactivation of Tumor Cells by Porphyrins and Chlorins.* 2006.
50. **Merle Uudsemaa**. *Quantum-Chemical Modeling of Solvated First Row Transition Metal Ions.* 2006.
51. **Tagli Pitsi**. *Nutrition Situation of Pre-School Children in Estonia from 1995 to 2004.* 2006.
52. **Angela Ivask**. *Luminescent Recombinant Sensor Bacteria for the Analysis of Bioavailable Heavy Metals.* 2006.
53. **Tiina Lõugas**. *Study on Physico-Chemical Properties and Some Bioactive Compounds of Sea Buckthorn (Hippophae rhamnoides L.).* 2006.
54. **Kaja Kasemets**. *Effect of Changing Environmental Conditions on the Fermentative Growth of Saccharomyces cerevisae S288C: Auxo-accelerostat Study.* 2006.
55. **Ildar Nisamedtinov**. *Application of 13C and Fluorescence Labeling in Metabolic Studies of Saccharomyces spp.* 2006.
56. **Alar Leibak**. *On Additive Generalisation of Voronoi's Theory of Perfect Forms over Algebraic Number Fields.* 2006.
57. **Andri Jagomägi**. *Photoluminescence of Chalcopyrite Tellurides.* 2006.
58. **Tõnu Martma**. *Application of Carbon Isotopes to the Study of the Ordovician and Silurian of the Baltic.* 2006.
59. **Marit Kauk**. *Chemical Composition of CuInSe 2 Monograin Powders for Solar Cell Application.* 2006.
60. **Julia Kois**. *Electrochemical Deposition of CuInSe2 Thin Films for Photovoltaic Applications.* 2006.
61. **Ilona Oja Açik**. *Sol-Gel Deposition of Titanium Dioxide Films.* 2007.
62. **Tiia Anmann**. *Integrated and Organized Cellular Bioenergetic Systems in Heart and Brain.* 2007.
63. **Katrin Trummal**. *Purification, Characterization and Specificity Studies of Metalloproteinases from Vipera lebetina Snake Venom.* 2007.
64. **Gennadi Lessin**. *Biochemical Definition of Coastal Zone Using Numerical Modeling and Measurement Data.* 2007.
65. **Enno Pais**. *Inverse problems to determine non-homogeneous degenerate memory kernels in heat flow.* 2007.
66. **Maria Borissova**. *Capillary Electrophoresis on Alkylimidazolium Salts.* 2007.
67. **Karin Valmsen**. *Prostaglandin Synthesis in the Coral Plexaura homomalla: Control of Prostaglandin Stereochemistry at Carbon 15 by Cyclooxygenases.* 2007.
68. **Kristjan Piirimäe**. *Long-Term Changes of Nutrient Fluxes in the Drainage Basin of the Gulf of Finland – Application of the PolFlow Model.* 2007.
69. **Tatjana Dedova**. *Chemical Spray Pyrolysis Deposition of Zinc Sulfide Thin Films and Zinc Oxide Nanostructured Layers.* 2007.
70. **Katrin Tomson**. *Production of Labelled Recombinant Proteins in Fed-Batch Systems in Escherichia coli.* 2007.
71. **Cecilia Sarmiento**. *Suppressors of RNA Silencing in Plants.* 2008.
72. **Vilja Mardla**. *Inhibition of Platelet Aggregation with Combination of Antiplatelet Agents.* 2008.
73. **Maie Bachmann**. *Effect of Modulated Microwave Radiation on Human Resting Electroencephalographic Signal.* 2008.
74. **Dan Hüvonen**. *Terahertz Spectroscopy of Low-Dimensional Spin Systems.* 2008.
75. **Ly Villo**. *Stereoselective Chemoenzymatic Synthesis of Deoxy Sugar Esters Involving Candida antarctica Lipase B.* 2008.
76. **Johan Anton**. *Technology of Integrated Photoelasticity for Residual Stress Measurement in Glass Articles of Axisymmetric Shape.* 2008.

77. **Olga Volobujeva**. *SEM Study of Selenization of Different Thin Metallic Films.* 2008.
78. **Artur Jõgi**. *Synthesis of 4'-Substituted 2,3'-dideoxynucleoside Analogues.* 2008.
79. **Mario Kadastik**. *Doubly Charged Higgs Boson Decays and Implications on Neutrino Physics.* 2008.
80. **Fernando Pérez-Caballero**. *Carbon Aerogels from 5-Methylresorcinol-Formaldehyde Gels.* 2008.
81. **Sirje Vaask**. *The Comparability, Reproducibility and Validity of Estonian Food Consumption Surveys.* 2008.
82. **Anna Menaker**. *Electrosynthesized Conducting Polymers, Polypyrrole and Poly(3,4-ethylenedioxythiophene), for Molecular Imprinting.* 2009.
83. **Lauri Ilison**. *Solitons and Solitary Waves in Hierarchical Korteweg-de Vries Type Systems.* 2009.
84. **Kaia Ernits**. *Study of In2S3 and ZnS Thin Films Deposited by Ultrasonic Spray Pyrolysis and Chemical Deposition.* 2009.
85. **Veljo Sinivee**. *Portable Spectrometer for Ionizing Radiation "Gammamapper".* 2009.
86. **Jüri Virkepu**. *On Lagrange Formalism for Lie Theory and Operadic Harmonic Oscillator in Low Dimensions.* 2009.
87. **Marko Piirsoo**. *Deciphering Molecular Basis of Schwann Cell Development.* 2009.
88. **Kati Helmja**. *Determination of Phenolic Compounds and Their Antioxidative Capability in Plant Extracts.* 2010.
89. **Merike Sõmera**. *Sobemoviruses: Genomic Organization, Potential for Recombination and Necessity of P1 in Systemic Infection.* 2010.
90. **Kristjan Laes**. *Preparation and Impedance Spectroscopy of Hybrid Structures Based on CuIn3Se5 Photoabsorber.* 2010.
91. **Kristin Lippur**. *Asymmetric Synthesis of 2,2'-Bimorpholine and its 5,5'-Substituted Derivatives.* 2010.
92. **Merike Luman**. *Dialysis Dose and Nutrition Assessment by an Optical Method.* 2010.
93. **Mihhail Berezovski**. *Numerical Simulation of Wave Propagation in Heterogeneous and Microstructured Materials.* 2010.
94. **Tamara Aid-Pavlidis**. *Structure and Regulation of BDNF Gene.* 2010.
95. **Olga Bragina**. *The Role of Sonic Hedgehog Pathway in Neuro- and Tumorigenesis.* 2010.
96. **Merle Randrüüt**. *Wave Propagation in Microstructured Solids: Solitary and Periodic Waves.* 2010.
97. **Marju Laars**. *Asymmetric Organocatalytic Michael and Aldol Reactions Mediated by Cyclic Amines.* 2010.
98. **Maarja Grossberg**. *Optical Properties of Multinary Semiconductor Compounds for Photovoltaic Applications.* 2010.
99. **Alla Maloverjan**. *Vertebrate Homologues of Drosophila Fused Kinase and Their Role in Sonic Hedgehog Signalling Pathway.* 2010.
100. **Priit Pruunsild**. *Neuronal Activity-Dependent Transcription Factors and Regulation of Human BDNF Gene.* 2010.
101. **Tatjana Knjazeva**. *New Approaches in Capillary Electrophoresis for Separation and Study of Proteins.* 2011.
102. **Atanas Katerski**. *Chemical Composition of Sprayed Copper Indium Disulfide Films for Nanostructured Solar Cells.* 2011.
103. **Kristi Timmo**. *Formation of Properties of CuInSe2 and Cu2ZnSn(S,Se)4 Monograin Powders Synthesized in Molten KI.* 2011.
104. **Kert Tamm**. *Wave Propagation and Interaction in Mindlin-Type Microstructured Solids: Numerical Simulation.* 2011.
105. **Adrian Popp**. *Ordovician Proetid Trilobites in Baltoscandia and Germany.* 2011.
106. **Ove Pärn**. *Sea Ice Deformation Events in the Gulf of Finland and This Impact on Shipping.* 2011.
107. **Germo Väli**. *Numerical Experiments on Matter Transport in the Baltic Sea.* 2011.
108. **Andrus Seiman**. *Point-of-Care Analyser Based on Capillary Electrophoresis.* 2011.
109. **Olga Katargina**. *Tick-Borne Pathogens Circulating in Estonia (Tick-Borne Encephalitis Virus, Anaplasma phagocytophilum, Babesia Species): Their Prevalence and Genetic Characterization.* 2011.
110. **Ingrid Sumeri**. *The Study of Probiotic Bacteria in Human Gastrointestinal Tract Simulator.* 2011.
111. **Kairit Zovo**. *Functional Characterization of Cellular Copper Proteome.* 2011.
112. **Natalja Makarytsheva**. *Analysis of Organic Species in Sediments and Soil by High Performance Separation Methods.* 2011.
113. **Monika Mortimer**. *Evaluation of the Biological Effects of Engineered Nanoparticles on Unicellular Pro- and Eukaryotic Organisms.* 2011.
114. **Kersti Tepp**. *Molecular System Bioenergetics of Cardiac Cells: Quantitative Analysis of Structure-Function Relationship.* 2011.
115. **Anna-Liisa Peikolainen**. *Organic Aerogels Based on 5-Methylresorcinol.* 2011.

116. **Leeli Amon**. *Palaeoecological Reconstruction of Late-Glacial Vegetation Dynamics in Eastern Baltic Area: A View Based on Plant Macrofossil Analysis.* 2011.
117. **Tanel Peets**. *Dispersion Analysis of Wave Motion in Microstructured Solids.* 2011.
118. **Liina Kaupmees**. *Selenization of Molybdenum as Contact Material in Solar Cells.* 2011.
119. **Allan Olspert**. *Properties of VPg and Coat Protein of Sobemoviruses.* 2011.
120. **Kadri Koppel**. *Food Category Appraisal Using Sensory Methods.* 2011.
121. **Jelena Gorbatšova**. *Development of Methods for CE Analysis of Plant Phenolics and Vitamins.* 2011.
122. **Karin Viipsi**. *Impact of EDTA and Humic Substances on the Removal of Cd and Zn from Aqueous Solutions by Apatite.* 2012.